

IDENTIFICATION, VALIDATION, AND STRUCTURAL STUDIES  
OF MULTITARGETING INHIBITORS  
AGAINST *MYCOBACTERIUM TUBERCULOSIS* MYCOLIC ACID  
METHYLTRANSFERASES

A Dissertation

by

JEREMY LEE WOOD

Submitted to the Office of Graduate and Professional Studies of  
Texas A&M University  
in partial fulfillment of the requirements for the degree of

DOCTOR OF PHILOSOPHY

Chair of Committee,	James Sacchettini
Committee Members,	Jeffrey Cirillo
	Thomas Meek
	Xiuren Zhang
Head of Department,	Dorothy Shippen

May 2019

Major Subject: Biochemistry

Copyright 2019 Jeremy Lee Wood

## ABSTRACT

Combating the persistent threat and low therapeutic success of treating multidrug-resistant *Mycobacterium tuberculosis* (Mtb), the causative agent of tuberculosis, demands a worldwide effort to discover and develop new antitubercular drugs. *M. tuberculosis* harbors a lipid-rich cell wall that poses a formidable barrier to small molecules including antibiotics. Mycolic acids are the predominant very long chain extensively-modified fatty acids found in the cell wall of Mtb that are determinant of cell wall permeability, intrinsic drug resistance, and virulence. Mycolic acids are modified by a family of mycolic acid methyltransferases (MA-MTs) that have been shown to be simultaneously inhibited by a single small molecule, dioctylamine. As cyclopropane mycolic acid synthases (CMAS) were the primary MA-MT targets of the compound, we believe targeting this family of synthases is a promising antibiotic strategy, as their simultaneous inhibition results in enhanced drug penetration and synergistic killing when combined with established antimycobacterial drugs. Due to the lack of suitable in vitro assays for drug screening, no drug-like molecules have been identified to establish whether simultaneous inhibition of this family of enzymes is a viable therapeutic strategy for the treatment of tuberculosis.

We first combined differential scanning fluorimetry (DSF) screening and organic synthesis to design a set of nitrobenzoxadiazole fluorescence enhancement probes suitable for in vitro CMAS multitarget assessment. Furthermore, we show that the CmaA2 displacement assay was suitable for HTS. Small molecule screening revealed that CMAS bind amine-based amphipathic ligands of broad structural diversity.

We then tested the power of our assays for identifying multitarget CMAS inhibitors *in vivo* by incubating mycobacteria with a selected collection of ligands with diverse chemical scaffolds and looked for changes in mycolic acid modification using radio two-dimensional thin layer chromatography. We found that the majority of these molecules inhibited multiple pathways of mycolic acid modification.

Using X-ray crystallography to examine the molecular basis of inhibition, we found that these drug-like molecules mimic the carbocation reaction intermediate. The studies provide a structural foundation for further structure-based inhibitor design.

Finally, we tested compound lethality using *Mtb* kill-curve assays where we found that simultaneous inhibition of mycolic acid modification is unlikely to be bactericidal to *Mtb* in planktonic culture.

In sum, we have developed an unprecedented CmaA2 HTS assay platform that enables the identification of drug-like small molecules that bind to and inhibit multiple CMAS *in vitro* and *in vivo*. We characterized the chemical space of CMAS ligands, that provides an experimental framework for multi-target drug development against *Mtb*.

## CONTRIBUTORS AND FUNDING SOURCES

### **Contributors**

This work was supported by a dissertation committee consisting of Professors James Sacchettini, Thomas Meek, and Xiuren Zhang of the Department of Biochemistry and Biophysics and Regents Professor Jeffery Cirillo at the Department of Microbial and Molecular Pathogenesis.

Our in-house *Mycobacterium tuberculosis* mc<sup>2</sup>7000 whole-cell active small molecule collection, that we used to test against the *M. tuberculosis* CmaA2-SAM-NBD-A complex in Chapter 3, was generated from high throughput screening performed by Dr. Ryan Hughes. Organic synthesis and chemical structure analysis of NBD-A and NBD-B fluorophores in Chapter 2 were performed by Dr. Abhijit Roychowdhury. Dr. Michael Glickman at the Memorial Sloan Kettering Cancer Center provided the radio two-dimensional thin layer chromatography data of isolated and purified mycolic acids from the cell walls of *Mycobacterium bovis* bacillus Calmette - Guérin Russia cultured in the presence and absence of inhibitors in Chapter 3. Data analysis of CmaA2-SAH-Compound 2 co-crystal subjected to liquid chromatography mass spectrometry was performed by Mr. Andres Silva in Chapter 3. Mrs. Wen Dong conducted the human dermal fibroblast and HepG2 cytotoxicity assays in Chapter 3.

All other work conducted for the dissertation was completed by the student independently.

### **Funding Sources**

The work was supported by a grant from the US National Institutes of Health (2P01AI095208-05A1) awarded to Professor James Sacchettini.

## NOMENCLATURE

BCG-P	<i>Mycobacterium bovis</i> bacillus Calmette - Guérin (Pasteur)
BCG-R	<i>Mycobacterium bovis</i> bacillus Calmette - Guérin (Russia)
CFAS	Cyclopropane fatty acid synthase
CMAS	Cyclopropane mycolic acid synthase
DSF	Differential scanning fluorimetry
HTS	High-throughput screening
MA-MT	Mycolic acid methyltransferase
MDR-TB	Multidrug-resistant tuberculosis
Msmeg	<i>Mycobacterium smegmatis</i>
MTA	5-thiomethyladenosine
Mtb	<i>Mycobacterium tuberculosis</i>
NBD	Nitrobenzoxadiazole
NBD-A	N <sup>1</sup> -methyl-N <sup>3</sup> -(7-nitrobenzo[c][1,2,5]oxadiazol-4-yl)propane -1,3-diamine
NBD-B	N <sup>1</sup> -(7-nitrobenz[c][1,2,5]oxadiazol-4-yl)propane-1,3- diamine
SAH	S-adenosyl homocysteine
SAM	S-adenosyl methionine
TB	Tuberculosis

## TABLE OF CONTENTS

	Page
ABSTRACT .....	ii
CONTRIBUTORS AND FUNDING SOURCES.....	iv
NOMENCLATURE.....	v
TABLE OF CONTENTS .....	vi
LIST OF FIGURES.....	viii
LIST OF TABLES .....	x
CHAPTER I INTRODUCTION AND LITERATURE REVIEW .....	1
Mycolic acid is the predominant lipid in the mycobacterial cell wall .....	3
Mycolic acid biosynthesis.....	9
Biosynthesis of unsaturated meromycolates: desaturases .....	12
Mycolic acids are modified by S-adenosyl methionine-dependent mycolic acid methyltransferases.....	25
Functional role of mycolic acid modification in <i>Mycobacterium         tuberculosis</i> physiology .....	37
Physiologic role of the <i>Mycobacterium tuberculosis</i> mycolic acid modifications during host infection .....	41
Biofilm formation .....	46
Mycolic acid methyltransferases as drug targets .....	48
CHAPTER II DESIGN AND DEVELOPMENT OF A NOVEL CYCLOPROPANE MYCOLIC ACID SYNTHASE FLUORESCENCE-BASED COMPETITION DISPLACEMENT ASSAY .....	54
Overview.....	54
Introduction.....	55
Results.....	59
Discussion.....	70
Materials and Methods.....	74
CHAPTER III HIGH THROUGHPUT SCREENING AND STRUCTURE GUIDED INHIBITOR DISCOVERY .....	79
Overview.....	79
Introduction.....	80
Results.....	84

Materials and Methods.....	124
Discussion.....	130
CHAPTER IV CONCLUSIONS .....	137
REFERENCES.....	145

## LIST OF FIGURES

	Page
Figure 1. Schematic representation of the <i>Mycobacterium tuberculosis</i> cell wall.....	4
Figure 2. Mycolic acid structure. ....	7
Figure 3. Mycolic acids of <i>Mycobacterium tuberculosis</i> and <i>Mycobacterium smegmatis</i> . ....	8
Figure 4. Mycolic acid biosynthetic pathway. ....	10
Figure 5. Putative roles of EchA proteins in meromycolate anaerobic desaturation. ....	18
Figure 6. Mycolic acid methyltransferases modify <i>Mycobacterium tuberculosis</i> mycolic acids. ....	27
Figure 7. The nitrobenzoxadiazole fluorophore is structurally similar to the 4-chloronaphthyl group in Compounds 4 and 5.....	60
Figure 8. Two-step synthetic route for N <sup>1</sup> -methyl-N <sup>3</sup> -(7-nitrobenzo[c][1,2,5]oxadiazol-4-yl)propane-1,3-diamine (NBD-A).....	61
Figure 9. Spectral properties of for N <sup>1</sup> -methyl-N <sup>3</sup> -(7-nitrobenzo[c][1,2,5]oxadiazol-4-yl)propane-1,3-diamine (NBD-A) in the presence of cyclopropane mycolic acid synthases. ....	62
Figure 10. Spectral properties of for N <sup>1</sup> -(7-nitrobenz[c][1,2,5]oxadiazol-4-yl)propane-1,3-diamine (NBD-B) in the presence of cyclopropane mycolic acid synthases. ....	63
Figure 11. Binding isotherms of CmaA2 and MmaA2 titrated with nitrobenzoxadiazole analogs of Compound 4. ....	64
Figure 12. CmaA2 in complex with N <sup>1</sup> -methyl-N <sup>3</sup> -(7-nitrobenzo[c][1,2,5]oxadiazol-4-yl)propane-1,3-diamine (NBD-A) and S-adenosyl homocysteine.....	66
Figure 13. Small molecules compete with nitrobenzoxadiazole probes for the active sites of cyclopropane mycolic acid synthases. ....	68
Figure 14. Thermal denaturation profiles of cyclopropane mycolic acid synthases in various buffer conditions.....	85



Figure 15. Dioctylamine and differential scanning fluorimetry-identified small molecules are active site competitors of cyclopropane mycolic acid synthases.....	89
Figure 16. CmaA2 high throughput screening plate <i>Z'</i> -factors.....	91
Figure 17. Chemical structures of 30 compounds identified via CmaA2 high throughput screening .....	92
Figure 18. Chemical structures of commercially available CmaA2 ligands identified via high throughput screening.....	93
Figure 19. Automated ligand identification system screening identified putative multitarget mycolic acid methyltransferase compounds.....	101
Figure 20. Multitargeting cyclopropane mycolic acid synthase ligands inhibit mycolic acid cyclopropanation biosynthesis in vivo.....	103
Figure 21. Compound 1 is a dose-dependent inhibitor of multiple pathways of mycolic acid modification.....	106
Figure 22. Molecule 4 is a dose-dependent inhibitor of multiple pathways of mycolic acid modification.....	107
Figure 23. Molecule H23 inhibits multiple pathways of mycolic acid modification.....	109
Figure 24. Crystal structures of CmaA2 in complex with Compounds 1 and 4.....	111
Figure 25. H23 induces an active site occluding conformational change upon binding CmaA2.....	115
Figure 26. H29 and dioctylamine similarly orient in the active site of CmaA2.....	119
Figure 27. Crystal structures of CmaA2 in complex with Compound 2 and S-adenosyl homocysteine.....	122
Figure 28. <i>Mycobacterium tuberculosis</i> kill-curve analysis of multitargeting cyclopropane mycolic acid synthase inhibitors.....	124
Figure 29. Putative model for CmaA2 active site closure via T198 phosphorylation.....	136

## LIST OF TABLES

	Page
Table 1. Data collection and refinement statistics for CmaA2 in complex with N1-methyl-N3-(7-nitrobenzo[c][1,2,5]oxadiazol-4-yl)propane-1,3-diamine (NBD-A) and S-adenosyl homocysteine.....	65
Table 2. $K_d$ and $EC_{50}$ values of the selected small molecule cyclopropane mycolic acid synthase active site competitor ligands.....	69
Table 3. Chemical structures of five small molecules identified as CmaA2 thermal stabilizers via differential scanning fluorimetry screening. ....	87
Table 4. $K_d$ and $IC_{50}$ values of differential scanning fluorimetry-identified small molecules. ....	89
Table 5. $K_d$ and $IC_{50}$ values of selected compounds identified through CmaA2 high throughput screening. ....	94
Table 6. $K_d$ values of selected compounds identified through differential scanning fluorimetry and high throughput screening in the presence of S-adenosyl homocysteine.....	96
Table 7. Cyclopropane mycolic acid synthase equilibrium dissociation constants for hit molecules identified via screening the Sanofi <i>Mycobacterium tuberculosis</i> whole cell active collection.....	98
Table 8. Total number of binding events identified for each mycolic acid methyltransferase via automated ligand identification system screening.....	99
Table 9. Data collection and refinement statistics for CmaA2 in complex with Compound 1 and 4.....	110
Table 10. Data collection and refinement statistics for CmaA2 in complex with H23 and S-adenosyl homocysteine.....	114
Table 11. Data collection and refinement statistics for CmaA2 in complex with H29 and S-adenosyl homocysteine.....	117
Table 12. Data collection and refinement statistics for CmaA2 in complex with H20 and S-adenosyl homocysteine.....	121

## CHAPTER I

### INTRODUCTION AND LITERATURE REVIEW

Tuberculosis (TB) is a highly contagious airborne disease caused by an infection with the bacterium *Mycobacterium tuberculosis* (Mtb). TB is one of the greatest causes of human mortality in history by a microbial pathogen and is a major global health threat due to the increased prevalence of multidrug-resistance (Daniel, 2006; World Health Organization, 2018). Until the groundbreaking discoveries by Robert Koch and Jean-Antoine Villemin in the late 19<sup>th</sup> century, wherein the unequivocal bacterial origin and transmissibility of the disease were determined, consumption, now called TB, was thought to be either an inherited, congenital, or spontaneous disease (Cambau and Drancourt, 2014). During the late nineteenth century, one in seven people died from the disease (Koch, 1882). In 2017, that number equates to approximately 1.1 billion deaths per year, compared to the near thousand-fold smaller 1.6 million deaths reported by the World Health Organization in the same year from drug-sensitive TB alone (World Health Organization, 2018). The works of Villemin and Koch, in addition to the discovery of X-rays by Wilhelm Röntgen, Ziel-Neelsen acid-fast mycobacterial stain by Franz Ziel and Friedrich Neelsen, and small-molecule chemotherapy by Paul Ehrlich, together provided a means to diagnose the sick and pursue a cure. Today, drug-sensitive TB is often curable with a 6 to 9-month standard combination drug treatment with four first-line antitubercular drugs: isoniazid, rifampicin, pyrazinamide, and ethambutol. Despite available treatment, this disease continues to cause extensive human mortality. A major global concern is the emergence of multidrug-resistant TB (MDR-TB) that is resistant to both isoniazid and rifampicin. An additional 230,000

deaths were reported from MDR-TB and rifampicin-resistant TB combined (World Health Organization, 2018). The persistent threat of drug-resistant Mtb demands the discovery of novel chemical agents with unique modes of action and the potential to shorten the duration of treatment. The urgent need for new therapeutic entities is compounded by the presence of bacilli with extended drug resistance profiles, where curative options are limited or currently unavailable (Dheda et al., 2017).

The cell wall of Mtb contains a complex array of lipid constituents whereby mycolic acids are the major and hallmark lipid, and are known to play roles in the cell wall permeability, intrinsic resistance to therapeutic reagents, and virulence (Barry III et al., 1998; Brennan and Nikaido, 1995; Jackson, 2014; Marrakchi et al., 2014). Mycolic acids account for approximately 50 % of the cell wall weight and are required for Mtb survival, as established by the therapeutic efficacy of isoniazid and ethionamide, inhibitors of mycolic acid biosynthesis (Draper, 1998). Aided by the Mtb genome sequence, a near complete picture of the enzymatic players involved in the mycolic acid biosynthetic pathway has been established (Cole et al., 1998; Pawelczyk and Kremer, 2014). Unlike *de novo* fatty acid biosynthesis in humans, that requires a single fatty acid synthase (FASI), mycolic acid biosynthesis in Mtb requires two FAS systems, FASI and FASII (Marrakchi et al., 2014). Since FASII is pathogen-specific, a significant effort has been directed towards identifying inhibitors against discrete enzymes in the pathway. A powerful method to identify the cellular protein target of an inhibitor is through the generation of spontaneous resistant mutants combined with whole-genome sequencing. This method has been successfully used to identify FASII enzymes as the targets of various whole-cell active growth inhibitors of Mtb (Aggarwal et al., 2017; La Rosa et al., 2012; Stanley et al., 2013). With regards to

established antitubercular drugs, a multitude of drug-resistant mutations have been identified within either the gene of the protein target or drug-activating enzyme (Dheda et al., 2017). Given the substantial risk of producing drug-resistant infections, TB curative therapy requires a multi-drug regimen. An alternative approach is to employ a therapeutic agent into a combination regimen that has the capacity to inhibit multiple targets simultaneously that may delay the onset of antimicrobial drug resistance. Previous studies demonstrated that S-adenosyl methionine (SAM)-dependent mycolic acid methyltransferases (MAMTs), that are highly similar enzymes responsible for modifying cell wall mycolic acids, are suitable targets for multitarget drug discovery (Barkan et al., 2009).

This chapter focuses on the biosynthetic processes involved in mycolic acid synthesis and their Mtb-specific modifications. It also emphasizes the functional roles of mycolic acid modification during host infection and mycolic acid modifying enzymes as promising drug targets for the treatment of tuberculosis.

### **Mycolic acid is the predominant lipid in the mycobacterial cell wall**

Encapsulating the cytoplasm of the mycobacterial cell is a tripartite cell wall structure consisting of a plasma membrane, cell wall core, and capsule (Figure 1). The major lipid constituents of the mycobacterial inner membrane (plasma membrane) are derivatives of phosphatidic acid (phosphatidylglycerol, phosphatidylethanolamine, phosphatidylinositol, and cardiolipin) and mannosylated phosphatidylinositol variants (Brennan and Nikaido, 1995). This phospholipid-rich milieu is critical for physiological processes such as peptidoglycan synthesis, nutrient acquisition, electron transport, and DNA replication (Jackson, 2014). The cell wall core surrounding the plasma membrane is a covalently-linked macromolecular assembly composed of peptidoglycan, arabinogalactan,

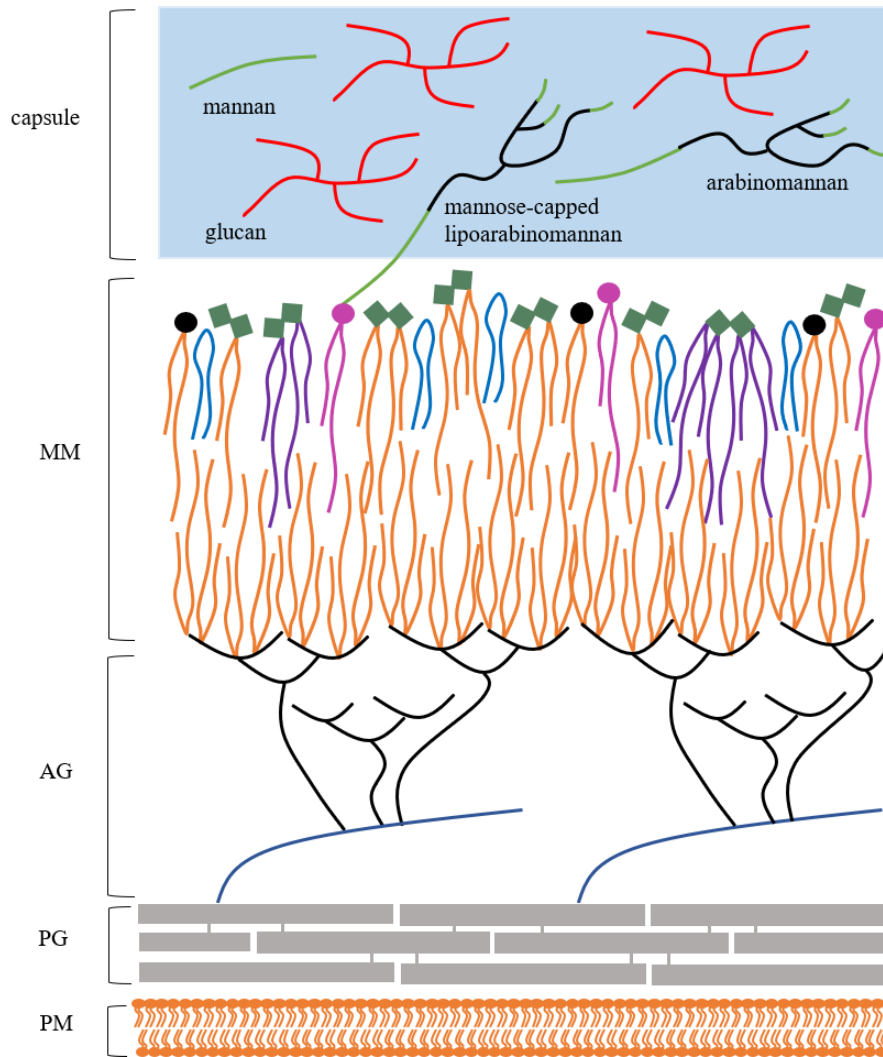


**Figure 1. Schematic representation of the *Mycobacterium tuberculosis* cell wall.**

The cell wall is a tripartite structure consisting of a plasma membrane (PM), a cell wall core composed of peptidoglycan (PG), arabinogalactan (AG), a mycomembrane (MM), and capsule. A layered peptidoglycan mesh surrounds the inner membrane and is covalently-attached to the heteropolysaccharide polymer, arabinogalactan (galactose represented in red, arabinose represented in blue). Mycolic acids, represented in green, in the inner leaflet of the outer membrane are covalently-attached to two-thirds of the arabinose branches of arabinogalactan. The outer leaflet, consists of an array of complex lipids, including mycolate-conjugates represented as orange/green species. This representation of the mycomembrane is consistent with the model proposed by Minnikin, where the lipids in the inner and outer leaflets intercalate (Minnikin, 1982). A polysaccharide-rich (glucose represented in black, mannose represented in brown) capsule layer surrounds the mycomembrane. This schematic representation of the Mtb cell wall was adapted from Jackson, 2014.

and mycolic acids, commonly referred to as the mycolyl-arabinogalactan-peptidoglycan complex (Jankute et al., 2015). The outer layer of the cell wall consists primarily of mycolic acids, that are found incorporated into to the inner and outer leaflets of the mycomembrane, recently resolved using cryo-electron microscopy (Hoffmann et al., 2008; Sani et al., 2010; Zuber et al., 2008). Mycolic acids in the inner leaflet are covalently attached to a highlycross-linked peptidoglycan mesh (mycobacteria: 70 - 80 %; *E. coil*: 50 %) by a large, approximately 100 residue, heteropolysaccharide arabinogalactan bridge (Daffé et al., 1990; Matsushashi, 1966; McNeil et al., 1991; Vollmer and Höltje, 2004). The base of arabinogalactan consists of an approximately 30-residue galactose polymer that is covalently-attached to the peptidoglycan through a disaccharide linker, rhamnose-N-acetylglucosamine (Daffé et al., 1990; Grzegorzewicz et al., 2016; Mikušová et al., 1996). At three distinct positions along the polymer, three 31-residue arabinose chains extend towards the outer cell wall, whereby two-thirds of the branched termini are esterified with mycolic acids (Bhamidi et al., 2008; McNeil et al., 1991). Mycolic acids are also found esterified to polyols (glycerol, glucose, trehalose) in the outer extractable leaflet (Quemard, 2016). Together, mycolic acids have been found to play key roles in cell wall fluidity, permeability, modulating the host immune system, foamy macrophage differentiation, and biofilm formation (Barkan et al., 2012; Vander Beken et al., 2011; Dubnau et al., 2000; Glickman et al., 2000; Ojha et al., 2008, 2010; Rao et al., 2006; Yuan et al., 1997, 1998a) The outermost layer of the cell wall consists of a capsule-like structure that has been a matter of debate, is composed almost entirely of carbohydrates and polypeptides, with a small amount (2 - 3 %) of lipids (Lemassu and Daffe, 1994; Ortalo-Magne et al., 1995, 1996) The existence of this layer has been shown to dependent on in vitro growth conditions, whereby

the presence of detergent and/or agitation results in the disruption of the structure with its components released into the surround medium (Daffé and Etienne, 1999; Ortalo-Magne et al., 1996; Sani et al., 2010). The major components of this cellular coat are  $\alpha$ -glucan, a branched structure similar to glycogen that approximates 90 % of the polysaccharide content, and extensively mannose-capped arabinomannan and mannan (Lemassu and Daffe, 1994).

Mycolic acids are the hallmark lipids of the outer bacterial cell wall of the *Actinomycetales* suborder *Corynebacterineae*, that include the important human pathogen *Mtb* (Asselineau and Lederer, 1950; Marrakchi et al., 2014). These fatty acids harbor a characteristic 3-carbon mycolate motif (C1-carboxyl, C2-alkyl branch, and a C3-hydroxyl group), and are commonly called  $\alpha$ -alkyl  $\beta$ -hydroxy fatty acids (Barry III et al., 1998). A particular property of mycolic acids is their ability to undergo thermolytic cleavage at high temperatures, where the C2-C3 bond is broken to free the  $\alpha$  and  $\beta$  constituents (Figure 2A). Pyrolytic cleavage results in two products, a fatty acid (an  $\alpha$ -branch derived fatty acid extended by two carbon atoms) and a meroaldehyde (commonly called the meromycolate chain) from the  $\alpha$  and  $\beta$  positions, respectively (Etemadi, 1967). Mycolic acids show significant variation in total carbon length and overall chemical structure. Mycolic acids have been identified from as short as C<sub>22</sub> in the genus *Corynebacterium* to as long as C<sub>100</sub> in *Segniliparus* (Collins et al., 1982; Hong et al., 2018). Mycolic acids found in *Mycobacteria* are near the longest identified in nature with carbon lengths between C<sub>60</sub> - C<sub>90</sub> (Barry III et al., 1998). In addition, mycolic acids contain considerable structural variation in the acyl constituents located at the  $\alpha$  and  $\beta$  positions. Fatty acids liberated from mycolic acids vary widely in total carbon length, from as short as C<sub>8</sub> in *Corynebacteria* to as long as C<sub>26</sub> in *Mycobacteria*, and have been largely identified as fully saturated lipids, although



unsaturated variants are have been found in *Tsukamurella* (Barry III et al., 1998; Collins et al., 1982; Tomiyasu and Yano, 1984). Unlike the  $\alpha$ -branch, meromycolate chains are largely found modified with double bonds, cyclopropane rings, methyl branches, or oxygenated

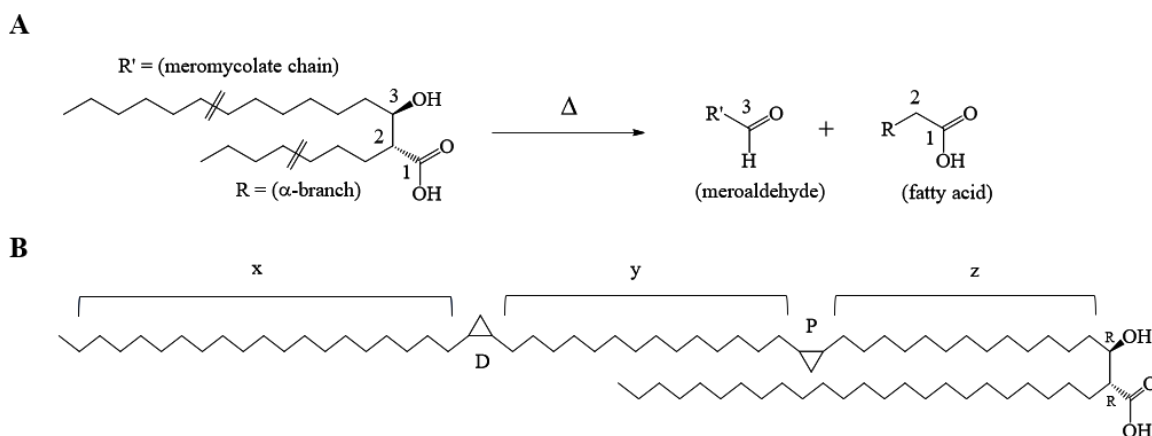


**Figure 2. Mycolic acid structure.**

A) Mycolic acids are characterized by a signature  $\alpha$ -alkyl  $\beta$ -hydroxy 3-carbon mycolate motif. The C2-C3 bond is labile at high temperature. Mycolic acid pyrolysis results in the C2-C3 bond cleavage generating a fatty acid and a meroaldehyde. B) Chemical structure of an  $\alpha$ -mycolate from *Mycobacterium tuberculosis* (Mtb). This mycolic acid shows the general features of mycolic acids found in the cell wall of Mtb. The stereochemistry of the mycolate motif is 2R, 3R with the meromycolate chain significantly longer than the  $\alpha$ -branch. Meromycolate chains contain two modification sites, distal (D) and proximal (P) with respect the  $\beta$ -hydroxy group, and three (x, y, z) acyl chain spacings.

functionalities (Barry III et al., 1998; Marrakchi et al., 2014). Fine structural differences within mycolic acids reveal species-specific signatures when analyzed by two-dimensional thin layer chromatography (Minnikin et al., 1984). Mtb and *M. smegmatis* (Msmeg) both synthesize three distinct mycolic acids types that differ most significantly in the modifications incorporated into their meromycolate chains (Figure 3). Mtb synthesizes three

mycolic acid types ( $\alpha$ -mycolates, methoxy mycolates, and keto mycolates) that strictly contain cyclopropanate rings. However, Msmeg synthesizes  $\alpha$ -mycolates,  $\alpha'$ -mycolates, and epoxy mycolates that lack cyclopropane rings but instead harbor double bonds. An additional layer of structural diversity in mycobacterial mycolic acid results from

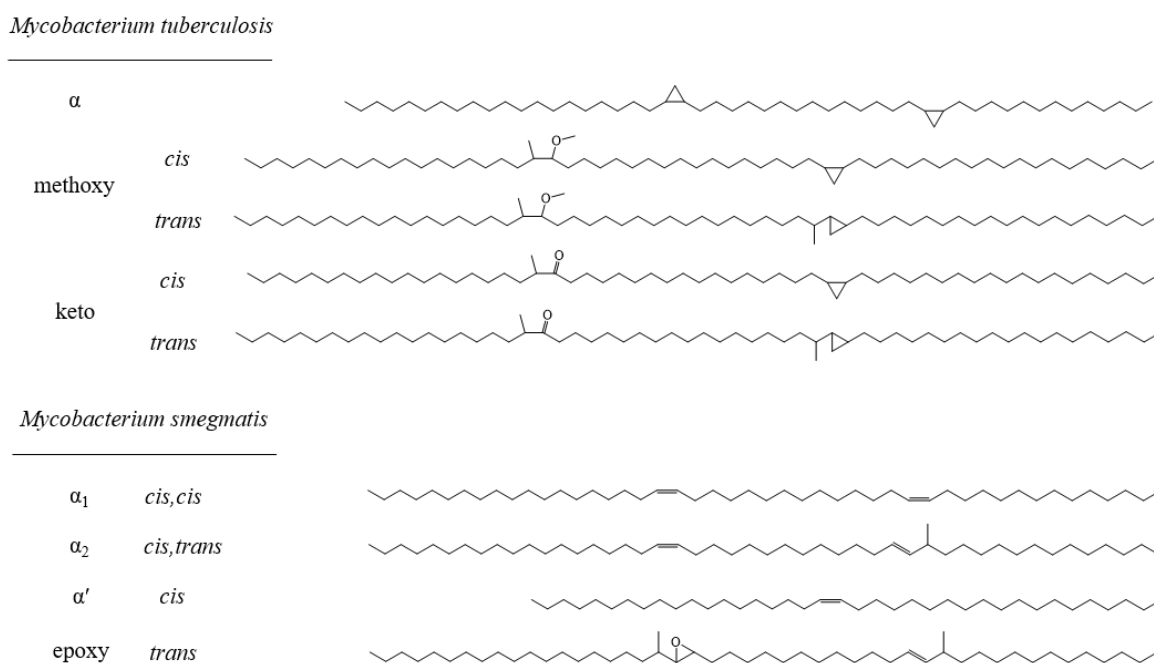


**Figure 3. Mycolic acids of *Mycobacterium tuberculosis* and *Mycobacterium smegmatis*.**

The meromycolate chains of *M. tuberculosis* (Mtb) and *M. smegmatis* (Msmeg) mycolic acids contain two modification sites, distal (D) and proximal (P) with respect the  $\beta$ -hydroxy group. Msmeg  $\alpha'$ -meromycolates contain a single modification. Top, Mtb synthesizes three mycolic acid types,  $\alpha$ -mycolate, methoxy mycolate, and keto mycolate. The distal modification is either a cyclopropane ring or oxygenated functional group, with a cyclopropane ring strictly located to the proximal position. Hydroxymycolate is a precursor of both methoxy and keto mycolate and has only been found in the Mtb cell wall in trace amounts (only the *trans*-species is shown). Bottom, Msmeg synthesizes three mycolic acid types,  $\alpha$ -mycolate ( $\alpha_1$  and  $\alpha_2$ ),  $\alpha'$ -mycolate, and epoxy mycolate. In Msmeg  $\alpha$ -mycolates, a *cis*-double bond strictly locates to the distal position whereas a *cis*- or *trans*-double bond are found at the proximal position.

microheterogeneity or the variation in carbon length of the acyl chain spacings (distal, internal, and proximal) between functional groups along the meromycolate chain. Meromycolate chains of Mtb contain three distinct acyl chains (x, y, z) between the terminal methyl and  $\beta$ -hydroxy groups, separated by two functional groups (Figure 2B). Watanabe et al. showed that the acyl chain lengths of mature Mtb  $\alpha$ -mycolates are x = 19, y = 14, and z = variable (11 -17), methoxymycolates are x = 17, y = 16 - 18, z = variable (17 - 18), and ketomycolates are x = 15 - 19 (major: 17), y = 14 - 20 (major: 16 or 18), z = variable (11 - 19) (Watanabe et al., 2002). As variable acyl chain length spacings affect mycolic acid total carbon length, subsequent analysis using MALDI-TOF MS clearly showed the chain length distribution of individual mycolate types synthesized by Mtb (major species,  $\alpha$ -mycolates: C<sub>76</sub> - C<sub>84</sub>; methoxymycolates: C<sub>79</sub> - C<sub>89</sub>; ketomycolates: C<sub>80</sub> - C<sub>88</sub>) (Teramoto et al., 2015).

### **Mycolic acid biosynthesis**

The Mtb mycolic acid biosynthetic pathway consists of two fatty acid synthases (FAS), FASI and FASII (Figure 4). Mycolic acid biosynthesis is initiated by *de novo* fatty acid synthesis via the eukaryotic-like FASI system. Encoded by Rv2524c, Mtb FASI is a single multifunctional polypeptide containing six enzymatic domains and an acyl carrier protein (ACP) (Zhang and Rock, 2016; Zimhony et al., 2004). FASI iteratively elongates an acetyl coenzyme A (acetyl-CoA) primer using malonyl-CoA as the two-carbon donor. The FASI system is uncommon in bacteria and nearly restricted to order *Actinomycetales* (Boehringer et al., 2013). The mycobacterial FASI synthesizes acyl-CoA products in a bimodal distribution of C<sub>16</sub> - C<sub>18</sub> and C<sub>24</sub> - C<sub>26</sub>, in contrast to the unimodal products of mammalian and yeast FASI of C<sub>16</sub> - C<sub>18</sub> (Lehner and Quiroga, 2016; Smith, 1994; Tehlivets et al., 2007; Zimhony et al., 2004). FASI-derived long chain acyl-CoAs products are used as

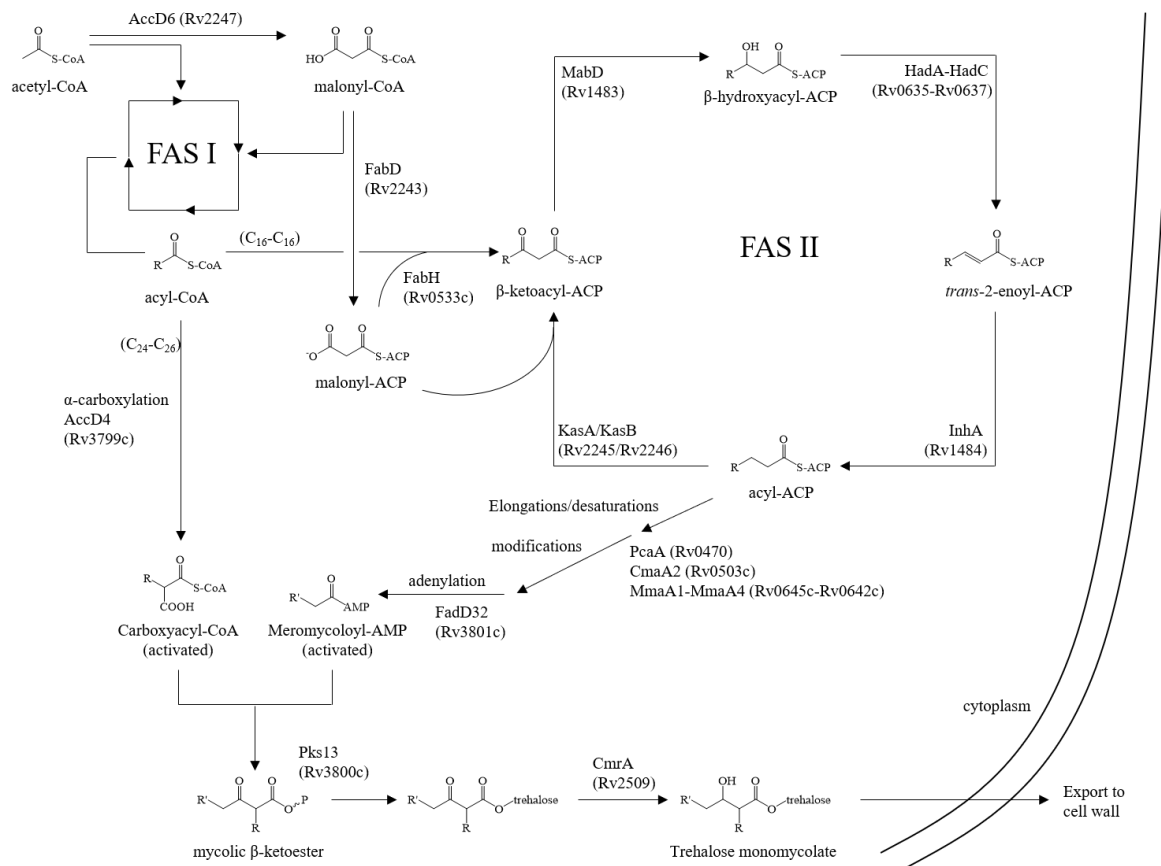


**Figure 4. Mycolic acid biosynthetic pathway.**

Mycolic acid biosynthesis requires two fatty acid synthase systems, FASI and FASII. Biosynthesis of mycolic acids is initiated by *de novo* fatty acid synthesis via FASI, whereby two acyl-CoA products are synthesized: an  $\alpha$ -branch precursor and a FASII primer. The acyl-CoA primer is elongated and modified via the FASII system. The  $\alpha$  branch precursor and FASII meromycolate chain are activated and condensed forming a premature mycolic acid, the mycolic  $\beta$ -ketoester. Following reduction of the mycolic  $\beta$ -ketoester, the mature mycolic acid is exported to the cell wall. PM represents the plasma membrane.

substrates for the synthesis of inner membrane phospholipids, outer membrane mycolic acids, and other complex lipids (Kolattukudy et al., 1997; Zimhony et al., 2004). In bacteria and plants, the canonical pathway for *de novo* lipid biosynthesis requires a bacteria-like FASII system (Schmid, 2016; Zhang and Rock, 2016). Unlike FASI, FASII entails multiple discrete soluble cytoplasmic enzymes and a soluble ACP to support fatty acid elongation.

However, both FAS systems typically require acetyl-CoA and malonyl-CoA substrates. In contrast, Mtb harbors a unique FASII system that is primed with FASI-derived acyl-CoAs. Once primed, acyl-ACP is iteratively elongated forming the meromycolate chain that is then modified with cyclopropane rings, methyl branches, and oxygen moieties prior to its condensation with the  $\alpha$ -branch. This condensation product is further processed to a mature mycolic acid and transported out of the cytosol to be incorporated into the inner or outer leaflets of the mycomembrane.

Mtb FASII relies on a discrete soluble ACP to prime fatty acids for elongation and to ferry the growing meromycolate chain to each active site throughout the dissociated system. To initiate meromycolate synthesis, the small acidic acyl carrier protein AcpM (12.5kDa, Rv2244) is first activated via the covalent attachment of a 4'-phosphopantethine arm by the 4'-phosphopantethinyl transferase PptT (Rv2794), generating holo-AcpM (Burstein and Shakked, 2015; Schaeffer et al., 2001; Wong et al., 2002). In this form, AcpM is subsequently converted to the essential FASII building block malonyl-AcpM by malonyl-CoA:ACP transacylase, FabD (Rv2243) (Kremer et al., 2001). Subsequently, a FASI-derived acyl-CoA is condensed with malonyl-AcpM by  $\beta$ -ketoacyl-ACP synthase, FabH, generating  $\beta$ -ketoacyl-AcpM (Rv0533c) (Brown et al., 2005; Sachdeva et al., 2008). The FASII catalytic assembly line is composed of four enzymatic steps carried out by the following enzymes: MabA (Rv1483), HadAB/HadBC (Rv0635-0637), InhA (Rv1484), and KasA/KasB (Rv2245/Rv2246). Subsequent to the initial C<sub>2</sub> extension,  $\beta$ -ketoacyl-AcpM is reduced to  $\beta$ -hydroxyacyl-AcpM by the  $\beta$ -ketoacyl-ACP reductase, MabA, followed by dehydration to *trans*-2-enoyl-AcpM by the heterodimer  $\beta$ -hydroxyacyl-ACP dehydratase complexes, HadAB or HadBC (Ducasse-Cabanot et al., 2004; Sacco et al., 2007). To

complete an elongation cycle, *trans*-2-enoyl-AcpM is reduced by the *trans*-2-enoyl-ACP reductase, InhA, generating a saturated acyl-AcpM extended by two carbons (Quemard et al., 1995). To initiate further rounds of elongation, the  $\beta$ -ketoacyl-ACP synthases, KasA or KasB, extend the growing chain by two carbons supplied by malonyl-AcpM (Swanson et al., 2009). At predetermined sites, marked by double bonds, the meromycolate chains are further modified by enzymes of the mycolic acid methyltransferase family.

Activated FASI- and FASII-derived acyl products are condensed by the polyketide synthase 13, Pks13 (Rv3800c), and further processed prior to being exported to the cell wall. The FASI-derived acyl-CoA destined as the mycolic acid  $\alpha$ -branch undergoes activation via  $\alpha$ -carboxylation by the acetyl-CoA carboxylase complex AccA3:AccD4:AccD5:AccE5 (Rv3285:Rv3799c:Rv3280:Rv3281), generating  $\alpha$ -carboxylacyl-CoA (Lyonnet et al., 2017). The meromycolate chain synthesized by FASII is activated via adenylation by the fatty acyl-AMP ligase, FadD32 (Rv3801c) (Portevin et al., 2005). The activated fatty acids are condensed by Pks13 to the mycolic  $\beta$ -ketoester precursor and transferred to trehalose (Gavalda et al., 2014; Trivedi et al., 2004). Following reduction by CmrA (Rv2509), the mature  $\beta$ -hydroxy mycolic acid is exported out of the cytoplasm to the outer bounds of the cell wall (Lea-smith et al., 2007).

### **Biosynthesis of unsaturated meromycolates: desaturases**

Modified mycolic acids in the cell wall of Mtb are derived from unsaturated meromycolate precursors, although the mechanistic details of how double bonds are incorporated into saturated meromycolates is currently unknown. The last twenty years of research has revealed the biosynthetic pathways responsible for mycolic acid modification and clearly established the essential role of unsaturated meromycolate chains as substrates

for the modifying enzymes (Dubnau et al., 2000; George et al., 1995; Glickman, 2003; Glickman et al., 2000, 2001; Yuan and Barry III, 1996; Yuan et al., 1995, 1998a). However, progress in identifying the enzymes responsible for introducing the double bonds has been slow.

The fact that Takayama and Qureshi isolated and characterized a series of long-chain monounsaturated fatty acids derivatives of  $C_{24:1}\Delta^5$  up to 32 carbons, suggests that the first double bond of the growing meromycolate is inserted at an early stage (Takayama and Qureshi, 1978). Inhibition studies using isoniazid, an inhibitor of *trans*-2-enoyl-ACP reductase InhA, showed that Mtb accumulated the  $\alpha$ -branch precursor hexacosanoic acid ( $C_{26}$ ) and inhibited the synthesis of  $C_{24:1}$  and longer derivatives (Davidson and Takayama, 1979; Takayama et al., 1975). Taken together, Takayama et. al. proposed that  $C_{20}$ -CoA is the FASII primer whereby the first *cis*-double bond is incorporated during the first round of elongation (Takayama et al., 2005). They proposed that  $C_{20}$ -CoA is first extended by two carbons upon covalent attachment to AcpM and converted to the (*trans*- $\Delta^2$ - $C_{22:1}$ ) *trans*-2-enoyl-AcpM intermediate in two enzymatic steps (by MabA and HadAB, respectively). With InhA inhibited by isoniazid, the intermediate is not reduced but isomerized to (*cis*- $\Delta^3$ - $C_{22:1}$ ) *cis*-3-docosenoyl-AcpM by an uncharacterized *cis-trans* isomerase. Subsequently, the *cis*-3-docosenoyl-AcpM intermediate is elongated by two carbons, presumably by KasA or another uncharacterized  $\beta$ -ketoacyl-AcpM synthase, and converted in two enzymatic steps to the (*cis,trans*- $\Delta^{5,2}$ - $C_{24:1}$ ) *cis,trans*-5,2-enoyl-AcpM intermediate. When InhA is inhibited, this diunsaturated intermediate is not reduced and is expected to accumulate. However, inferring from prior reports for  $\beta$ -hydroxyacyl-ACP dehydratase proteins, the reaction equilibrium favors the  $\beta$ -hydroxylated-AcpM intermediate, *cis*-5- $\beta$ -hydroxyacyl-AcpM

(Rock and Cronan, 1996; Sacco et al., 2007). Accumulation of this intermediate has not been reported but C<sub>24:1</sub> would be expected to deplete, that is observed. As Mtb H<sub>37</sub>Ra, the strain used in the aforementioned studies, predominately synthesizes  $\alpha$ -mycolates with a major terminal acyl carbon length of  $x = 17$ , C<sub>20</sub>-CoA is likely the primer for these mycolic acids (Figure 2B) (Grzegorzewicz et al., 2012; Watanabe et al., 2002). Similarly, methoxy and keto mycolates are less abundant and have shorter ( $x = 15$ ) terminal carbon lengths, suggesting that a shorter primer (C<sub>18</sub>-CoA) would be required for their synthesis. A recent study has shown that Mtb H37Ra treated with thiacetazone, an antitubercular drug that inhibits the upstream catalytic step to InhA performed by the  $\beta$ -hydroxy-ACP dehydratases HadAB/BC, accumulates  $\beta$ -hydroxy-C<sub>18</sub> to C<sub>22</sub> fatty acids (Grzegorzewicz et al., 2012). These data indicate that FASI-derived C<sub>16</sub> to C<sub>20</sub>-CoAs are used as FASII-priming substrates. Moreover, thiacetazone treatment resulted in a substantial accumulation of  $\beta$ -hydroxy-C<sub>18</sub> and C<sub>20</sub> fatty acids with C<sub>22</sub> to a lesser extent. Prior reports showed that thiacetazone severely depletes  $\alpha$ -mycolates whereas oxygenated mycolates were less effected (Belardinelli and Morbidoni, 2012; Coxon et al., 2013). This increased abundance of  $\beta$ -hydroxy-C<sub>20</sub> fatty acids, with respect to  $\beta$ -hydroxy-C<sub>22</sub> fatty acids, may be explained by Mtb diverting mycolic acid biosynthetic pathways towards oxygenated types when  $\alpha$ -mycolate synthesis is inhibited. A similar effect on mycolic acid abundance has been previously described for Mtb lacking a functional cyclopropane mycolic acid synthase, PcaA (Glickman et al., 2000). In absence of drug, these  $\beta$ -hydroxy-AcpM substrates undergo dehydration, followed by *cis*-double bond formation, and then elongated. Interestingly, these growing meromycolate chains would have terminal length spacings of C<sub>17</sub> and C<sub>15</sub>, that perfectly agrees with the distal acyl spacings found in  $\alpha$ - and oxygenated mycolates,



respectively (Watanabe et al., 2002). FASII primed with C<sub>16</sub>-CoA may require additional round(s) of elongation prior to double bond incorporation as a terminal acyl carbon length of  $x = 13$  was not reported, likely due to either extremely low abundance or was never identified. Together, these data strongly suggest that Mtb uses an anaerobic desaturase pathway to incorporate the distal double bond into growing meromycolate chains.

Qureshi et al. found that a cell extract of Mtb incorporates [<sup>14</sup>C]-malonate into long-chain fatty acids, up to C<sub>56</sub>, containing multiple double bonds (Qureshi et al., 1984). In addition, the [methyl-<sup>14</sup>C] SAM label, in the presence of malonate, was only found within short-chain ( $\leq$  approximately C<sub>22</sub>) and C<sub>48</sub> - C<sub>56</sub> fatty acids. This data suggested that the incorporated proximal and distal double bonds are preserved until the introduction of cyclopropane rings, methyl-branches, or oxygen functional groups and that modification reactions occur prior to their condensation with the  $\alpha$ -branch. However, the order of double bond modification is unclear, although multiple pathways have been proposed (Glickman et al., 2000; Yuan and Barry III, 1996; Yuan et al., 1997, 1998b).

In *Escherichia coli*, unsaturated fatty acid synthesis occurs during FASII elongation and requires two anaerobic desaturation pathway enzymes, FabA and FabB (Zhang and Rock, 2016). During the initial first four rounds of oleic acid (C<sub>18:1</sub> $\Delta^9$ ) biosynthesis acyl chain elongation proceeds through the canonical FASII pathway, wherein the  $\beta$ -hydroxyacyl-ACP intermediates are dehydrated to *trans*-2-enoyl-ACP by the  $\beta$ -hydroxyacyl-ACP dehydratase FabZ (Mtb HadAB/BC). To complete an iterative round of elongation, *trans*-2-enoyl-ACP is reduced to a fully saturated acyl chain by the *trans*-2-enoyl-ACP reductase FabI (Mtb InhA). On the fifth round, the dual-functional enzyme with dehydratase and isomerase activities, FabA, diverts saturated fatty acid synthesis to the

unsaturated pathway by converting the 3-hydroxydecanoyl-ACP to *cis*-3-decenoyl-ACP. However, this intermediate is not reduced by FabI but further elongated. *E. coli* encodes two  $\beta$ -keto-ACP synthases, FabZ and FabB, required to catalyze acyl chain elongation. During canonical saturated C<sub>2</sub> elongation, FabZ extends the saturated nascent chain by two carbon units. In contrast, the *cis*-3-decenoyl-ACP synthesized by FabA requires FabB to complete the diversion of unsaturated fatty acid biosynthesis.

Mtb has been reported to lack FabA and FabB enzymes, hinting at the existence of an analog pathway that fulfills the synthesis of unsaturated meromycolate chains to support the incorporation of various functional groups (Marrakchi et al., 2014). Indeed, an alternative mechanism of anaerobic desaturation has been discovered through the functional characterization of FabM in *Streptococcus pneumoniae* (Marrakchi et al., 2002a). Unlike the dual-function FabA, FabM is a monofunctional *cis-trans* isomerase that converts a *trans*-2-enoyl-ACP to *cis*-3-acyl-ACP. The Mtb genome encodes twenty one putative enoyl-CoA hydratases/isomerases (EchA), two of which are highly similar to FabM, echA10 (Rv1142c) and echA11 (Rv1141c) (Cole et al., 1998; Takayama et al., 2005). A recent study by Srivastava et al. identified five EchA proteins (EchA10; EchA11; EchA2, Rv0456c; EchA5, Rv0675; and EchA16, Rv2831) that demonstrated FabM-like activity in vitro, as they catalyzed the isomerization of *cis*-3-octanoyl-CoA to *trans*-2-octenoyl-CoA (Srivastava et al., 2015). These biochemical data suggest that either these enzymes are involved in the  $\beta$ -oxidation pathway for degrading *cis*-unsaturated lipids or they are involved in fatty acid biosynthesis where the reverse reaction was assessed using the CoA substrate. The authors further identified three EchA proteins (EchA1, Rv0222; EchA8, Rv1070c; and EchA9, Rv1071c) as having dual isomerase/hydratase activities, similar to reverse reaction of FabA,

that were shown to convert *cis*-3-octenoyl-CoA to 3-hydroxyoctanoyl-CoA, although the stereochemistry of the products was not characterized. This is important because the 3-hydroxyacyl-CoA intermediates of  $\beta$ -oxidation and fatty acid synthesis have a distinct stereochemistry. Specifically, during  $\beta$ -oxidation the  $\beta$ -hydroxyacyl intermediate resides as a CoA-derivative with 3S stereochemistry; whereas the fatty acid synthesis intermediate ACP-derivative has a 3R stereochemistry (Zhang and Rock, 2016).

The functional characterization of the Mtb H<sub>37</sub>Rv EchA and  $\beta$ -oxidation enzymes FadAB proteins *in vivo* entailed heterologous complementation experiments, using the inability of an *E. coli*  $\Delta$ *fadAB* mutant to use fatty acids as the sole carbon source (Srivastava et al., 2015). Expression of Mtb FadAB complemented the growth defect of *E. coli* in the presence of lauric acid (C<sub>12</sub>) but not oleic acid (C<sub>18:1</sub> $\Delta^9$ ). This indicates that unlike *E. coli* FadAB, Mtb FadAB lacks the essential *cis-trans* isomerase activity required to degrade *cis*-unsaturated fatty acids. Regarding the five identified FabM-like EchA *cis-trans* isomerases, only EchA5 and EchA10 when coexpressed with Mtb FadAB sustained cell growth on oleic acid, suggesting their involvement in the  $\beta$ -oxidation pathway. Therefore, EchA2, EchA11, and EchA16 may be involved in diverting FASII elongation to the unsaturated mode (Figure 5A) Regarding the three identified dual hydratase/isomerase EchA proteins, only FadAB EchA1 coexpression sustained cell growth on oleic acid, suggesting that EchA1 converts the *cis*-3-octenoyl-CoA intermediate to (S)-3-hydroxyoctanoyl-CoA that is then degraded by FadAB. Since both EchA8 and EchA9 showed *E. coli* FabB-like activity *in vitro* (reverse reaction), the lack of complementation of the cell growth defect in the Mtb FadAB/EchA8 and FadAB/EchA9 coexpression strains may result from the production of (R)-3-

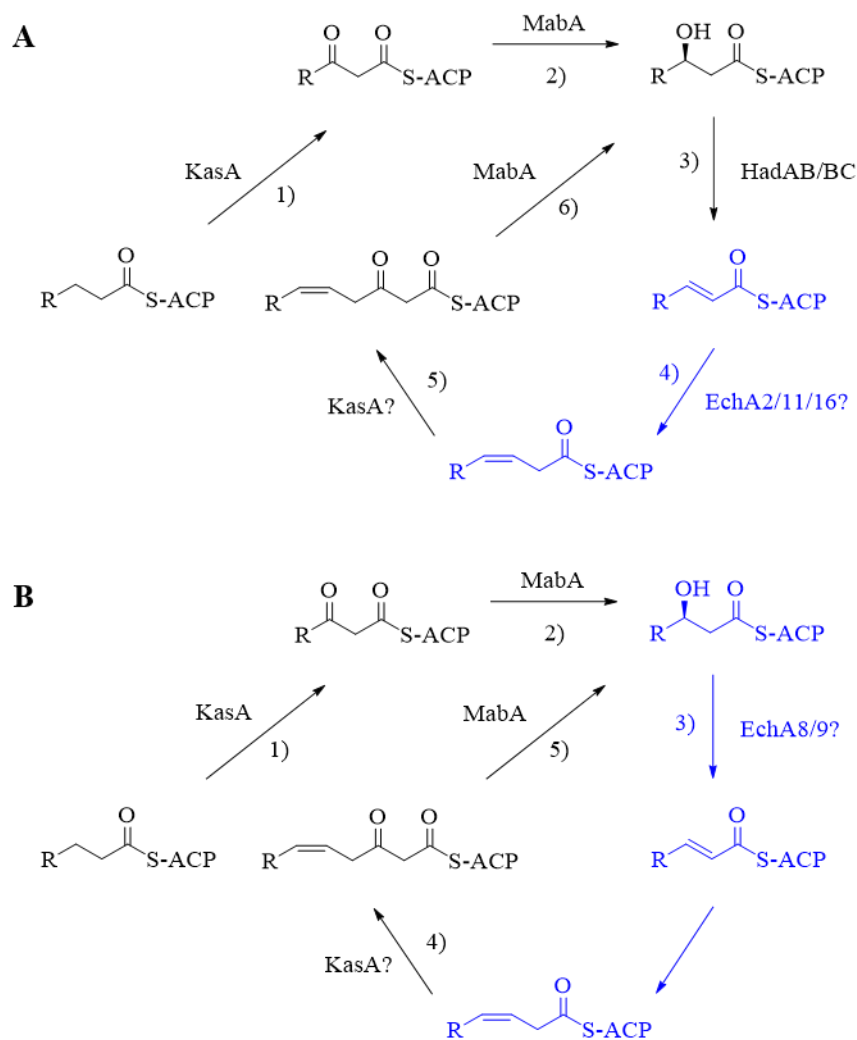


**Figure 5. Putative roles of EchA proteins in meromycolate anaerobic desaturation.**

A) Putative model for the diversion of saturated meromycolate chain elongation to unsaturation mode by EchA proteins with *cis-trans* isomerase FabM-like activity. B) Putative model for the diversion of saturated meromycolate chain elongation to unsaturated mode by EchA proteins with dual-function dehydratase/isomerase FabA-like activity. In these models, saturated meromycolate chain elongation proceeds until EchA proteins insert *cis*-double bonds into the growing chain. Chain elongation of *cis*-3-acyl-AcpM intermediates by KasA or other uncharacterized  $\beta$ -ketoacyl-AcpM synthase would complete the diversion to the unsaturated mode, wherein subsequent rounds of chain elongation will proceed via the canonical fatty acid synthase II reaction series.

hydroxyoctanoyl-CoA that is not a FadB substrate. Therefore, EchA8 and EchA9 may be involved in the anaerobic desaturase pathway (Figure 5B). If EchA8/9 generate (R)-3-

hydroxyoctanoyl-CoA in vitro, these enzymes may be responsible for diverting canonical FASII elongation to the unsaturated pathway by competing with HadAB/BC complexes for the  $\beta$ -hydroxylated substrate of appropriate chain length. In this study, only short chain unsaturated acyl-CoAs were used. To provide further indication for a functional role of EchA proteins in an anaerobic biosynthetic pathway, much longer ( $C_{22}$  -  $C_{24}\Delta^3$ ) *cis*-unsaturated-CoA substrates require investigation (Quemard et al., 1995). These acyl chain length substrates would represent the FASII intermediates found during the biosynthesis of Mtb H<sub>37</sub>Rv  $\alpha$ - and oxygenated mycolates, as the distal chain length spacings are  $x = 19$  and  $x = 17$ , respectively (two carbons longer than those previously described for Mtb H<sub>37</sub>Ra)(Watanabe et al., 2002). Notably, while the biologically relevant substrates for the anaerobic desaturase pathway are ACP derivatives, mycobacterial FASII enzymes have been shown to use CoA substrates (Marrakchi et al., 2002b; Quemard et al., 1995; Sacco et al., 2007). An alternative approach to assess putative EchA protein activity is to use the most biologically relevant ( $C_{22}$  -  $C_{24}$ ) acyl-AcpM substrates in FASII reconstitution assays, in a similar fashion as previously reported for the characterization of *S. pneumoniae* FabM (Marrakchi et al., 2002a). This approach requires successful loading of  $C_{20}$ - to  $C_{22}$ -CoA substrates onto AcpM by Mtb FabH, that has been reported (Brown et al., 2005). The inability to demonstrate enzymatic activity, using these approaches above, would strongly suggest that EchA proteins are not involved in anaerobic desaturation of the distal double bond in growing meromycolates. As mycolic acids are essential for Mtb viability and have not been found unmodified (lacking double bonds), the proteins involved in the incorporation of *cis* double bonds should be essential. However, all *echA* genes are predicted to be non-essential by transposon mutagenesis, hinting to functional redundancy in the Mtb

genome or a nonfunctional role in double bond incorporation (DeJesus et al., 2017; Griffin et al., 2011).

The formation of *cis*-double bonds via the anaerobic desaturation pathway requires a  $\beta$ -ketoacyl-ACP synthase with FabB-like activity to elongate *cis*-3-acyl-AcpM intermediates and prompt the unsaturation mode. Of the two established Mtb  $\beta$ -ketoacyl-ACP synthases KasA and KasB, KasA is an essential component of the FASII system and the only probable one to have FabB-like activity. In contrast to Marrakchi et al. whom reported that mycobacteria lack FabA and FabB enzymes, the crystal structures of *E. coli* FabB in complex with a decanoic acid and Mtb KasA have been solved and show a near identical tertiary structure (Luckner et al., 2009; Marrakchi et al., 2014; Olsen et al., 2001). In fact, structural superimposition revealed that the amino acid residues within 5 Å of the bound lipid are nearly identical in both structures. This structural data suggests that KasA may have FabB-like activity to catalyze chain elongation of *cis*-3-acyl-AcpM intermediates. However, experimental confirmation of the FabB-like activity of KasA awaits the identification of the biologically relevant substrates, specifically C<sub>22</sub> - C<sub>24</sub> *cis*-3-acyl-AcpM, possibly synthesized by EchA proteins. The inability for Mtb to elongate growing meromycolate chains harboring *cis*-double bonds incorporated by anaerobic desaturases would be expected to have lethal consequences. As such, if *cis*-double bonds are incorporated by the anaerobic desaturation pathway, lack of FabB-like activity by KasA would imply the existence of another yet undefined  $\beta$ -ketoacyl-ACP synthase in the Mtb genome. Alternatively, *cis*-double bonds may be incorporated via the aerobic desaturase pathway.

In contrast to the anaerobic desaturase pathway, Asselineau et. al. proposed that the C<sub>24:1</sub> fatty acid likely resulted from oxygen-dependent aerobic desaturation of a C<sub>24</sub> meromycolate precursor via a  $\Delta^5$  desaturase (Asselineau et al., 1970). This model was derived from the observation that various mycobacteria strains abundantly synthesize oleic ( $\Delta^9$ -C<sub>18:1</sub>) and palmitoleic ( $\Delta^9$ -C<sub>16:1</sub>) acids via aerobic desaturation, and the most frequently encountered long-chain fatty acids were C<sub>24</sub> and C<sub>26</sub> with their unsaturated derivatives harboring a double bond located in the  $\Delta^5$  position.

Plants synthesize fatty acids *de novo* via the dissociated FASII system; however, *cis* double bonds are not introduced during iterative elongation cycles but are reserved until saturated fatty acid synthesis is complete (Schmid, 2016). Oleic acid (C<sub>18:1</sub> $\Delta^9$ ), a commonly found fatty acid in the lipid bilayers, is synthesized by  $\Delta^9$ -desaturase that requires NAD(P)H and molecular oxygen to introduce a *cis*-double bond between C9 and C10 of octadecanoic acid (C<sub>18</sub>). Likewise, an acyl lipid desaturase,  $\Delta^5$  desaturase, encoded by the *des* gene in *Bacillus subtilis* is required for the synthesis of *cis*-5-hexaenoic acid from palmitic acid (Aguilar and Cronan, 1998; Altabe et al., 2003).

Analysis of the complete Mtb genome sequence by Cole and collaborators led to the identification of three putative aerobic desaturase genes (*desA1*, Rv0824c; *desA2*, Rv1094; *desA3*, Rv3229c) resembling plant diiron-dependent desaturases that incorporate double bonds into acyl-ACP substrates (Cole et al., 1998). In contrast to the predicted nonessentiality of the EchA proteins, putatively involved in the proposed anaerobic desaturation pathway, all three *desA* genes are predicted to be essential (Griffin et al., 2011). In a recent study, phage-mediated mutagenesis of Msmeg failed to recover mutants in the *desA1* gene (MSMEG\_5773), suggesting its essentiality (Singh et al., 2016). Interestingly,

it was possible to obtain a *Msmeg*  $\Delta$ *desA1* mutant, but only in the presence of acetamide with a second copy of *desA1* under an acetamide-inducible promoter. Moreover, bacterial stasis was observed after eight hours of acetamide withdrawal, accompanied by complete inhibition of mycolic acid biosynthesis and accumulation of mono-unsaturated mycolates, as evidenced by mass spectrometry. *Msmeg*  $\alpha$ -mycolates contain two sites of unsaturation; however, whether the proximal or distal double bond was lost upon acetamide withdrawal was not determined. Since *Msmeg* DesA1 depletion does not alter medium-chain fatty acid abundance or composition, it was proposed that DesA1 plays a fundamental role in mycolic acid biosynthesis. *Msmeg* *desA1* is an *Mtb* *desA1* ortholog, sharing 80% identity and 90% similarity. In addition, genetic complementation with the heterologous *Mtb* *desA1* rescues the growth inhibition phenotype of the merodiploid strain in the absence of acetamide, unfortunately the recovery of mycolic acid biosynthesis was not investigated.

Conversely, the function of *Mtb* DesA2 is unclear, although the crystal structure of the protein showed a highly similar quaternary dimer structure to that of the stearyl-ACP  $\Delta^9$  desaturase from castor seed (Dyer et al., 2009). *Mtb* DesA2 harbors two metal binding motifs found in class II diiron-oxo enzymes, with an unusually positioned lysine residue within the first site where a conserved glutamate typically resides (Fox et al., 1994; Lindqvist et al., 1996). As no iron atoms were found bound to the protein, suggesting that the lysine residue disrupts iron chelation. These data suggest that DesA2 has likely evolved away from a diiron-dependent desaturase to some other biological function that is currently unknown.

Unlike the uncharacterized roles of *Mtb* DesA1 and DesA2, DesA3 has been established as an essential enzyme involved in oleic acid biosynthesis. The biological role of DesA3 was first established in a mode of action study of isoxyl, a thiourea antitubercular



drug (Phetsuksiri et al., 2003). Isoxyl was found to simultaneously inhibit mycolic acid and oleic acid biosynthetic pathways. The DesA3-dependent conversion of stearyl-CoA to the oleic acid derivative was later shown to require Rv3230c to complete the desaturase system. Rv3230c contains flavin binding, NAD binding, and [2Fe-2S] ferredoxin domains that are three essential components for the abstraction and subsequent transfer of electrons to the iron reaction center, wherein stearyl-CoA is oxidized to oleoyl-CoA (Chang and Fox, 2006; Fox et al., 2004).

Mtb  $\alpha$ - and oxygenated mycolic acids show variable, yet distinct, acyl chain spacings between the distal and proximal modifications, whereby site-specific double bonds introduced into the growing meromycolate chain may serve to direct the biosynthetic pathway. As previously mentioned, Watanabe and collaborators characterized all Mtb H<sub>37</sub>Rv mycolate types. The authors found that the distal acyl chain spacings (not including the terminal methyl group) had a conserved length of 17 - 19 carbons, whereas the length of the internal and proximal spacings show considerable variation (Watanabe et al., 2002). Specifically, the  $\alpha$ -mycolate distal spacing is C<sub>19</sub> whereas oxygenated mycolates are C<sub>17</sub>. Although the length of the internal and proximal spacings appears to be strain specific, the internal spacings are shorter in  $\alpha$ -mycolates (10 - 14 carbons) than those found in the oxygenated types (14 - 18 carbons). Mtb H<sub>37</sub>Rv harbors  $\alpha$ -mycolates with a conserved internal spacing length of 14 carbons, whereas the oxygenated types are slightly longer with 16 - 18 carbons. The carbon length of the internal spacings in H<sub>37</sub>Rv and H<sub>37</sub>Ra strains are distinct, with H<sub>37</sub>Ra containing the shortest carbon lengths within the aforementioned ranges. In all mycolate types the proximal spacing is highly variable yet longer in oxygenated forms than those of  $\alpha$ -mycolates, that likely results from differential termination of

meromycolate biosynthesis. Differential acyl chain spacings, determined by site-specific double bonds incorporated into premature  $\alpha$ - and oxygenated meromycolate chains, may function as a type of molecular ruler for the introduction of the various functional groups. Together, these distinct acyl chain spacings may provide a molecular mark to shunt the meromycolate to  $\alpha$ - or oxygenated meromycolate synthesis. Corroborating this hypothesis was the finding that the Mtb  $\Delta mmaA4$  mutant solely synthesizes  $\alpha$ -mycolates that contain mature  $\alpha$ -mycolates ( $\alpha_1$ ) and a set  $\alpha$ -mycolate derivatives,  $\alpha_2$  and  $\alpha_3$  (Dinadayala et al., 2003; Laval et al., 2001).  $\alpha_2$ -mycolates contained a distal double bond and a proximal *cis*-cyclopropane ring, whereas  $\alpha_3$ -mycolates was diunsaturated. The distal acyl chain spacings were identical to those found in mature oxygenated mycolates, although the total carbon length was slightly shorter. Surprisingly, the derivatives were found to lack *trans*-double bonds. In a recent study by Sambandan et al., 2D-TLC analysis of purified total mycolic acids from  $\Delta mmaA4$  mutant showed four  $\alpha$ -mycolates,  $\alpha_1$  -  $\alpha_4$  (Sambandan et al., 2013). Although the mycolic acids were not characterized in the study, the  $\alpha_3$  and  $\alpha_4$  are likely *trans*- and *cis*-diunsaturated  $\alpha$ -mycolates, respectively. These putative assignments were based on their relative migration behavior in the second dimension (silver) and overall abundance. Mycolic acids harboring *trans*-double bonds migrate faster in the silver dimension than their *cis*-derivatives and are lower in abundance when incorporated into oxygenated mycolates (*trans*- $\alpha_3$ -mycolate were less abundant than *cis*- $\alpha_4$ -mycolate). Moreover, 2D-TLC analysis of purified mycolic acids from transposon mutants in a  $\Delta mmaA4$  background may aid in the identification of desaturases involved in oxygenated mycolic acid biosynthesis, as these mutants should be devoid of  $\alpha_2$  -  $\alpha_4$  mycolates. However, genetic inactivation of the genes responsible for incorporating double bonds into precursor oxygenated mycolates may be

inviability due to the rationale described above. With regards to putative EchA desaturases described above, *MmaA4/EchA* double mutants warrant investigation. Alternatively, putative desaturases involved in mycolic acid synthesis may be identified as up- and down-regulated genes in the *Mtb ΔpcaA* mutant, as oxygenated mycolates predominate severely depleted  $\alpha$ -mycolates (Glickman et al., 2000). In the case that mutants can be isolated, the mycolic acid composition and fine chemical structure should be fully characterized for all mycolate types in null mutants of putative *Mtb* desaturases.

### **Mycolic acids are modified by S-adenosyl methionine-dependent mycolic acid methyltransferases**

Double bonds incorporated into the meromycolate chain are functionalized by a set of mycolic acid methyltransferase (MA-MTs), generating the three characteristic mycolic acid types found in the cell wall of *Mtb*. Whereas eight MA-MTs are encoded in four loci, six have been functionally characterized (*PcaA*, *CmaA2*, *MmaA1-4*). A role in mycolic acid modification has not been found for *CmaA1* or *UmaA1*. MA-MTs share extensive primary and tertiary structure similarity but distinctly modify the fine chemical structure of meromycolate chains (Figure 6A to C). MA-MT functions were initially discovered by overexpressing the genes in *Msmeg*, a species where the mycolic acids primarily contain double bonds (Figure 3). Then, their biologically relevant functions were tested once the genetic tools for generating *Mtb* null mutants had been established.

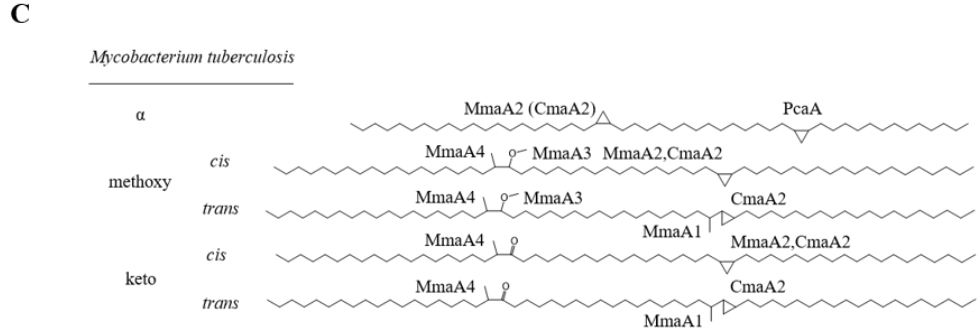
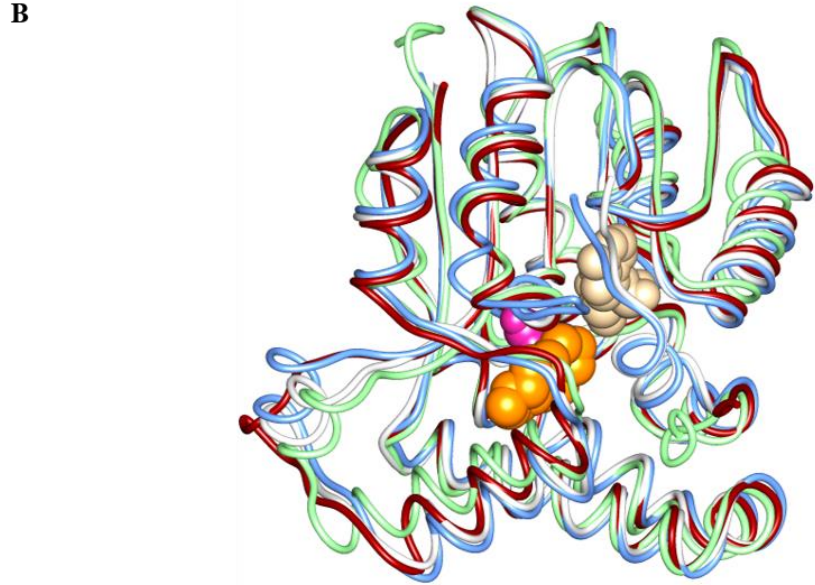
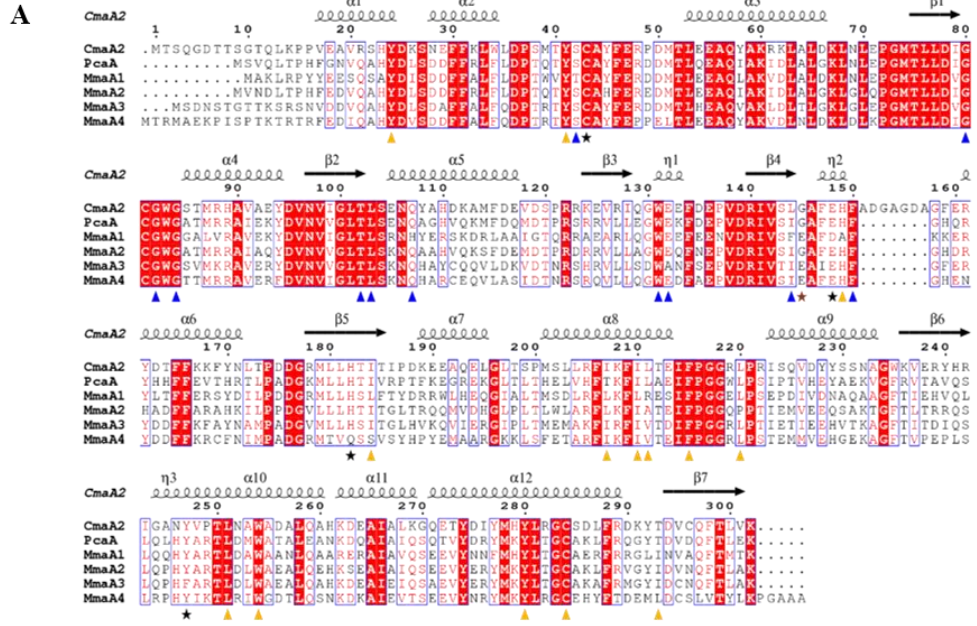
The first evidence that confirmed cyclopropanated mycolic acids were derived from unsaturated precursors came from the identification of an H<sub>37</sub>Ra-derived cosmid clone that conferred *Msmeg* with the ability to accumulate hybrid cyclopropanated  $\alpha$ -mycolic acids in the cell wall. Of the three open reading frames, expression of the single gene *cmaA1* was

sufficient for incorporating a *cis*-cyclopropane ring at the distal position of  $\alpha_2$ -mycolates (Yuan et al., 1995). CmaA1 shares 35 % amino acid sequence identity with *E. coli* cyclopropane fatty acid synthase (CFAS) that cyclopropanates unsaturated phospholipids via a methyl transfer from SAM (Wang et al., 1992). In addition, CmaA1 harbors a sequence element, LLDXGXGXG, that is a conserved SAM binding motif (Ingrosso et al., 1989). Despite the ability of CmaA1 to cyclopropanate  $\alpha_2$ -mycolates in *Msmeg*, no change in mycolic acid composition was observed in the *Mtb*  $\Delta$ *cmaA1* mutant (Glickman, 2003). This data suggests that CmaA1 is not involved in mycolic acid modification but may methylate other cellular lipids or that its function is redundant.

A *cmaA1* sequence similarity search revealed *cmaA2* as an unannotated gene sequence in the *Mycobacterium leprae* genome (George et al., 1995). The *Mtb* homolog was identified by polymerase chain reaction (PCR) screening of an H<sub>37</sub>Ra cosmid library in *E. coli*. *Mtb* CmaA2 shares 73 % amino acid sequence identity with *M. leprae* CmaA2, and 52 % with *Mtb* CmaA1. *Mtb* and *M. leprae* CmaA2 contain the SAM binding motif, LLDXGXGXG, and a unique stretch of amino acids, 151 - 157 (*Mtb* CmaA2 numbering), that is not present in CmaA1. Overexpressing CmaA2 in *Msmeg* revealed that the enzyme functions as a proximal *cis*-cyclopropane synthase of  $\alpha_1$ - and epoxy mycolates. This established CmaA2 as the first identified cyclopropane mycolic acid synthase (CMAS) of both  $\alpha$ - and oxygenated mycolates. Interestingly, *Msmeg* coexpressing CmaA1 and CmaA2 resulted in the accumulation of mycolic acids similar to mature dicyclopropanated  $\alpha$ -mycolates found in the cell wall of *Mtb*. Since *Mtb* synthesizes oxygenated mycolates modified with *trans*-cyclopropane rings at the proximal position, the CMAS responsible for this chemical transformation remained unknown. Interestingly, characterization of the *Mtb*

**Figure 6. Mycolic acid methyltransferases modify *Mycobacterium tuberculosis* mycolic acids.**

A) Primary structure alignment of the six established *Mycobacterium tuberculosis* mycolic acid methyltransferases (MA-MTs). Regions of high amino acid similarity are boxed in blue with conserved residues highlighted in red. CmaA2 amino acids within 5 Å of dialkylamine inhibitor dioctylamine, designate the acyl binding site with orange triangles. Amino acid residues interacting with S-adenosyl homocysteine are represented with blue triangles. Black stars designate amino acid residues that ligand the bicarbonate ion within cyclopropane mycolic acid synthase enzymes (CMAS: CmaA2, MmaA2, and PcaA). E145, brown star, of MmaA4 (similarly observed in the sequence of MmaA1 and MmaA3) replaces the bicarbonate ion that resides within cyclopropane mycolic acid synthase enzymes. Primary structure alignment and secondary structure representation was constructed using ESPript 3.0. B) Superimposition of the Ca trace of MA-MT crystal structures: CmaA2 (blue, PDB code 3HEM), MmaA2 (grey, PDB code 1TPY), PcaA (maroon, PDB code 1L1E), and MmaA4 (green, PDB code 3HA3). Dioctylamine (orange spheres), S-adenosyl homocysteine (brown spheres), and bicarbonate (pink spheres) in complex with CmaA2 designates the overall active site of MA-MT. C) *Mycobacterium tuberculosis* synthesizes three mycolic acid types characterized by modifications incorporated into the meromycolate chain by a family of MA-MTs. A functional role of CmaA2, represented in parenthesis, in distal cyclopropanation of  $\alpha$ -mycolates was only observed in the  $\Delta mmaA2\Delta cmaA2$  double mutant. Figure 6C was adapted from Marrakchi et al. 2014.



*ΔcmaA2* null mutant revealed that CmaA2 modifies oxygenated mycolic acids with a proximal *trans*-cyclopropane ring (Glickman et al., 2001).

The keen observation of a cross-reactive band in a Southern blot when analyzing the genetic conservation of *cmaA1* among various pathogenic mycobacteria, revealed a DNA fragment that was used to identify an operon of four additional MA-MTs genes, *mmaA1-4* (Yuan and Barry III, 1996). The single cosmid clone that cross-reacted with the *cmaA1* hybridization probe conferred Msmeg the ability to produce a hybrid mycolic acid that comigrated with authentic Mtb methoxymycolates. Notably, expression of a cosmid fragment containing the *mma* (methoxy mycolic acid) locus in Msmeg was sufficient to sustain accumulation of methoxy mycolates and hydroxy mycolates as the principal mycolate types. Moreover, the fragment harbored four closely related genes to Mtb *cmaA1* and *E. coli cfas* that encode for proteins with the SAM binding motif, LLDXGXGXG. The proteins were named MmaA1-4 for their involvement in methoxy mycolic acid biosynthesis. Their individual roles in mycolic acid modification were further established by analyzing the mycolic acid species that accumulate upon overexpressing the proteins individually or in combination with others. No change was observed when expressing MmaA1 and MmaA3 alone, whereas distinct mycolate profiles were produced upon expression of MmaA2 and MmaA4. MmaA2 exhibited a CmaA2-like function, as only the proximal position of  $\alpha_1$ - and epoxy mycolates were modified with *cis*-cyclopropane rings. Overexpression of MmaA4 completely abolished  $\alpha_1$ - and  $\alpha_2$ -mycolate biosynthesis, as all mycolates were converted to distal methyl-branched hydroxylated derivatives. Coexpression of MmaA4 with either MmaA2 or MmaA3 (MmaA4 + MmaA2, and MmaA4 + MmaA3) resulted in cell walls rich in *cis*-cyclopropanated hydroxy mycolates and *cis*- and *trans*-methoxy mycolates,

respectively. Interestingly, coexpression of MmaA2 and MmaA4 produced a strain devoid of *trans*-cyclopropanated hydroxy mycolate and solely accumulated the *cis*-derivative, that appeared to result from enhanced MmaA2 activity. These data suggested that distal hydroxylation precedes *cis-trans* isomerization, although not a strict requirement as MmaA2 *cis*-cyclopropanates mycolic acids in the absence of MmaA4.

The functional roles of MmaA1 - 4 have been corroborated by characterizing the mycolic acid phenotypes of null mutants and overexpression strains of Mtb and *M. bovis*. Overexpression of MmaA1 in Mtb demonstrated a profound increase in the overall *trans*-content of oxygenated mycolates, a phenotype not observed when overexpressed in Msmeg (Yuan et al., 1997). The total *trans*-content of oxygenated mycolates in Mtb H<sub>37</sub>Rv cultured in vitro is approximately 20 % and nearly restricted to ketomycolates (methoxymycolate: < 5 %; ketomycolate: 20 %). Overexpression of MmaA1 resulted in increased methoxy and keto mycolate *trans* content to 60 % and 100 %, respectively. This increase in *trans* configuration resulted in methoxymycolate depletion with an accumulation of ketomycolates to an unusually high level that exceeded methoxymycolates ( $\alpha$ , m, k; H<sub>37</sub>Rv: 51 %, 36 %, 13 %; H<sub>37</sub>Rv::*mmaA1*: 59 %, 12 %, 29 %). These data suggest that the ketomycolate biosynthetic pathway may favor proximal *trans*-configured substrates or that ketomycolate overexpression is a compensatory response to increasing cell wall rigidity by the accumulation of *trans*-mycolate species. In contrast, while the Mtb  $\Delta$ *mmaA1* mutant completely lacked *trans*-cyclopropane rings and *trans*-double bonds, the overall mycolate composition was similar to WT (Barkan et al., 2010). Together, these data showed that MmaA1 plays a fundamental role in modifying oxygenated mycolic acids with *trans*-cyclopropane rings by functioning as a *cis-trans* isomerase. Characterization of the Mtb



*ΔmmaA2* mutant identified MmaA2 as a major player in the incorporation of *cis*-cyclopropane rings into  $\alpha$ - and methoxymycolates, and as the principal distal cyclopropane mycolic acid synthase of  $\alpha$ -mycolates (Glickman, 2003). Moreover, the Mtb *ΔcmaA2ΔmmaA2* double mutant lacks mature  $\alpha$ -mycolates and accumulates distal monounsaturated  $\alpha$ -mycolates, in addition to a near complete loss of *cis*-cyclopropanated oxygenated mycolates. These data showed that CmaA2 and MmaA2 are functionally redundant (Barkan et al., 2010). On the other hand, Mtb *ΔmmaA3* mutants have been isolated but their mycolic acid composition have not been reported (Alahari et al., 2009; Dao et al., 2008). However, overexpression of MmaA3 in Mtb and various *M. bovis* strains resulted in a cell wall completely devoid of ketomycolates and contain methoxymycolates as the major mycolate type (Yuan et al., 1998a). These data support the hypothesis that hydroxymycolates synthesized by MmaA4 are precursors for both methoxy- and ketomycolates. In contrast to MmaA3 overexpression, the vaccine strain *Mycobacterium bovis* BCG Pasteur (BCG-P) synthesizes similar mycolates to Mtb but lacks methoxymycolates resulting from mutations in *mmaA3* (Behr et al., 2000; Yuan et al., 1998a). Moreover, the Mtb *ΔmmaA4* mutant solely synthesizes  $\alpha$ -mycolates, as the strain is unable to produce the hydroxymycolate precursor for methoxy- and ketomycolate biosynthesis (Dubnau et al., 2000).

The functional role of UmaA2 (renamed as PcaA) in mycolic acid modification was identified through characterizing a Mtb cording-deficient mutant. Mycobacteria grown in detergent-free media aggregate into ordered microscopic bundles with a rope-like structure, also known as cording. Cording has history been correlated with Mtb virulence, however, many non-pathogenic mycobacteria also form cords (Julián et al., 2010; Middlebrook et al.,

1947). The function of *umaA2* was established subsequent to isolating a BCG-P transposon mutant defective in microscopic cording. Inactivation of the *umaA2* gene in *M. bovis* and Mtb resulted in mutants with granular colony morphologies and disordered aggregation (Glickman et al., 2000). UmaA2 shares 68 % identity and 77 % similarity with Mtb CmaA1 and 33 % identity and 46 % similarity with CFAS. Mycolic acid analysis of the Mtb  $\Delta$ *umaA2* mutant via 2D-TLC revealed an  $\alpha$ -mycolate derivative that migrated slower in the silver dimension than the mature mycolate, indicating the loss of a cyclopropane ring. Structural analysis of the mycolate derivative confirmed the lack of cyclopropanation and located the unmodified double bond to the proximal position. UmaA2 was named PcaA (proximal cyclopropane of  $\alpha$ -mycolates) for the role in incorporating a cyclopropane ring at the proximal position of  $\alpha$ -mycolates.

The functional role of UmaA1 has remained elusive and is not involved in modifying Mtb mycolic acids. Mtb CDC1551 is a natural  $\Delta$ *umaA1* mutant resulting from a frameshift mutation within the *umaA1* gene. The mycolic acid composition of CDC1551 does not significantly differ from that of wild type Mtb H<sub>37</sub>Rv (Laval et al., 2008). Moreover, extensive analysis of the mycolate composition of the Mtb H<sub>37</sub>Rv  $\Delta$ *umaA1* mutant confirmed that UmaA1 is not involved in mycolic acid modification (Laval et al., 2008).

The currently accepted reaction mechanism for MA-MT-mediated methylation of an isolated and unactivated double bond incorporated into the meromycolate chain involves the formation of a carbocation transition state intermediate. The carbocation-based mechanism for double bond methylation was first proposed by Lederer and subsequently used by Yuan et al. to propose the reaction mechanism for incorporating cyclopropane rings and oxygenated functional groups into the meromycolate chain (Lederer, 1969; Yuan and Barry

III, 1996). Despite decades of research and a variety of intriguing approaches, the cyclopropanation reaction mechanism of fatty/mycolic acids remains unclear. What is known about the cyclopropanation reaction has been derived from pulse-chase (feed and bacterial extract) experiments, crystal structures of Mtb CMAS, and in vitro kinetic studies of CFAS. Initial feed and bacterial extract studies showed that the cyclopropane methylene bridge is derived from SAM, with two of the three methyl protons retained in the product, and preservation of the *cis*-configuration and vinyl/allylic protons from the unsaturated fatty acid substrate (Buist and Maclean, 1981; Cronan, J. E et al., 1974; Pohl et al., 1963; Polacheck et al., 1966; Zalkin et al., 1963). The latter observations rule out the possible alternate cyclopropene, exomethylene, and methylalkene reaction intermediates.

Crystal structure analysis of multiple CMAS (CmaA1, CmaA2, and PcaA) evidenced a common trigonal electron density at the catalytic core that was attributed to a bicarbonate ion that copurified with the enzymes and was proposed as the active site base responsible for abstracting a proton from the carbocation intermediate (Huang et al., 2002). Five amino acids were identified to ligand the bicarbonate ion (CmaA2 numbering: C43, E148, H182, I184, and Y247) and are conserved among CMAS and CFAS enzymes. As CMAS share significant amino acid sequence identity with CFAS, the enzymes likely undergo a similar reaction mechanism. Indeed, CFAS has been used as the working model for all in vitro mechanistic studies, primarily because CMAS substrates are unknown and the enzymes demonstrate poor in vitro activity with nonauthentic substrates. Through assessing pH effects on CFAS activity, Courtois et al. found maximum catalytic activity at pH 7.5, with two ionizable groups ( $pK_{a1}$  of 6.8 and  $pK_{a2}$  of 8.7) involved in catalysis (Courtois et al., 2004). Structural studies of CMAS enzymes revealed the presence of two ionizable amino

acids in the active site (CmaA2 numbering: H149 and E148) in addition to the bicarbonate ion. Together with the structural studies of CMAS in complex with a quaternary ammonium lipophilic ligand DDDMAB (didecyldimethylammonium bromide) and the  $pK_a$  of carbonate ( $pK_a = 6.4$ ), the active site base that performs proton abstraction during catalytic cyclopropanation has been attributed to the bicarbonate ion. Kinetic studies using various CFAS mutants and a bicarbonate scrubbing system have clearly established an essential role for the bicarbonate ion and E148 (CmaA2 numbering) in catalysis; however, the role of the bicarbonate ion as a catalytic base or stabilizer of the carbocation intermediate has not been elucidated (Courtois and Ploux, 2005; Iwig et al., 2005). An alternative reaction mechanism that has been proposed for the cyclopropane synthase reaction involves ylide formation. This mechanism involves a metal ion whereby hydrogens atoms of the carbenoid species readily exchange with solvent protons in the absence of substrate. CFAS is devoid of metal ions and methyl protons of SAM are not readily exchanged with solvent protons. These data disagree with a ylide-based mechanism and provides strong scientific evidence to support a carbocation-based reaction mechanism (Courtois and Ploux, 2005; Courtois et al., 2004; Iwig et al., 2004).

The current proposed mechanism for the methylation and hydroxylation of an isolated and unactivated double bond by MmaA4 involves nucleophilic attack of a water molecule to the carbocation center formed subsequent to methyl transfer (Dubnau et al., 1997; Yuan and Barry III, 1996). Primary structure alignment of multiple MA-MTs showed that the CMAS-conserved G145 (CmaA2 numbering) is a glutamate residue in MmaA3 and MmaA4 (Figure 6A) (Huang et al., 2002). Crystal structure analysis of multiple CMAS showed that the conserved glycine residue locates adjacent to the bicarbonate ion binding

site (Huang et al., 2002). However, a bicarbonate ion is absent in the crystal structure of MmaA4-SAM as E146 occupies the same position (Boissier et al., 2006). In agreement with the proposed mechanism, two ordered water molecules were found within the active site, one that forms a hydrogen bond with E146 at a distance of 3.2 Å. Superimposition of MmaA4-SAM and CmaA1-DDDMAB/CTAB structures showed that the water molecule locates within 1 Å of the positively charged quaternary amines. As this proposed mechanism is based on in vivo and crystallographic data, further kinetic studies are required to delineate the reaction mechanism once in vitro assays have been established.

In a recent study, Guangqi et al. provided additional support for the carbocation-based mechanism by investigating the enzyme activity of a CFAS mutant whereby the CMAS-conserved active site glycine was mutated to the corresponding glutamate found in MmaA4 (Guangqi et al., 2013). The CFAS G236E mutant enzyme demonstrated less than 1 % enzymatic activity in vitro. This reduced enzyme activity was also observed in vivo, as overexpressing the CFAS G236E mutant in an *E. coli* CFAS-deficient strain resulted in a substantial reduction in cyclopropanated fatty acids. However, fatty acid analysis revealed that the strain synthesized multiple methyl-branched unsaturated fatty acid products. The multitude of products formed indicates that the CFAS mutant harbored an active site base in the absence of a bicarbonate ion. These data suggest that the conserved active site glutamate (conserved bicarbonate ligand) may be involved in proton abstraction from the reaction intermediates. Together these data suggest that cyclopropane synthases may have evolved to incorporate a bicarbonate ion to direct and preserve the carbocation center near the ion during catalysis. The inability to preserve the location of the cation center, as observed with the CFAS G236E mutant, would be deleterious to the cyclopropane reaction by allowing

carbocation migration from a secondary to a more stable tertiary center resulting from a hydride shift. Proton abstraction from these intermediates would likely result in multiple side products that was observed. As for MmaA4, the carbocation center may be rapidly quenched via nucleophilic attack by a water molecule, prohibiting carbocation migration, wherein the precursor methyl-branched hydroxymycolate required for methoxy- and ketomycolate biosynthesis is generated. Alternatively, catalysis may be initiated by nucleophilic attack of the double bond by a hydroxide ion followed by methylation. No  $\alpha$ -methyl hydroxylated fatty acid products were reported by the CFAS G236E mutant.

Since dioctylamine has been shown to inhibit CMAS function *in vivo* and the compound has been crystallized in the active site of CmaA2, crystal structures of CmaA2 bound to enantiomeric dioctylamine analogs that mimic intermediates of the proposed reaction mechanism, would be useful to establish the location of the carbocation center and the active-site base. Specifically, dioctylamine analogs harboring an adjacent methyl group to the nitrogen atom, would provide insight into the location of a carbocation and methyl group in the earliest stage of the methyl transfer reaction. In addition, analogs harboring an aziridine ring (cyclopropane ring with one carbon atom substituted for nitrogen) mimicking the reaction intermediate undergoing cyclopropane ring formation would serve in the identification of the active-site base. Coupling this structural information with CMAS/CFAS *in vitro* inhibition studies using these reaction intermediate analogs would provide strong support for defining the location of the carbocation center and active-site base during catalysis.

## **Functional role of mycolic acid modification in *Mycobacterium tuberculosis***

### **physiology**

The role of the mycolic acid modification in the physiology of Mtb is currently obscure, as they have not been explored in detail. Cyclopropane rings were first hypothesized as an intrinsic protection mechanism of labile double bonds from oxidative degradation by host defense microbicidal effectors, such as hydrogen peroxide, because Mtb lacks an OxyR-like inducible protective response (Yuan et al., 1995). Msmeg overexpressing either CmaA1 or CmaA2, resulted in cell walls containing approximately 25 % cyclopropanated mycolic acids. Incorporation of distal cyclopropane rings by CmaA1 provided a 10-fold increase in H<sub>2</sub>O<sub>2</sub> resistance, while no protective advantage was observed with proximal cyclopropanation by CmaA2 (George et al., 1995; Yuan et al., 1995). With the multitude of Mtb mutants generated that lack a single CMAS gene (*cmaA2*, *mmaA2*, and *pcaA*) in addition to a cyclopropane-deficient Mtb mutant, only the  $\Delta$ *pcaA* mutant has been assessed for chemical sensitivity towards hydrogen peroxide whereby sensitivity was comparable to WT (Glickman et al., 2000). A similar result was obtained upon acidified nitrite treatment, a host source of reactive nitrogen species (Chan et al., 1992).

Cyclopropane rings were later hypothesized to play a role in cell wall fluidity and permeability. Using the same aforementioned Msmeg strains, differential scanning calorimetry analysis of purified mycolic acids showed that proximal cyclopropane modification increased the thermal transition temperature by 3 °C, suggesting that the modification plays a role in enhancing cell wall rigidity (George et al., 1995). The opposite effect resulted from distal cyclopropanation. In both Msmeg and Mtb, *cis*-modifications are globally distributed as they are found at the proximal and distal positions. However, *trans*-

modifications are restricted to the proximal position. The mycolic acid composition (57 %  $\alpha$ -mycolate, 33 % methoxymycolate, 10 % ketomycolate) and overall *cis* and *trans* distribution (90 % *cis*, 10 % *trans*) are similar throughout Mtb strains (Yuan et al., 1997). Notably, a set of Mtb clinical isolates with minimal animal passage showed an overall increase in *trans* content, approximately 10 % as compared to 2 - 3 % of the extensive laboratory passaged H<sub>37</sub>Rv and H<sub>37</sub>Ra strains (Yuan et al., 1997). The mycobacterial cell wall resides in a state of extremely low fluidity and is highly impermeable to many substances (Brennan and Nikaido, 1995). Differential scanning calorimetry analysis of purified cell walls and total mycolic acids from Mtb H<sub>37</sub>Rv showed clear thermal transition temperatures of 61 °C and 41 °C, respectively (Liu et al., 1996). These data suggest that under physiologic growth temperatures, 37 °C, the cell wall resides in a highly ordered state, with mycolic acid as the principle contributor to the unusually low fluidity. Similar transition temperatures have been observed for purified cell walls and total mycolic acids from Msmeg, that lack cyclopropane rings and harbor significantly higher *trans*-content (~ 68 %) (Liu et al., 1996). Msmeg and *M. avium* maintain cell wall viscosity by altering mycolate *trans/cis* ratios in a temperature-dependent manner. Bacteria grown in elevated temperatures, increasingly rigidify their cell wall through the accumulation of *trans*-configured mycolic acids. In the study by Liu et al., *trans*-olefins and *trans*-cyclopropane modification were shown to similarly contribute to the overall fluidity of the mycobacterial cell wall (Liu et al., 1996). As Mtb is a facultative intracellular pathogen, that spends most of its life cycle within a host, the thermal adaptive effect on the *trans/cis* ratio is unlikely but has not been investigated.



Investigating the physiologic roles of *cis*- or *trans*-cyclopropane rings within the cell wall using isolated Mtb mutants is difficult as compensatory changes may occur or multiple mycolic acid types are effected that will undoubtedly complicate interpretation (Yuan et al., 1997). Selectively removing the proximal *cis*-cyclopropane of  $\alpha$ -mycolates requires the inactivation of the *pcaA* gene. The  $\Delta$ *pcaA* mutant loses the enzyme-specific modification but also dramatically depletes  $\alpha$ -mycolate abundance and accumulates oxygenated mycolates to an unusually high level (Glickman et al., 2000). Eliminating distal *cis*-cyclopropanes of  $\alpha$ -mycolates requires inactivation of the *cmaA2* and *mmaA2* genes but the cell wall accumulates proximal unsaturated oxygenated mycolates (Glickman, 2003). Deletion of the *cis*-cyclopropanes of oxygenated mycolates also requires inactivation of both *cmaA2* and *mmaA2*, but the cell wall accumulates distal unsaturated  $\alpha$ -mycolates and *trans*-unsaturated oxygenated mycolates (Barkan et al., 2010). Removal of *trans*-cyclopropanes of oxygenated mycolates requires inactivation of *cmaA2*, but the cell wall accumulates *cis*-unsaturated oxygenated mycolates. However, as previously mentioned, a *trans*-deficient strain has been generated through genetic inactivation of the *mmaA1* gene (Barkan et al., 2010). The  $\Delta$ *mmaA1* mutant synthesizes a WT mycolic acid composition but solely contains *cis*-cyclopropane rings. Therefore, generating a *trans* cyclopropane-deficient strain is not possible through genetic deletion of MA-MTs. However, deletion of KasB has been found to solely lack *trans*-cyclopropane rings and harbors a wild type mycolic acid composition (Bhatt et al., 2007). Generation of a cyclopropane-deficient Mtb strain requires multiple CMAS deletions (*pcaA*, *cmaA2*, *mmaA2*). As this particular strain is currently unavailable, it is unknown whether a WT mycolic acid composition remains intact. In contrast, an alternative cyclopropane-deficient strain has been generated (*pcaA*, *cmaA2*, *mmaA1-2*) but

as *mmaA1* was inactivated this strain is devoid of *trans*-configured mycolic acids but retains a WT composition (Barkan et al., 2012). A Mtb strain solely lacking *cis*- and *trans*-cyclopropane rings is not available but could be generated with the latter strain complemented with *mmaA1*. Therefore, investigating the net contribution of cyclopropane rings on cell wall function is likely possible, but establishing their individual contributions is difficult.

Despite very little evidence suggesting the physiologic role of oxygenated mycolic acid in the physiology of Mtb, their presence clearly affects cell wall permeability. As previously mentioned, Mtb overexpressing *mmaA1* depletes methoxymycolate abundance and increases the ketomycolate content to an unusually high level. In addition, these oxygenated mycolates were predominately *trans*-configured (Yuan et al., 1997). Isolated and purified Mtb ketomycolates containing proximal *trans*-cyclopropane rings showed a substantial increase in melting temperature, ~10 °C, relative to their *cis*-derivatives (Liu et al., 1996). This data suggests that the *trans*-cyclopropanated ketomycolates may provide a rigidifying effect when incorporated into the cell wall. However, Mtb::*mmaA1* resulted in a dramatic reduction in growth rate at elevated temperature with enhanced cell wall permeability, indicative of a more fluid cell wall (Yuan et al., 1997). A similar overall increase in ketomycolate was reported for Mtb grown within the macrophage and under reduced oxygen tension (Yuan et al., 1998a). This data is corroborated by a genome-wide transcriptomic analysis of clinical lungs samples showing the up- and downregulation of *mmaA4* and *pcaA*, respectively (Rachman et al., 2006). With regards to cell wall permeability, this altered cell wall architecture may be more suitable for nutrient acquisition in the host. In contrast, the Mtb  $\Delta$ *mmaA4* mutant, that is devoid of oxygenated mycolates

and solely synthesizes  $\alpha$ -mycolates, has a more rigid cell wall marked by a dramatic decrease in cellular uptake of glycerol and chenodeoxycholate. (Dubnau et al., 2000).

### **Physiologic role of the *Mycobacterium tuberculosis* mycolic acid modifications during host infection**

The first evidence supporting a role of mycolic acid cyclopropanation in Mtb pathogenesis was through the isolation and characterization of a cording-defective mutant resulting from inactivating the *pcaA* gene. Cording is a colony or microscopic morphology wherein the bacteria form serpentine rope-like bundles that correlates with their virulence (Middlebrook et al., 1947). As previously mentioned, the BCG-P and Mtb  $\Delta$ *pcaA* mutants lack well-defined serpentine cords and shows diffuse aggregation. The mycolic acid composition of the Mtb  $\Delta$ *pcaA* mutant is inverted, whereby oxygenated mycolates predominate severely depleted proximal cyclopropane-deficient  $\alpha$ -mycolates (Glickman et al., 2000). When infected in a mouse model, the  $\Delta$ *pcaA* mutant has an early growth defect within the first week, but grew to higher bacterial loads than WT just prior to the onset of the adaptive immune response at 3 weeks (Glickman et al., 2000; Rao et al., 2005). In all organs tested (liver, lung, and spleen), the  $\Delta$ *pcaA* mutant was cleared at a faster rate than WT. This enhanced rate of bacterial clearance has been interpreted as a persistence defect. However, bacterial loads began to stabilize to WT levels in the lungs and spleen at day 72 but were lower than WT at the end of a 135-day infection, and approximately 10-fold less in the liver. Notably, in a 219-day mortality study all mice survived the  $\Delta$ *pcaA* mutant infection whereas all WT-infected mice perished. However, bacterial loads were only examined during the first 135 days, questioning the author's proposed long-term persistence defect. The difference in mortality was attributed to an altered host immune response, as

histology sections of the lung showed dramatic differences in pulmonary damage. In a following study, WT and  $\Delta pcaA$  mutants were shown to be differentially recognized by host-derived macrophages. Altered host recognition was attributed to the dramatic change in the fine chemical structure of the surface extractable glycolipid trehalose dimycolate (TDM), as macrophage treated with  $\Delta pcaA$  TDM showed reduced tumor necrosis factor- $\alpha$  (TNF- $\alpha$ ) secretion (Rao et al., 2005). The mycolic acid composition of WT-derived TDM resembles those found esterified to the cell wall, whereas ketomycolates are the principle constituents of  $\Delta pcaA$  TDM with  $\alpha$ - and methoxymycolates considerably lower in abundance. In addition, mice injected with  $\Delta pcaA$  TDM showed a marked reduction in lung granulomatous inflammation. Together, the proximal cyclopropane ring of  $\alpha$ -mycolates has been characterized as a proinflammatory modification wherein the presence or absence of this modification profoundly effects the fine chemical structure of TDM, host recognition, and infection outcome.

The relationship between the fine chemical structure of TDM and host immune response was further substantiated with murine infection studies using the Mtb  $\Delta cmaA2$  mutant. As noted above, CmaA2 functions to incorporate proximal *trans*-cyclopropane rings into oxygenated mycolates. In addition, CmaA2 is functionally redundant with MmaA2 in incorporating proximal *cis*-cyclopropanation in oxygenated mycolates and distal cyclopropanation of  $\alpha$ -mycolates. The mycolic acid composition is overall similar to WT Mtb but lacks *trans*-cyclopropanation and a subset of *cis*-cyclopropanated oxygenated mycolates. In contrast to the  $\Delta pcaA$  mutant, inactivation of the *cmaA2* gene did not affect bacterial growth in vivo but generated a hypervirulent strain that reduced the mean survival time of infected mice by approximately 100 days (Rao et al., 2006). Mice infected with the

*ΔcmaA2* mutant caused larger lymphopenic granulomas in the liver that appears as a necrotic-like lesion. In addition, as hypervirulence of the *ΔcmaA2* mutant required an active TNF- $\alpha$ , interferon- $\gamma$ , and intact lymphocyte population, these data suggest that the cause of larger/altere d granulomas and enhanced mortality rate was due to an elevated immune response. In contrast to macrophage TNF- $\alpha$  hypostimulation by *ΔpcaA* TDM, *ΔcmaA2* TDM was hyperstimulatory but varied with macrophage source. Macrophage derived from C57Bl/J6 mice, the same mouse strain used in the histology and mortality studies previously described, were unresponsive to *ΔcmaA2* TDM stimulation. In contrast, BALB/C mice infected with the *ΔcmaA2* mutant also resulted in premature death, but host-derived macrophage showed enhanced TNF- $\alpha$  stimulation when treated with *ΔcmaA2* TDM. This source-dependent data indicates that other immune cell types are likely the primary source of TNF- $\alpha$ . Together, the functional role of *trans*-cyclopropane rings were marked as an immune suppressing modification, unlike the proinflammatory role of proximal *cis*-cyclopropane rings of  $\alpha$ -mycolates. The interpretation that the role of *trans*-cyclopropanation as an immunosuppressive modification is complicated by the accumulation of *cis*- and *trans*-unsaturated mycolic acids. Interestingly, the Mtb *ΔkasB* mutant is devoid of oxygenated mycolates that harbor *trans*-cyclopropane rings and are shorter by 2 - 6 carbons (Bhatt et al., 2007). Surprisingly, mice infected with the *ΔkasB* mutant survive 600 days of infection, despite ~1000 colony forming units present in the lung. This data suggests that the hypervirulence of the *ΔcmaA2* mutant is unrelated to the lack of *trans*-cyclopropane rings but resulted from accumulating approximately half of the oxygenated mycolates as *cis*-unsaturated derivatives. An alternative approach to the test the immune suppressive role of *trans*-oxygenated mycolates is through murine infection studies

using the Mtb  $\Delta$ *mmaA1* mutant but these investigations have not been reported (Barkan et al., 2010). In addition, examining the potential immunosuppressive role of *cis*-cyclopropane rings within oxygenated mycolates is currently not possible with the available Mtb mutants.

To address the net effect of cyclopropanation during infection, a cyclopropane-deficient strain was generated and infected in a mouse model (Barkan et al., 2012). The cell wall contains diunsaturated  $\alpha$ -mycolates and proximal *cis*-unsaturated oxygenated mycolates. The strain was devoid of *trans*-configured oxygenated mycolates as *mmaA1* was genetically inactivated. Interestingly, the colony morphology is identical to wild type but highly sensitive to tyloxapol, a detergent media supplement commonly used to prevent mycobacteria from aggregating in liquid culture. Upon murine infection, the strain was severely growth attenuated prior to the onset of the adaptive immune response, 80-fold lower CFUs than wild type, with subsequent growth arrest throughout the remaining 126-day infection study. Growth attenuation was attributed to an enhanced immune response, specifically TNF- $\alpha$ , IL-17, and INF- $\gamma$ . Whether this immune response is beneficial or detrimental to the outcome of infection is currently unknown as mortality studies were not undertaken and histology sections of the lungs or other organs were not analyzed. Taken together, these data suggest that Mtb cyclopropanates cell wall mycolic acids to dampen the host immune response.

In experimental mouse models and in human disease, Mtb infection is characterized by accumulation of lipid-rich foamy macrophages (FM), a host response currently thought to be contributed in part by cell wall ketomycolic acids (Dkhar et al., 2014; Hunter, 2012; Peyron et al., 2008; Russell et al., 2009). Upon infection, the internalization of Mtb by host macrophage triggers the granuloma formation, immune cellular aggregates used to contain

the infection. Within the granuloma, resident macrophages differentiate into FM, characterized by the accumulation of numerous lipid bodies. Korf et al. first showed that upon administering mycolic acids to the peritoneal cavity or the airway of mice, resident macrophage had a foam-like morphology similar to those found in human tuberculosis granulomas (Korf et al., 2005). The cells were larger, contained numerous large vacuoles, and accumulated neutral lipids including cholesterol, suggesting interference with host lipid metabolism. Macrophage lipid accumulation was later attributed to Mtb-specific oxygenated mycolates, as only upon infection with Msmeg overexpressing Mtb *mmaA4* induced FM formation (Peyron et al., 2008). The reported source of the Msmeg strain used in the study was not clearly defined. An earlier study reported that Msmeg overexpressing Mtb *mmaA4* harbors hydroxymycolate as the principle cell wall mycolate but ketomycolate may have been synthesized, observed as an uncharacterized spot upon 2D-TLC analysis of purified cell wall mycolates (Yuan and Barry III, 1996). Alternatively, the cell wall of Msmeg overexpressing a similar *mmaA* locus from BCG-P (named *cmaA-D*) accumulates substantial quantities of ketomycolate and hydroxymycolate (Dubnau et al., 1997). As Mtb has been found to incorporate trace amounts of hydroxymycolate in the cell wall, the contribution of individual oxygenated mycolates on FM induction was not addressed (Quémard et al., 1997). The more relevant strains to test the hypothesis that oxygenated mycolic acids induce FM formation is the Mtb  $\Delta mmaA3$  and  $\Delta mmaA4$  mutants (Dubnau et al., 2000). The former mutant has not been tested and the later mutant was reported to drastically reduce FM induction but the data was not provided. Moreover, Mtb overexpressing *mmaA3* is also devoid of ketomycolate, but this strain has not been tested either. However, as BCG-P is a natural  $\Delta mmaA3$  mutant and has been shown to induce FM formation, these data provide

support for the involvement in ketomycolate in macrophage differentiation (Holla et al., 2016). With regard to prior reports showing that mycobacterial cell wall lipids are actively trafficked out of the phagosome during infection, lipid-sensing nuclear receptors peroxisome proliferator-activated receptor gamma and testicular receptor 4 (TR4) are activated by Mtb lipids and are essential for FM biogenesis, and macrophage lipid accumulation is essential for Mtb viability, Dkhar et al. searched for the activating lipid of TR4 (Beatty et al., 2000; Dkhar et al., 2014; Mahajan et al., 2012; Xie et al., 2009). They found that ketomycolates directly bind to TR4 and induce lipid droplet accumulation in human monocyte derived macrophages.

### **Biofilm formation**

Mtb biofilm formation has been implicated in the generation of pulmonary cavitation, the hallmark characteristic of post primary TB in immunocompetent individuals, and transmission of the disease (Basaraba and Ojha, 2017; Kulka et al., 2012). Biofilm formation has been shown to be intimately involved in the chronicity and drug-tolerance associated with many bacterial diseases but this association in TB remains unclear (Costerton et al., 1999; Olsen, 2015). Biofilms are self-assembled multicellular aggregates embedded in an extracellular matrix. Within the biofilm, bacteria reside in a gradient of microenvironments conducive to generating a phenotypically distinct population, resulting in microbial communities that are difficult to clear by the host immune system and antibiotic treatment (Hall-Stoodley et al., 2004; Wong and Jacobs, 2016). During the early stages of a primary infection, Mtb bacilli engulfed by resident alveolar macrophages are quarantined within a granuloma. Granulomas found in infected humans undergo significant necrosis leading to a caseous granuloma. Resident bacilli are found within and adjacent to the necrotic



center and have been observed to form extracellular communities called necrosis-associated extracellular clusters (NECs), cellular structures reminiscent of biofilms (Lenaerts et al., 2007; Orme, 2011, 2014). Adaption to life in the necrotic granuloma likely provides long term persistence in a dormant state, whereby reactivation and escape results in a post primary infection (Wong and Jacobs, 2016). It has been proposed that dystrophic calcification of the necrotic center pushes NECs towards the oxygen-rich alveoli resulting in lipid pneumonia (Orme, 2014; Wong and Jacobs, 2016). Subsequent to foamy macrophage necrosis, alveoli are filled with soft caseous material that is then coughed out resulting in a pulmonary cavity. This vacant cavity forms a suitable surface environment for Mtb biofilm formation, a significant source of bacilli for disease transmission (Hunter, 2012; Rich, 1951).

Mtb has historically been grown as a surface pellicle, a biofilm-like structure at the liquid-air interface of a detergent-free liquid medium (Wayne, 1994). Within the pellicle, Mtb are encased in an extracellular matrix consisting of a complex mixture of lipids and free mycolic acids that harbor drug-tolerant populations when treated with high levels of antibiotics (Ojha et al., 2008). The free mycolic acid constituents of the extracellular matrix are predominately methoxymycolates (roughly 80% abundance) with  $\alpha$ - and ketomycolates as minor species. Despite the minor abundance, ketomycolates were established as essential matrix components for pellicle formation (Sambandan et al., 2013). To assess pellicle-drug tolerance, Mtb H<sub>37</sub>Rv and the Mtb  $\Delta$ *mmaA4* mutant (pellicle-deficient) were subjected to rifampicin treatment. As the  $\Delta$ *mmaA4* mutant was hypersensitive to rifampicin, drug sensitivity was attributed to the pellicle-forming deficiency, but the lack of methoxymycolate was not clearly ruled out. The Mtb  $\Delta$ *mmaA3* mutant is devoid of methoxymycolates but synthesizes  $\alpha$ - and ketomycolates but forms biofilms that

phenotypically differ from WT. In contrast, the cell wall and matrix mycolic acid composition of Mtb overexpressing *mmaA3* was similar to the free mycolic acids found in WT Mtb but lack ketomycolates and was pellicle-deficient. Neither of the aforementioned strains were tested for antibiotic sensitivity. Therefore, drug tolerance may result from pellicle formation or abundant methoxymycolate present in the extracellular matrix. Despite a previous report showing that Mtb overexpressing *mmaA3* had increased sensitivity to rifampicin treatment in planktonic culture, methoxymycolate deficiency cannot be ruled out as the cause of rifampicin sensitivity to the  $\Delta$ *mmaA4* mutant in pellicle-forming conditions (Yuan et al., 1998a).

A significant contribution to the overall abundance of free mycolic acids found in the extracellular matrix results from hydrolysis of newly synthesized TDM. In Msmeg, the accumulation of free mycolic acids within the matrix during biofilm growth coincided with depletion of extractable TDM, but the total TDM levels remained unchanged (Ojha et al., 2010). TDM hydrolysis was proposed to occur during translocation and not subsequent to glycolipid deposition into the cell wall. Moreover, it was shown that biofilm lysates of Msmeg and Mtb harbor TDM esterase activity. A TDM-specific esterase was identified and strongly predicted as extracytoplasmic enzyme, but the cellular location was not characterized (Yang et al., 2014).

### **Mycolic acid methyltransferases as drug targets**

CMAS were first proposed as potential drugs targets when overexpressing Mtb *cmaA1* and *cmaA2* in Msmeg were found to provide enhanced protection against hydrogen peroxide treatment and increased cell wall rigidity, respectively (George et al., 1995; Yuan et al., 1995). Cell walls containing approximately 25 % distal *cis*-cyclopropanated  $\alpha_2$ -

mycolates, resulting from CmaA1 overexpression, provided Msmeg increased resistance to hydrogen peroxide killing. Overexpression of *cmaA2* resulted in a similar abundance of proximal *cis*-cyclopropanated  $\alpha_1$ -mycolates and decreased the fluidity of the cell wall. These data suggested that inhibiting CMAS may provide a means to increase bacterial susceptibility to host antimicrobial effectors and membrane permeability.

Crystal structure analysis of mycolic acid methyltransferases revealed that the enzymes share an overall similar fold and active site architecture that predicts that CMAS can be targeted by a single chemical entity (Figure 6B). The eight mycolic acid methyltransferases identified from the Mtb genome share 50 - 70 % amino acid sequence identity. Of those confirmed to play a functional role in mycolic acid modification, crystal structures have been solved for PcaA, CmaA2, MmaA2, and MmaA4 (Boissier et al., 2006; Huang et al., 2002). The SAM binding domains, containing the conserved glycine-rich motif, all show a similar fold commonly found among SAM-dependent methyltransferases that consists of seven aligned  $\beta$ -stands, six parallel and one antiparallel, flanked by  $\alpha$ -helices (Cheng and Roberts, 2001; Schluckebier et al., 1995). All of the MA-MT structures solved in complex with SAM or SAH have a small portal adjacent to the sulfur atom of the cofactor. The portal extends towards a larger hydrophobic tunnel, the acyl substrate binding site, that are  $\sim 10$  Å wide and  $\sim 15$  Å long (Huang et al., 2002). The acyl binding sites differ significantly in polarity as they extend from the cofactor site towards the bulk solvent. At the base of the tunnel, adjacent to the small portal that houses the activated methyl group of SAM, locates the polar catalytic core. The residues positioned at the core are highly conserved between MA-MTs, with differences specifically occurring to the amino acid E146 in MmaA4 (E143 in MmaA3). As mention previously, a bicarbonate ion was absent in the

MmaA4 crystal structure, as E146 occupies the position (Boissier et al., 2006). All bicarbonate-stabilizing amino acids are strictly conserved in CMAS. The amino acids that constitute the acyl binding site entrances are not strictly conserved although the resident amino acids are extensively hydrophobic.

Thiacetazone, a second-line antitubercular prodrug, was the first small molecule inhibitor identified to target multiple mycolic acid cyclopropane synthases (Alahari et al., 2007). CMAS function was found to be highly sensitive to the inhibitory effect of the compound. BCG-P treated with the compound resulted in  $\alpha$ -mycolate depletion with a concomitant accumulation of ketomycolate and unsaturated derivatives of both mycolate types. As significant inhibition of mycolic acid cyclopropanation was observed well below the minimum inhibitory concentration and the lack of reduced drug sensitivity when CMAS genes were overexpressed, the effect on CMAS function was not the basis of growth inhibition. Moreover, it was later shown that thiacetazone solely inhibits Mtb mycolic acid biosynthesis without affecting mycolic acid modification (Belardinelli and Morbidoni, 2012). Therefore, Mtb CMAS enzymes were ruled out as targets of thiacetazone. It was recently shown that the primary targets of thiacetazone are the FAS II  $\beta$ -hydroxyacyl-ACP dehydratase complexes, HadAB/BC (Belardinelli and Morbidoni, 2012; Coxon et al., 2013; Grzegorzewicz et al., 2012).

Through the use of the tool compound dioctylamine, it was shown that simultaneous inhibition of MA-MTs with a single compound is possible and causes pleiotropic effects on Mtb cells. Dioctylamine was first identified as an inhibitor of *E. coli* CFAS and later found to demonstrate dose-dependent inhibition of multiple pathways of mycolic acids modification that paralleled bacterial cell growth inhibition (Barkan et al., 2009;

Guianvarc'h et al., 2006). Through the use of chemical and genetic approaches, CMAS were established as the primary targets of the compound. Although DOA inhibits methoxymycolate synthesis, MmaA3 was found to be indirectly targeted by the compound. DOA additionally targets MmaA4 but higher concentrations were required. The molecular basis of inhibition was attributed to the compound's ability to mimic the common carbocation intermediate formed upon methyl transfer to unsaturated mycolate precursors (Yuan and Barry III, 1996). In addition to DOA's effect on cell wall integrity and cell viability, the compound demonstrates synergistic killing with ciprofloxacin and isoniazid. Enhanced drug penetration and/or the combined effect on mycolic acid biosynthesis was proposed as the mechanism of synergy, respectively. Interestingly, overexpression of any one MA-MT gene was unable to confer resistance to DOA, however, cells overexpressing all six established MA-MTs resulted in partial resistance. To clearly establish cyclopropane mycolic acid synthases as the cause of cellular growth inhibition, and rule out CMAS as target decoys, the growth inhibitory effect of dioctylamine on a recently report cyclopropane-deficient strain is required (Barkan et al., 2012). It is worthy to note that the compound's effect on the mycolic acid modification in the cell wall of Mtb has been inferred from data obtained from *M. bovis* BCG-R, a mycobacterium that synthesizes an overall similar mycolic acid composition as Mtb, but has not been directly shown.

Mycolic acid modifications also have important roles in Mtb host-pathogen interactions. Mtb lacking specific MA-MTs, and consequently specific cyclopropane modifications of cell wall extractable and esterified mycolates, have altered virulence and inflammatory activity for host cells, a phenotype that is mediated through TDM (Dao et al., 2008; Rao et al., 2005, 2006). Mtb lacking all cyclopropane modifications is severely

attenuated in the mouse model of infection and elicits hyperinflammation in vivo, confirming that the net effect of the cyclopropane modification is to suppress host immunity (Barkan et al., 2012). Taken together, these data indicate that pharmacologic inhibition of this methyltransferase family would have the dual effect of compromising cell viability while eliciting an enhanced host immune response.

The essential nature of ketomycolic acids in Mtb biofilms formation, FM differentiation, and virulence, suggests MmaA4 is a unprecedented antibiotic target for the treatment of TB (Dao et al., 2008; Dkhar et al., 2014; Dubnau et al., 2000; Sambandan et al., 2013). Currently, two compounds have been identified to inhibit MmaA4, dioctylamine and S-adenosyl-N-decyl-aminoethyl, but neither compound is MmaA4-specific (Barkan et al., 2009; Vaubourgeix et al., 2009). As previously described, CMAS enzymes were reported as the primary targets of dioctylamine, but higher concentrations of the compound are required to inhibit MmaA4 function. S-adenosyl-N-decyl-aminoethyl is a SAM-analog that was shown to inhibit cellular growth of both Msmeg and Mtb at similar concentrations. As the former lacks the *mmaA4* gene, this strongly suggests that off-target inhibition is responsible for the observed growth inhibition. In addition, reduced drug susceptibility was not observed when MmaA4 was overexpressed. Together with the lack of evidence showing reduced drug susceptibility of Mtb overexpressing MmaA4, the proposed mechanism of inhibition is unclear. Given that MmaA4-specific inhibitors are currently unavailable and in vitro assays for drug screening have not been developed, novel assay methodologies are urgently needed to exploit this putative drug.

In sum, mycolic acid modification plays important roles in cell wall permeability and host-pathogen interactions. Since the loss of cell wall cyclopropane rings, resulting from

multitarget chemical intervention or combined genetic deletions, causes a loss in Mtb viability, enhanced drug penetration, an enhanced immune response, and severe growth attenuation within the host, we sought multitarget drug-like inhibitors of cyclopropane mycolic acid synthases. As established in vitro assays for this enzyme family are not suitable for drug discovery, we pursued the development of a novel assay strategy to unlock this family of currently intractable protein targets for drug discovery. Chapter 2 focuses on the design and development of fluorescence-based competition displacement assays suitable for multitarget assessment of small-drug like molecules towards CMAS. Wherein Chapter 3 emphasizes the suitability of this assay methodology as a high throughput screening platform, in vivo activity of identified inhibitors, and the structural basis of CMAS inhibition. Together, we show that the simultaneous inhibition of multiple CMAS will likely require small amphipathic molecules that mimic the common carbocation reaction intermediate. This work provides a framework for the discovery of multitarget CMAS inhibitors in addition to rational assay design strategies that could be used by the scientific community to initiate drug discovery for currently or forthcoming intractable drug targets.

## CHAPTER II

### DESIGN AND DEVELOPMENT OF A NOVEL CYCLOPROPANE MYCOLIC ACID SYNTHASE FLUORESCENCE-BASED COMPETITION DISPLACEMENT ASSAY

#### Overview

To combat the persistent threat and low therapeutic success of drug-resistant tuberculosis, chemotherapeutic agents with novel modes of action are urgently needed. Inhibition of mycolic acid biosynthesis is a well-established vulnerability to *Mycobacterium tuberculosis* and the pathway contains a myriad of protein targets that lack homology with host enzymes. *M. tuberculosis* mycolic acids are decorated with cyclopropane rings, methyl branches, and oxygenated functionalities through the catalytic action of six S-adenosyl methionine (SAM)-dependent mycolic acid methyltransferases. This family of enzymes share a highly similar primary and tertiary structure and have been shown to be simultaneously inhibited by the small molecule inhibitor dioctylamine. However, host toxicity renders the compound unsuitable for further development. Cyclopropane mycolic acid synthases (CMAS) were identified as the primary targets of the compound but are intractable to in vitro target-based screening, therefore novel biochemical assay platforms are needed to investigate their simultaneous inhibition as a multitarget antibiotic strategy against tuberculosis.

By chemically modifying a CmaA2 small-molecule ligand, identified via differential scanning fluorimetry screening, we generated a set of environment-sensitive nitrobenzoxadiazole (NBD) fluorescence enhancement probes suitable for CMAS drug discovery. NBD-probes show enhanced fluorescence intensity when bound to CMAS, that



likely results from the fluorophore experiencing a drastic change in environment polarity upon binding. The probes bind to CMAS with saturable single-site binding behavior and are effectively displaced by dioctylamine and nonfluorescent parent molecules. Our studies clearly demonstrate the utility of NBD-probes for establishing the binding affinity and multitargeting capacity of CMAS ligands.

## **Introduction**

Inhalation of contaminated aerosols harboring viable *Mycobacterium tuberculosis* (Mtb) bacilli causes one of mankind's most devastating diseases, tuberculosis. In 2017, tuberculosis was one of the top 10 causes of human mortality, resulting from a global estimate of 2 million deaths (World Health Organization, 2018). Drug-sensitive tuberculosis is often curable with standard 6 - 9 month combination drug treatment, but of significant global concern in the emergence of multidrug-resistant strains against these chemotherapeutic agents (Dheda et al., 2017). To combat and reduce the onset of drug-resistant Mtb, new antimycobacterial medicines with novel modes of action that shorten lengthy tuberculosis treatment are urgently needed.

Mycolic acids are the major and signature lipids that constitute the outer asymmetric bilayer in the cell wall of Mtb. These lipids are high-molecular-weight  $\alpha$ -alkyl  $\beta$ -hydroxy fatty acids ( $C_{76}$  -  $C_{90}$ ) extensively modified by cyclopropane rings, methyl branches, and oxygenated functionalities that produce the three signature mycolic acid types:  $\alpha$ -mycolate, methoxymycolate, and ketomycolate (Barry III et al., 1998). Mycolic acids are found within the inner leaflet esterified to the underlying arabinogalactan and in the outer leaflet as solvent-extractable glycolipids. Together, mycolic acids form an outer lipid bilayer with exceptionally low fluidity and permeability, including impermeability to antibacterial agents

(Barkan et al., 2009). Through a genetic approach, six S-adenosyl methionine (SAM)-dependent mycolic acid methyltransferases (MA-MTs: CmaA2, PcaA, MmaA1-4) have been shown to be responsible for incorporating these characteristic modifications into the meromycolate chain (Barkan et al., 2010; Dubnau et al., 2000; Glickman, 2003; Glickman et al., 2000, 2001; Yuan and Barry III, 1996; Yuan et al., 1997, 1998a). PcaA and MmaA2 cyclopropanate the proximal and distal positions of  $\alpha$ -mycolates, respectively (Glickman, 2003; Glickman et al., 2000). MmaA2 plays an additional functionally-redundant role with CmaA2 in *cis*-cyclopropanation of oxygenated mycolates. MmaA1 and CmaA2 function in concert to incorporate *trans*-cyclopropane rings. Two additional SAM-dependent methyltransferases, UmaA1 and CmaA1, have been identified to share significant similarity to MA-MTs, but have no functional role in mycolic acid modification. However, the latter enzyme has CMAS activity when overexpressed in *M. smegmatis*, a mycobacterial species that has been shown to cyclopropanate their mycolic acids when cultured in reduced growth temperatures (Barkan et al., 2010; Laval et al., 2008).

Mycolic acid cyclopropanation has been strongly implicated in bacterial virulence (Barkan et al., 2012; Glickman et al., 2000; Rao et al., 2005, 2006). Their role in mycobacterial pathogenesis was first evidenced through investigating the cording-deficient Mtb  $\Delta pcaA$  mutant infected in mice. The mutant showed an early growth defect, within the first week, but grew to highly bacterial loads prior to the onset the adaptive immune response at 3 weeks (Glickman et al., 2000; Rao et al., 2005). Subsequently, the mutant was cleared at a faster rate than wild type, indicative of a persistence defect. In addition, mice infected with the  $\Delta pcaA$  mutant had attenuated immunopathology in addition to a dramatic reduction in mortality. Conversely, the Mtb  $\Delta cmaA2$  mutant demonstrated an exaggerated host

immune response, resulting in extensive tissue damage with an accelerated host mortality rate (Rao et al., 2006). Recently, it has been shown that cyclopropane-deficient Mtb is severely growth attenuated in the mouse model, attributed to an enhanced immune response (Barkan et al., 2012).

We previously showed that simultaneously inhibiting multiple pathways of mycolic acid modification with a single small molecule is feasible and causes pleiotropic effects on the cell (Barkan et al., 2009). This dialkylamine inhibitor, dioctylamine, was first identified as an inhibitor of *E. coli* cyclopropane fatty acid synthase (CFAS) (Guianvarc'h et al., 2006). Using chemical and genetic approaches, CMAS were established as the primary targets of DOA. Despite DOA's ability to additionally inhibit methoxymycolate synthesis, MmaA3 was found as an indirect target of the compound. Moreover, DOA also inhibited MmaA4 function but higher concentrations were required. MA-MT enzymes possess nearly identical tertiary structures and active site amino acid composition, yet modify distinct lipid substrates (Figure 6A to C). While the relationship between tertiary structure and active site conservation with respect to enzyme function has not been resolved, their mycolic acid modification reactions likely proceeds through a common carbocation intermediate (Yuan and Barry III, 1996). The crystal structure of the CmaA2-DOA complex showed that the basic amine of the compound locates to the site of methyl transfer with the acyl chains positioned to the entrance, indicating that inhibition of mycolic acid modification by DOA results from mimicking the carbocation intermediate. In addition to DOA's effect on cell wall integrity and cell viability, the compound demonstrated synergistic killing with ciprofloxacin and isoniazid, two established antimycobacterial drugs (Barkan et al., 2009). Enhanced drug penetration and/or the combined effect on mycolic acid biosynthesis was

proposed as the mechanism of synergy, respectively. Interestingly, overexpression of any one MA-MT was unable to confer resistance to DOA. This data indirectly suggests that a single chromosomal mutation of any one MA-MT gene would be unable to confer the bacterial cell resistance to a multitargeting MA-MT compound. These data provide strong implications for targeting this enzyme family as a promising strategy to shorten the duration of tuberculosis treatment and slow the onset of antimicrobial drug resistance.

Current in vitro assays prohibit investigating MA-MTs as drug targets. Of the six validated MA-MTs, in vitro assays have been developed for three CMAS enzymes (CmaA2, MmaA2, and PcaA)(Barkan et al., 2009; Corrales et al., 2012). Since their native substrates have not been established and are part of a heterogenous lipid mixture covalently attached to acyl-carrier protein AcpM, these assays currently require nonauthentic fatty acid substrates (Barkan et al., 2009; Corrales et al., 2012; Yuan et al., 1998b). CMAS enzymes can cyclopropanate medium chain fatty acids, such as linoelaidic acid and *cis*-11,14-eicosadienoic acid (EA), but large amounts of protein are required and the kinetic constants (CmaA2:  $K_m = 16.8 \mu\text{M}$  and  $k_{\text{cat}} = 0.03 \text{ s}^{-1}$  for EA) prohibit further assay development as a high throughput screening platform.

In this chapter, a small molecular scaffold identified via differential scanning fluorimetry was chemically modified to afford a set of fluorescence probes that demonstrate enhanced fluorescence when bound with both CmaA2- and MmaA2-SAM complexes. We demonstrate that the probes bind to CMAS with single-site binding behavior, can be effectively displaced by small molecule ligands, and bind directly to the acyl binding site of CmaA2 using crystallographic analysis.

## Results

### *Nitrobenzoxadiazole-conjugated 1,3-diaminopropanes are fluorescence enhancement probes of multiple cyclopropane mycolic acid synthases*

Small-molecule differential scanning fluorimetry screening against purified recombinant Mtb CmaA2 (*see* Chapter 3) identified two compounds, **4** and **5**, that were particularly interesting because they contain a hydrophobic 4-chloronaphthyl group, that is structurally similar to the NBD fluorophore (Figure 7). NBD fluorescent probes demonstrate environment sensitivity, as they are weakly fluorescent in aqueous suspensions but show enhanced fluorescence when in an apolar environment (Fery-Forgues et al., 1993; Rohacova et al., 2010). We designed an NBD-analog similar to **4** and **5**, by naphthyl group replacement for NBD, based on the idea that the acyl binding site of CMAS would enhance NBD fluorescence. In fact, Shi *et al.* demonstrated that naphthyl group replacement for NBD has a minimal effect on the biochemical properties of the parent molecule (Shi et al., 2005). Moreover, NBD analogs have been used in drug discovery as active site competition probes for target-based small molecule screening (Berger et al., 2012). Therefore, our design would enable the development of a fluorescence-based competition displacement assay more suitable for HTS, with enhanced acyl binding site selectivity, as compared to the DSF assay described in Chapter 3.

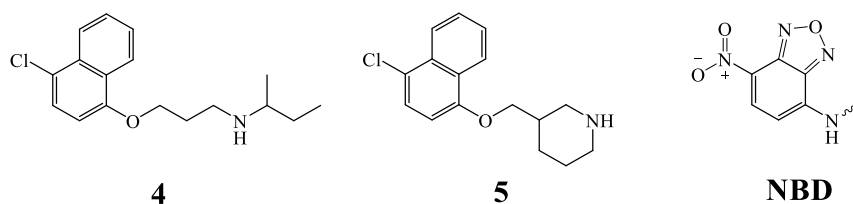


**Figure 7. The nitrobenzoxadiazole fluorophore is structurally similar to the 4-chloronaphthyl group in Compounds 4 and 5.**

The naphthyl and nitrobenzoxadiazole (NBD) groups are both bicyclic aromatic ring systems. Activation of the NBD fluorophore requires substituting the chlorine atom of nonfluorescent 4-chloro-7-nitrobenzoxadiazole for an amine substituent (NBD is represented in the activated form).

Using a facile two-step synthesis, we prepared N<sup>1</sup>-methyl-N<sup>3</sup>-(7-nitrobenzo[c][1,2,5]oxadiazol-4-yl)propane-1,3-diamine (NBD-A) (Figure 8) and tested whether CmaA2 binding enhanced NBD fluorescence intensity. The *in vitro* assay conditions 4 μM CmaA2 and 200 μM SAM when tested using a range of NBD-A concentrations (5 μM to 0.625 μM) resulted in a 4.9 to 10-fold increase in fluorescence intensity with a concomitant blue-shift in the excitation (485 nm to 475 nm) and emission wavelengths (545 nm to 530 nm) (Figure 9, left) (Barkan et al., 2009). NBD-A fluorescence enhancement was dependent on the presence of SAM bound to CmaA2, as NBD fluorescence was unaltered when incubated with CmaA2 or SAM alone. These data suggest that NBD fluorescence enhancement by CmaA2 is a SAM-dependent process. Incubating NBD-amine, NBD-A lacking N-methyl-1-propanamine, with the CmaA2-SAM complex resulted in no change in fluorescence intensity. Therefore, the N-methyl-1-propanamine constituent of NBD-A is critical for NBD fluorescence enhancement by anchoring the probe to the active site.

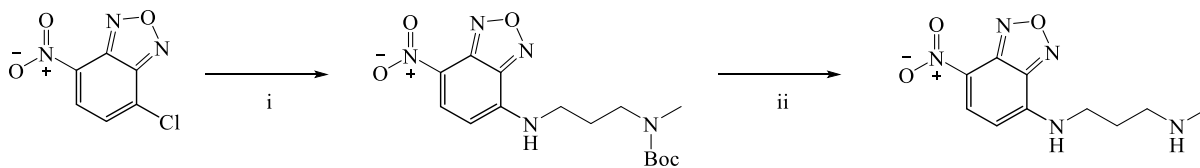


**Figure 8. Two-step synthetic route for N<sup>1</sup>-methyl-N<sup>3</sup>-(7-nitrobenzo[c][1,2,5]oxadiazol-4-yl)propane-1,3-diamine (NBD-A).**

*i)* K<sub>2</sub>CO<sub>3</sub>, ACN, 60 °C *(ii)* TFA, DCM, 0 - 25 °C

Structural superimposition of the three known Mtb CMAS enzymes (CmaA2, MmaA2, and PcaA) show an overall similar fold with nearly identical active site residues (Figure 6A and B). Moreover, the enzymes all contain an ordered bicarbonate ion that resides within their active sites and likely participates in the cyclopropanation reaction (Huang et al., 2002). Subsequent to methyl transfer, this ion has been proposed as the active site base responsible for abstracting a proton from a common carbocation transition state intermediate, generating the cyclopropanated product. The amino acids involved in stabilizing the bicarbonate ion and the carbocation reaction intermediate formed during catalysis are highly conserved in all three CMAS enzymes. This structural information predicts that these enzymes share the capacity to bind NBD-A.

We then tested whether MmaA2 and PcaA binding enhanced NBD-A fluorescence intensity. We were surprised to find that NBD-A fluorescence was significantly lower when bound to MmaA2 than previously observed for CmaA2 (53 to 62 % less, 5 μM to 0.625 μM NBD-A, respectively; Ex: 485 nm Em: 545 nm) with no observed shift in excitation or emission wavelengths (Figure 9, middle). Given the near identical active site architecture of CmaA2 and MmaA2, in addition to the available crystallographic data of the CmaA2-DOA

complex, the terminal methylamine of NBD-A is unlikely to be sterically hindered in the active site of MmaA2. Although steric hinderance is possible, we attempted to improve enhance NBD fluorescence by synthesizing a demethylated NBD-A analog (N<sup>1</sup>-(7-nitrobenz[c][1,2,5]oxadiazol-4-yl)propane-1,3-diamine, NBD-B). Incubation of MmaA2-SAM complex in the presence of varying concentrations of NBD-B (5  $\mu$ M to 0.625  $\mu$ M) averaged a 40 % increase in fluorescence enhancement as compared to NBD-A (Figure 10, middle). However, NBD-B fluorescence was not improved over NBD-A for CmaA2 (Figure 9 and Figure 10, left). PcaA produced negligible fluorescence enhancement upon titrating NBD-A (Figure 9, right) or NBD-B (Figure 10, right).

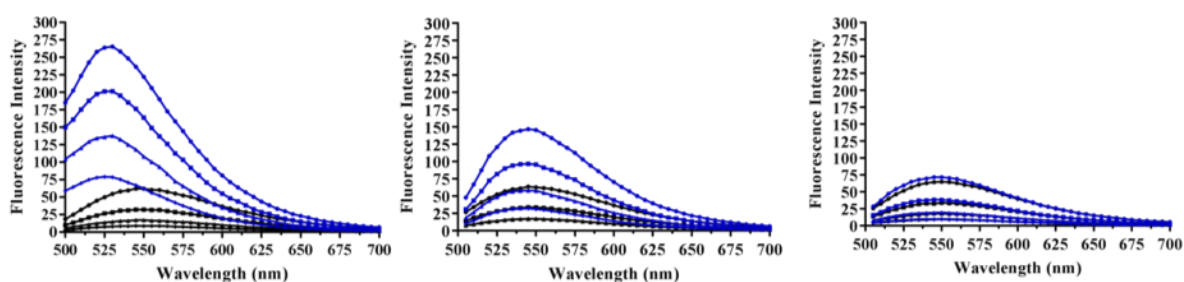


**Figure 9. Spectral properties of for N<sup>1</sup>-methyl-N<sup>3</sup>-(7-nitrobenzo[c][1,2,5]oxadiazol-4-yl)propane-1,3-diamine (NBD-A) in the presence of cyclopropane mycolic acid synthases.**

Fluorescence emission spectra of 5  $\mu$ M (circle), 2.5  $\mu$ M (square), 1.25  $\mu$ M (triangle), and 0.625  $\mu$ M (diamond) NBD-A in the presence of 4  $\mu$ M cyclopropane mycolic acid synthase (CMAS) supplemented with 200  $\mu$ M S-adenosyl methionine (blue) and 4  $\mu$ M CMAS alone (black) (CmaA2: left, MmaA2: middle, PcaA: right). Emission spectra are shown in the range of 500 - 700 nm upon excitation of the nitrobenzoxadiazole fluorophore at 475 nm (CmaA2) and 485 nm (MmaA2 and PcaA). Data points were collected in 5 nm intervals. Experiments were performed in triplicate with similar results.



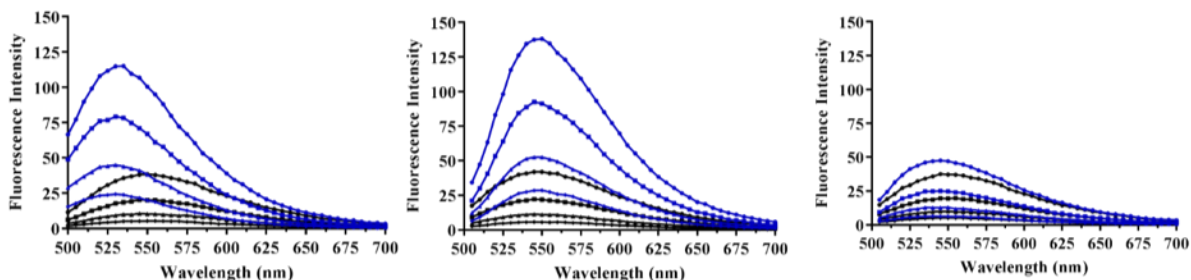


**Figure 10. Spectral properties of for N<sup>1</sup>-(7-nitrobenz[c][1,2,5]oxadiazol-4-yl)propane-1,3-diamine (NBD-B) in the presence of cyclopropane mycolic acid synthases.**

Fluorescence emission spectra of 5  $\mu$ M (circle), 2.5  $\mu$ M (square), 1.25  $\mu$ M (triangle), and 0.625  $\mu$ M (diamond) NBD-B in the presence of 4  $\mu$ M cyclopropane mycolic acid synthase (CMAS) supplemented with 200  $\mu$ M S-adenosyl methionine (blue) and 4  $\mu$ M CMAS alone (black) (CmaA2: left, MmaA2: middle, PcaA: right). Emission spectra are shown in the range of 500 - 700 nm upon excitation of the nitrobenzoxadiazole fluorophore at 475 nm (CmaA2) and 485 nm (MmaA2 and PcaA). Data points were collected in 5 nm intervals. Experiments were performed in triplicate with similar results.

Upon optimizing the assay conditions, we determined the dissociation constants of the CMAS-fluorophore complexes. NBD-A and NBD-B demonstrated saturable binding curves, wherein the data was fit to the general quadratic equation for single-site binding. The dissociation constant of CmaA2-SAM-NBD-A complex (Ex: 475 nm, Em: 530 nm) was  $K_d = 606 \pm 28$  nM (Figure 11, left). The dissociation constant of MmaA2-SAM-NBD-B (Ex: 485 nm, Em: 545 nm) complex was  $670 \pm 23$  nM (Figure 11, right). Together, these data show that NBD-analogs bind to CMAS with saturable single-site binding behavior.

To further demonstrate that NBD-A binds directly to CmaA2 and to explore the molecular basis of their interaction, we then solved the crystal structure in complex with NBD-A and SAH. Statistics for the crystallographic data collection and structure refinement are provided in Table 1. The overall fold of the ternary complex, solved at 2.1  $\text{\AA}$  resolution, was similar to the two previously reported structures of CmaA2 in complex with DOA and

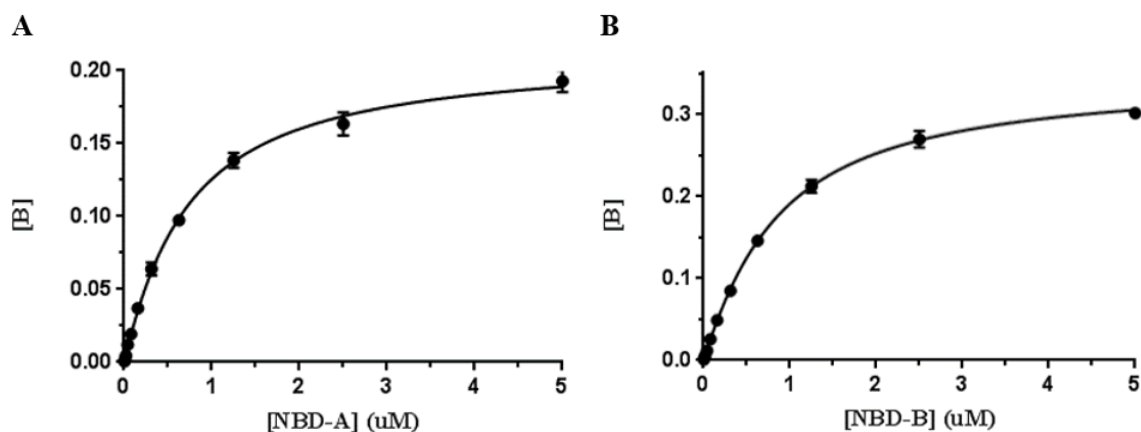


**Figure 11. Binding isotherms of CmaA2 and MmaA2 titrated with nitrobenzoxadiazole analogs of Compound 4.**

Nitrobenzoxadiazole analogs of Compound 4 demonstrate saturable binding when titrated (5  $\mu$ M to 5 nM) against 300 nM cyclopropane mycolic acid synthase supplemented with 300  $\mu$ M S-adenosyl methionine (SAM). A) Titration of N<sup>1</sup>-methyl-N<sup>3</sup>-(7-nitrobenzo[c][1,2,5]oxadiazol-4-yl)propane-1,3-diamine (NBD-A) against the CmaA2-SAM complex. B) Titration of N<sup>1</sup>-(7-nitrobenz[c][1,2,5]oxadiazol-4-yl)propane-1,3-diamine (NBD-B) against the MmaA2-SAM complex. Saturation binding data from triplicate experiments were fit to the general quadratic single-site binding equation using GraphPad software, whereby the dissociation constants of the complexes were determined.

DDDMAB (0.324 and 0.304  $\text{\AA}$ , respectively), with no major conformational changes to the polypeptide backbone or amino acids side chains in the acyl binding site (Barkan et al., 2009; Huang et al., 2002). Surface modeling of the CmaA2-NBD-A complex showed that the terminal basic amine (N02) was buried deep in the active site tunnel with the NBD fluorophore located to the extensively hydrophobic active site entrance (Figure 12A). N02 of NBD-A located to a near identical location at the base of the active site as previously described for the nitrogen atoms in DOA and DDDMAB (Barkan et al., 2009). The altered orientation of N02, as compared to N09 of dioctylamine, resulted in the formation of two hydrogen bonds, one with the bicarbonate ion and the other with the backbone oxygen of G145, at distances of 3.0 and 2.9  $\text{\AA}$ , respectively (Figure 12B). The N-methyl-1-

		CmaA2-SAH-NBD-A
Data collection	Space group	I4122
	Unit cell dimensions	
	a, b, c (Å)	106.39, 106.39, 227.11
	$\alpha$ , $\beta$ , $\gamma$ (°)	90, 90, 90
	Resolution <sup>a</sup>	48.18 - 2.04 (2.09 - 2.04)
	No. unique reflections	44918
	R <sub>merge</sub> (%) <sup>a</sup>	0.07 (1.18)
	I/ $\sigma$ <sup>a</sup>	43.1 (1.7)
	Redundancy <sup>a</sup>	12.9 (12.5)
	Completeness (%) <sup>a</sup>	99.68 (99.5)
Refinement	Resolution (Å)	48.18 - 2.04
	No. unique reflections	44918
	R <sub>work</sub> /R <sub>free</sub> (%)	16.2, 18.9
	R <sub>free</sub> test set (%)	4.45
	Wilson B-factor (Å <sup>2</sup> )	42.8
	Bulk solvent k <sub>sol</sub> (e/Å <sup>3</sup> ), B <sub>sol</sub> (Å <sup>2</sup> )	0.36, 55.6
	F <sub>o</sub> , F <sub>c</sub> correlation	0.97
	No. atoms	2584
	No. protein atoms	2392
	No. solvent atoms	143
	No. ligands	3
	RMSD bonds	0.017
	RMSD angles	1.26
	Average B, all atoms (Å <sup>2</sup> )	58
	Sidechain outliers (%)	1.58
	Ramachandran outliers (%)	0.35

**Table 1. Data collection and refinement statistics for CmaA2 in complex with N1-methyl-N3-(7-nitrobenzo[c][1,2,5]oxadiazol-4-yl)propane-1,3-diamine (NBD-A) and S-adenosyl homocysteine.** *a*, values in parenthesis are for the highest resolution shell

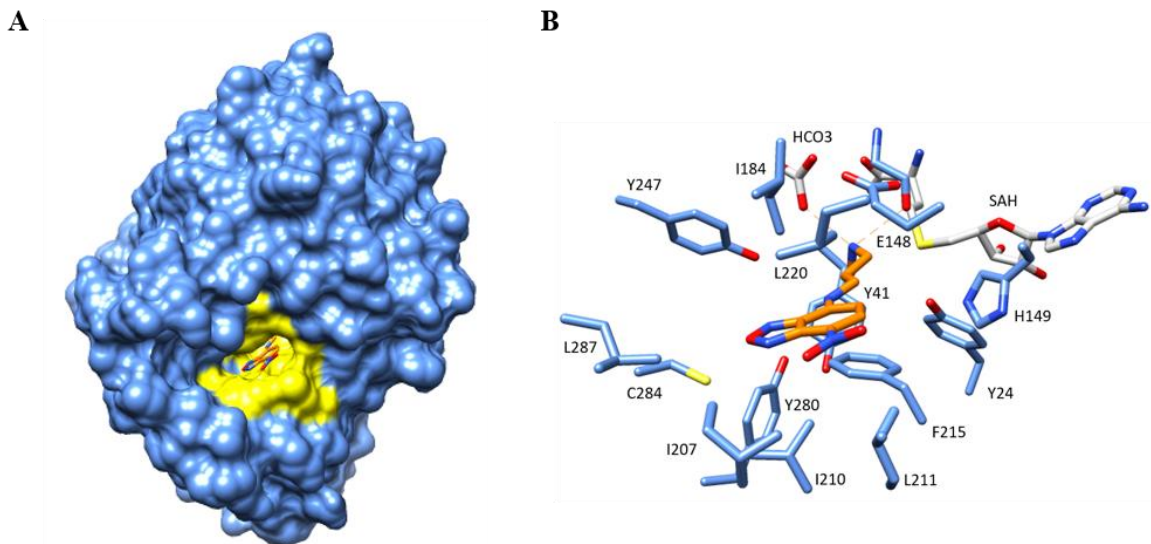


**Figure 12. CmaA2 in complex with N<sup>1</sup>-methyl-N<sup>3</sup>-(7-nitrobenzo[c][1,2,5]oxadiazol-4-yl)propane-1,3-diamine (NBD-A) and S-adenosyl homocysteine.**

A) Surface representation of CmaA2 in complex with S-adenosyl homocysteine (SAH) and NBD-A. Active site entrance residues (I184, I207, I210, L211, P215, L220, C284, L287, and T293) are highlighted in yellow, with NBD-A shown in stick representation. B) Amplified view of NBD-A bound to the active site. Amino acid residues at a distance of 5 Å from NBD-A are shown as light blue sticks with SAH and bicarbonate ion represented in grey. Carbon atoms of NBD-A are represented in orange, while heteroatoms are colored by convention. Hydrogen bonds are represented as orange dashed lines.

propanamine constituent of NBD-A traverses the active site tunnel positioning the NBD fluorophore to the entrance. At the entrance, the atoms of NBD are within the van der Waals radii of an array of hydrophobic amino acid residues (I184, I207, I210, L211, F215, L220, C284, and L287). These residues mark the residence site of the alkyl chain in the lipid substrate, that likely provides the apolar environment responsible for promoting NBD fluorescence enhancement. This structural analysis of the CmaA2-SAH-NBD-A ternary complex shows that upon CmaA2 binding, the NBD fluorophore experiences a significant change in environmental hydrophobicity as it relocates from the bulk aqueous solvent to the acyl binding site entrance.

*Small molecules competitively displace nitrobenzoxadiazole probes from multiple cyclopropane mycolic acid synthases*

To demonstrate that NBD analogs are competition displacement probes, we used the CMAS-fluorophore complexes in a DOA competitive assay. NBD-A and NBD-B were first bound to CmaA2 and MmaA2 then subjected to increasing concentrations of DOA. Probe displacement was measured by means of a decrease in fluorescence intensity (NBD-A Ex: 475 nm, Em: 530 nm; NBD-B Ex: 485 nm, Em: 545 nm) as DOA competes for the active sites. DOA reduced NBD fluorescence intensity in a dose-dependent fashion (Figure 13A and B). Analysis of the dose-response curves showed that this inhibitor was a highly effective active site competitor with  $K_d$  values of  $134 \pm 20$  nM (CmaA2) and  $103 \pm 22$  nM (MmaA2) (Table 2). This biochemical data agrees with our prior report showing that DOA inhibits CmaA2 and MmaA2 function in vivo (Barkan et al., 2009).

We then tested 4 and 5 as active site competitors in our displacement assays. Both molecules demonstrated dose-dependent displacement of the assay probes (Figure 13A and B). Analysis of the dose-response plots showed that both molecules were high affinity CMAS ligands (

Table 1), with  $K_d$  values  $\leq 40$  nM. We were unable to determine the binding affinity of Compound 5 towards either enzyme, likely resulting from a higher affinity than could be calculated with the current assay conditions. In addition, the binding affinity of compound 4 towards MmaA2 could not be accurately determined as the percent error was 50%. These data clearly demonstrate that our NBD competition displacement assays are suitable for multitarget assessment and are presumably limited to determining dissociation constants near single-digit nanomolar concentrations.

The dose-response plot for **5** showed that complete dissociation of the NBD fluorophores from CMAS resulted from 313 nM inhibitor. Given that complete dissociation of the NBD fluorophores by **5** would be achieved with concentrations between 156 and 313 nM, this dose-response data allowed the determination of a rough estimate of the binding stoichiometry between CMAS and NBD fluorophores. Throughout this study, CmaA2 ligand binding and competition displacement assays required 300 nM enzyme and 300  $\mu$ M SAM. When NBD-A was titrated the CmaA2-SAM complex (Figure 11, left), the maximum obtainable complex calculated was 213 nM with a  $K_d$  of 606 nM. The CmaA2 competition assays performed optimally with 600 nM NBD-A that resulted in an overall CmaA2-SAM-

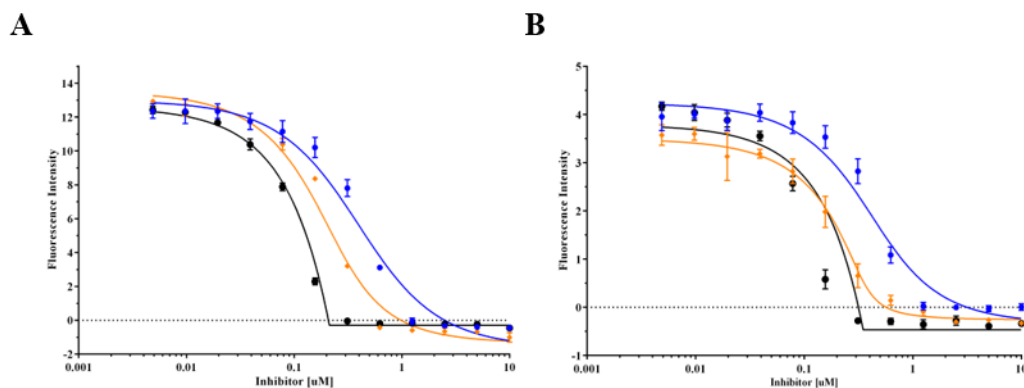


**Figure 13. Small molecules compete with nitrobenzoxadiazole probes for the active sites of cyclopropane mycolic acid synthases.**

A) Selected compounds were titrated against CmaA2 complexed with S-adenosyl methionine and N<sup>1</sup>-methyl-N<sup>3</sup>-(7-nitrobenzo[c][1,2,5]oxadiazol-4-yl)propane-1,3-diamine (NBD-A). B) Selected compounds were titrated against MmaA2 complexed with S-adenosyl methionine and N<sup>1</sup>-(7-nitrobenz[c][1,2,5]oxadiazol-4-yl)propane-1,3-diamine (NBD-B). Diocetylamine (blue), Compound 4 (orange), and Compound 5 (black). Competition displacement fluorescence intensity data was fit to the Wang model (Wang, 1995). Titration experiments were performed in triplicate.

NBD-A concentration of 160 nM. Under these conditions, complete displacement of NBD-A was established between 156 - 313 nM **5**, suggesting that the interaction between CmaA2-SAM and NBD-A closely approximates to a 1:1 binding stoichiometry. In a similar fashion, all of the MmaA2 assays required 300 nM enzyme and 300  $\mu$ M SAM. When NBD-B was titrated against MmaA2-SAM complex, the maximum obtainable complex calculated was 349 nM with a  $K_d$  of 670 nM (Figure 11, right). The MmaA2 competition assays performed optimally with a fixed NBD-B concentration of 600 nM, that resulted in a final MmaA2-SAM-NBD-B concentration of 237 nM. Under these conditions, complete displacement of NBD-B was established between 156 - 313 nM **5**, suggests that the interaction between MmaA2-SAM and NBD-B closely approximates to a 1:1 binding stoichiometry.

Compound	CmaA2 ( $K_d$ , nM)	MmaA2 ( $K_d$ , nM)	Binding Differential
dioctylamine	134 $\pm$ 20	103 $\pm$ 22	1.3
<b>4</b>	36 $\pm$ 5	8 $\pm$ 4	4.5
<b>5</b>	N/A	N/A	N/A

**Table 2.  $K_d$  and  $EC_{50}$  values of the selected small molecule cyclopropane mycolic acid synthase active site competitor ligands.**

Equilibrium dissociation constants were determined by fitting the competition displacement fluorescence intensity data to the Wang model (Wang, 1995). N/A represents data not available. The data represents the mean  $\pm$  standard error from triplicate experiments.

## Discussion

Since the first proposal of inhibiting mycolic acid cyclopropanation as an antibiotic strategy against Mtb, identification of inhibitors against CMAS has relied on in vitro drug screening using *E. coli* CFAS (George et al., 1995; Guianvarc'h et al., 2006, 2008). To date, this surrogate approach has only identified two multitargeting inhibitors of MA-MTs, dioctylamine and S-adenosyl-N-decyl-aminoethyl (Barkan et al., 2009; Guianvarc'h et al., 2006; Vaubourgeix et al., 2009). The lack of drug discovery progress may have resulted from insufficient drug screening efforts and/or poor translational growth inhibition of Mtb. As CMAS demonstrate poor in vitro enzymatic activity and MmaA3/4 assays have not been established, target-based screening small molecule collections have not been possible. Therefore, novel in vitro assay approaches for MA-MT drug screening are of dire need to assess this multitargeting strategy for the treatment of tuberculosis. Through combining differential scanning fluorimetry screening, chemical synthesis, ligand binding and competition displacement assays, we clearly demonstrated that a set of NBD fluorescence enhancement probes are well-suited for CMAS inhibitor discovery and multitarget assessment.

Our findings that the binding affinities of **4** and **5** were near or beyond the assay limit of detection, suggest that future inhibitor studies will require higher affinity assay probes. Despite our assay development success, molecules intended for structure-activity relationships will undoubtedly result in inhibitors with higher affinities than could be determined in our current assay conditions. Combining the observations that the N-methyl-1-propanamine constituent of NBD-A is critical for NBD fluorescence enhancement, the nitrogen atoms of DOA and NBD-A similarly locate at the site of methyl transfer, and that



DOA, **4**, and **5** effectively inhibit CMAS-NBD-A(B) complex formation, these data clearly establish a requirement for a terminal basic amine in future design strategies for generating higher affinity assay probes. The crystal structure of CmaA2 in complex with NBD-A provides a molecular framework for generating NBD-A analogs with enhanced binding affinity. Together, this structural data and observed differential binding affinity between **4** and **5** towards CMAS suggest that improving NBD probe affinity will entail modifying the constituents near the terminal nitrogen atom. This would require either repositioning the basic amine and/or enhancing the intermolecular contacts between the probe and polypeptide chain. Given that the binding affinity of **5** is near or beyond the detectable limit of our current assay conditions, NBD-**5** is currently the most promising starting point to increase the binding affinity of our assay probes.

An alternative method to improve CMAS assay limit of detection is through changing the assay methodology, from measuring direct fluorescence intensity to fluorescence polarization. The disadvantages of direct NBD fluorescence intensity measurements are intrinsic background fluorescence and low fluorescence brightness of the fluorophore. Resulting from the competitive nature of the NBD displacement assay, the assay limit of detection could be improved by increasing the CMAS-NBD-A complex concentration. This would require increasing the NBD probe concentration. However, the gain in fluorescence intensity by increasing the complex concentration will be offset by a higher background fluorescence signal, resulting in an increasingly diminished dynamic range of the assay. In addition, the NBD fluorophore is not very bright, that results in relatively low fluorescence emission output (Lancet and Pecht, 1977). Since fluorescence brightness plays a significant role in the measurable fluorescence signal, this assay format

requires relatively large amounts of enzyme. These unfavorable characteristics of our NBD approach could be alleviated through a fluorescence polarization assay, but a fluorescently-tethered ligand is required. The advantages of fluorescence polarization are the use of fluorophores with high fluorescence brightness and ratiometric detection with minimal background fluorescence, resulting in an assay platform where significantly less enzyme would be required with a large dynamic range (Lea and Simeonov, 2012). Fluorescence polarization assays have been developed for a wide-array of protein targets and are amenable to high throughput screening. Inferring from the structural similarity between **4**, **5**, and NBD-A, in addition to the observation that the nitro group of the NBD-A when complexed with CmaA2 is solvent exposed, these data suggest that the 4-chloro substituents on the high affinity ligands **4** and **5** should also be solvent exposed. Replacing the 4-chloro substituents on the naphthyl rings for a tethered fluorophore may generate suitable probes for fluorescence polarization assay development.

The development of fluorescent assay probes by naphthyl ring replacement for NBD reveals an assay development strategy that can be used to facilitate drug discovery for currently intractable protein targets. Current genome sequencing data far exceeds functional proteomics, and as a consequence the proteome of pathogenic organisms have not been functionally characterized. Exploiting this potentially vast drug target space will inevitably require novel assay methodologies. We envision that this assay development strategy can be implemented in two ways. The first approach follows the workflow used in this chapter. First, a small molecule library is screened against a protein target using DSF to identify naphthyl-containing ligands. Subsequently, NBD fluorescent analogs would be synthesized by naphthyl group replacement and assessed for fluorescence enhancement. The advantage

of this approach is the simultaneous identification of potential inhibitors in addition to parent molecule starting points for NBD-derivatization. As DSF-identified ligands may inevitably lack a naphthyl group, this chemical moiety may not be strictly required as a derivation starting point. Compound diversity libraries are strategically designed to survey vast chemical space that includes chemical moieties such as bicyclic ring systems and multi-substituted aromatics in that NBD replacement may generate suitable assay probes. DSF screening may afford molecules that lack a rational derivation starting point. If protein structure data is available, using a structure-guided design approach to strategically place an NBD fluorophore into an identified hydrophobic pocket, as similarly reported with NBD-dodecanoic acid bound to human serum albumin, may generate a viable assay probe (Wenskowsky et al., 2018). A major disadvantage of DSF is that not all proteins are suitable for the screening technique as observed with MmaA2 and PcaA in Chapter 3. In the second approach, an NBD-based diversity library would be synthesized and screened against a protein target. The advantage of this approach is ability to rapidly survey NBD-derivative chemical space. The major disadvantages of this approach, that may render the methodology impractical, are high cost and extensive chemical synthesis to generate the NBD-derivative library. Any fluorescent-enhancement probe identified, using either of the aforementioned approaches, may undergo further modification either to the non-fluorescent constituent or conjugated fluorophore that could significantly improve binding affinity and fluorescence signal output (Zhuang et al., 2013). Moreover, NBD probes that are effectively displaced by non-fluorescent ligands warrant further investigations into their suitability as a high throughput screening platform.

## Materials and Methods

### *Cloning, expression, and purification of recombinant Mycobacterium tuberculosis cyclopropane mycolic acid synthases*

*cmaA2* (Rv0503c), *mmaA2* (Rv0644c), and *pcaA* (Rv0470c) genes were amplified from H<sub>37</sub>Rv genomic DNA via polymerase chain reaction. *cmaA2* was cloned into pET28b-TEV whereas *mmaA2* and *pcaA* were cloned into pMCSG7. Positive clones, confirmed via DNA sequencing, were transformed into *E. coli* BL21 (DE3) for protein expression. Cell cultures were grown at 37 °C, in Luria-Bertani broth, until an OD<sub>600</sub> of ~ 0.8. The cultures were then chilled in an ice water bath for 20 mins. Protein expression was induced with 500 μM IPTG and protein production was allowed to proceed for 16 - 18 hr at 18 °C. Cell pellets were harvested and homogeneously suspended in an equal volume of 50 mM Tris-HCl, pH 8.0, 300 mM NaCl and lysed with a French press. Recovered supernatants were loaded onto Ni Sepharose 6 Fast Flow resin (GE Healthcare) and washed with 30-column volumes of 50 mM Tris-HCl, pH 8.0, 300 mM NaCl, 30 mM imidazole. His-tagged recombinant protein was eluted using 50 mM Tris-HCl, pH 8.0, 300 mM NaCl, 500 mM imidazole, then setup for his-tag removal via TEV proteolysis in 20 mM Tris-HCl, pH 8.0, 150 mM NaCl, 1 mM DTT for 2 hrs at 25 °C. The final purified protein was obtained after collecting the flow through fraction of a second pass through the Ni resin. As 6X-his-TEV-PcaA was observed to be a poor TEV protease substrate, the his-tag was not removed. Purified CMAS were buffer exchanged into 20 mM Tris-HCl, pH 8.0 and 50 mM NaCl using the concentrate and dilute method. All proteins were concentrated to 20 mg/mL and flash frozen in liquid nitrogen prior to storage at -80°.

*Synthesis of N<sup>1</sup>-methyl-N<sup>3</sup>-(7-nitrobenzo[c][1,2,5]oxadiazol-4-yl)propane-1,3-diamine (NBD-A) and N<sup>1</sup>-(7-nitrobenzo[c][1,2,5]oxadiazol-4-yl)propane-1,3-diamine (NBD-B)*

Step 1: In a 10mL microwave reaction vessel, respective N-boc-1,3-diaminopropanes (6.5 mmol, 1.3 equiv.) were dissolved in 2mL of anhydrous acetonitrile. Freshly activated potassium carbonate (1.5 mmol, 3.0 equiv.) was then added and stirred for 5 - 10 min at room temperature. After the addition of 4-chloro-7-nitrobenzofurazan (5.0 mmol, 1 equiv.), the reaction vessel was sealed and purged with nitrogen gas. The reaction was proceeded in a microwave reactor at 60 °C for 1.0 hr. The reaction mixture was cooled to room temperature and the contents were taken in ethyl acetate (25 ml) and washed with water (3 x 25 ml) and brine (2 x 25 ml). The combined organic layers were dried over anhydrous sodium sulfate and concentrated *in vacuo* to give brown residue that was purified by normal phase column chromatography. Elution at 30% ethyl acetate in hexane (v/v) gave the pure compounds as orange solids. *Tert*-butyl methyl(3-((7-nitrobenzo[c][1,2,5]oxadiazol-4-yl)amino)propyl)carbamate (NBD-A carbamate): Yield = 89 %; <sup>1</sup>H-NMR (400 MHz, CDCl<sub>3</sub>): δ 8.50 (d, 1H, 8.5 Hz), 7.76 (br, 1H), 6.20 (d, 1H, 8.5 Hz), 3.56 (t, 2H, 12 Hz), 3.44 (t, 2H, 12 Hz), 2.92 (s, 3H), 1.91-1.97 (m, 2H), 1.51 (s, 9H); HR-MS (FAB) *m/z* [M+H]<sup>+</sup>: 352.1615 (calc.), 352.1624 (found). *Tert*-butyl (3-((7-nitrobenzo[c][1,2,5]oxadiazol-4-yl)amino)propyl)carbamate (NBD-B carbamate): Yield = 86.0 %; <sup>1</sup>H-NMR (400 MHz, CDCl<sub>3</sub>): δ 8.50 (d, 1H, 8.5 Hz), 7.37 (br, 1H), 6.19 (d, 1H, 8.5 Hz), 4.77 (br, 1H), 3.32 (q, 2H, 6.2 Hz), 1.93 (q, 2H, 6.0 Hz), 1.49 (s, 9H); HR-MS (FAB) *m/z* [M+H]<sup>+</sup>: 338.1459 (calc.), 338.1472 (found).

Step 2: To a stirred solution of respective NBD-carbamates (0.5 mmol, 1 equiv.) in anhydrous dichloromethane (5.0 ml) at 0 °C, under a nitrogen atmosphere, 30% TFA in

DCM (3.0 equiv.) was added and stirred for 1 hr followed by 3 - 4 hr at room temperature. Reaction progress was monitored by TLC using dichloromethane:methanol:water (65:25:4 v/v) supplemented with 0.1 % triethylamine. Chilled ethyl ether (10 -15 ml) was then added to the reaction mixture and allowed to stand at 0 °C for one hour as the pure solid product precipitates. The product was filtered and washed thoroughly with diethyl ether. The solid product was then dried overnight under vacuum and purified by normal phase column chromatography. Elution at DCM: MeOH: H<sub>2</sub>O (60:30:4 v/v) with 0.1 % triethylamine gave the pure compounds as orange solids. N<sup>1</sup>-methyl-N<sup>3</sup>-(7-nitrobenzo[c][1,2,5]oxadiazol-4-yl)propane-1,3-diamine (NBD-A): Yield = 76 %; <sup>1</sup>H-NMR (DMSO-*d*<sub>6</sub>) δ 9.51 (br, 1H), 8.50 (d, 1H, 8.7Hz), 7.78 (br, 2h); 6.43 (d, 1H, 8.5Hz), 2.79-2.93 (m, 2H), 1.61-1.81 (m, 2H); <sup>13</sup>C-NMR (DMSO-*d*<sub>6</sub>) δ: 24.98, 38.95, 43.14, 99.69, 119.15, 121.19, 138.20, 144.86, 144.56; HR-MS (FAB) *m/z* [M+H]<sup>+</sup>: 238.0935 (calc.), 238.0934 (found). N<sup>1</sup>-(7-nitrobenzo[c][1,2,5]oxadiazol-4-yl)propane-1,3-diamine (NBD-B): Yield = 74 %; <sup>1</sup>H NMR (CD<sub>3</sub>OD) δ 8.50 (d, 1H, 8.7 Hz), 6.41 (d, 1H, 8.5 Hz), 3.69 (t, 4H, 6.3 Hz), 3.16-3.20 (m, 2H), 2.76 (s, 3H), 2.13-2.20 (m, 2H); <sup>13</sup>C-NMR (CD<sub>3</sub>OD) δ 24.69, 32.26, 40.29, 46.58, 98.86, 122.73, 133.52, 136.69, 144.07, 144.49; HR-MS (FAB) *m/z* [M+H]<sup>+</sup>: 252.1091 (calc.), 252.1101 (found).

#### *Direct fluorescence ligand binding assays*

Ligand binding assays were performed in Griener FluoTrac 600 96-well assay plates, 200 μL assay volume, in three steps. All liquid handing steps were performed using a Cybio Vario instrument. First, 96 μL of 100 mM NaH<sub>2</sub>PO<sub>4</sub>, pH 7.4, was transferred to each well of the assay plate. Second, 4 μL of a 50X NBD-A (or NBD-B) dilution series was added and mixed thoroughly. Third, 100 μL of 2X enzyme master mix (600 nM CmaA2/MmaA2 supplemented with 600 μM S-adenosyl methionine) was transferred to the assay plate. The

plates were then sealed and incubated overnight at 25 °C for 15 - 18 hrs. NBD-A and NBD-B fluorophores were used for CmaA2 and MmaA2, respectively. Then, the fluorescence intensity of each well was measured. using the following excitation and emission wavelengths (NBD-A Ex: 475 nm, Em: 530 nm; NBD-B Ex: 485 nm, Em: 545 nm). Analysis of the binding data was performed in a similar fashion as previously described (Bell, 1981).

#### *Fluorescence-based competition binding assays*

Competition binding assays were performed in Griener FluoTrac 600 96-well assay plates, 200  $\mu$ L assay volume, in three steps. All liquid handling steps were performed using a Cybio Vario instrument. First, 96  $\mu$ L of 100 mM NaH<sub>2</sub>PO<sub>4</sub>, pH 7.4, was transferred to each well. Second, 4  $\mu$ L of DMSO or 50X inhibitor dilution series was transferred to the plate and mixed thoroughly. Third, 100  $\mu$ L of 2X enzyme master mix (presence or absence of 600 nM CmaA2/MmaA2 supplemented with 600  $\mu$ M S-adenosylmethionine and 1.2  $\mu$ M fluorescent probe) was transferred to the assay plate. NBD-A or NBD-B fluorophores were used in CmaA2 or MmaA2 competition assays, respectively. Assay plates were then sealed and incubated overnight at 25°C for 15 - 18 hrs, then their fluorescence intensity measured (NBD-A, Ex/Em: 475 nm/530 nm; NBD-B, Ex/Em: 485 nm/545 nm). The dissociation constant of the inhibitors were calculated by fitting the data to the Wang model (Wang, 1995).

#### *Crystallization of CmaA2 in complex with N<sup>1</sup>-methyl-N<sup>3</sup>-(7-nitrobenzo[c][1,2,5]*

#### *oxadiazol-4-yl)propane-1,3-diamine and S-adenosyl homocysteine*

CmaA2 in complex SAH and NBD-A was co-crystallized using the hanging-drop vapor diffusion method. For co-crystallization of the CmaA2-SAH-NBD-A complex, the following procedure was carried out. A 2 mL solution containing 30  $\mu$ M (1 mg/mL) CmaA2,

200  $\mu$ M SAM, and 200  $\mu$ M NBD-A were incubated at 25 °C for 1 hr. The protein solution was concentrated to 10 mg/mL and mixed with equal portions of mother liquor to a final volume of 4  $\mu$ L. Mother liquor used: 0.1 M HEPES pH 7.2 and 1.0 M trisodium citrate. Crystals were ready for data collection in approximately one week at 18 °C. Crystals were cryo-preserved in mother liquor supplemented with 20 % glycerol prior to flash freezing in liquid nitrogen. The diffraction data were collected at beamline 19-ID at the Advanced Photon Source, Argonne National Laboratory. The data was processed and reduced using HKL2000 (Otwinowski and Minor, 1997).

#### *Structure determination and model refinement*

The structure of CmaA2 in complex with SAH and NBD-A was solved by molecular replacement using Phaser-MR in Phenix (Afonin et al., 2010). CmaA2-DOA (PDB code: 3HEM) was used as the search model once DOA and all solvent molecules were removed. The crystal was in the space group  $I4_122$ , with one molecule in the asymmetric unit with dimensions of  $a = b = 106.39$  and  $c = 227.11$  Å and  $\alpha = \beta = \gamma = 90^\circ$ . Subsequent to molecular replacement phasing, rigid body refinement was performed in PHENIX refine. The initial structure refinement produced a  $R_{\text{work}}$  and  $R_{\text{free}}$  of 24.9 % and 27.6 %, respectively (Afonin et al., 2010). Guided by the electron density within subsequent  $F_o - F_c$  maps examined in Coot, the three CmaA2 ligands, SAH, bicarbonate ion, and NBD-A were manually modelled. With further model building and PHENIX refinement cycles, 143 water molecules were added to yield a final  $R_{\text{work}}$  and  $R_{\text{free}}$  of 16.2 % and 18.9 %, respectively. The final model contained amino acids residues 12 - 302.



CHAPTER III  
CMAA2 HIGH THROUGHPUT SCREENING AND STRUCTURE GUIDED  
INHIBITOR DISCOVERY

**Overview**

To combat escalating rates and low treatment success of drug-resistant tuberculosis, novel chemotherapeutic agents that bypass current resistance mechanisms are urgently needed. Mycolic acids are the predominate lipid constituents found in the cell wall of *Mycobacterium tuberculosis* and are essential for cell viability. *M. tuberculosis* mycolic acids are extensively modified by cyclopropane rings, methyl branches, and oxygenated functional groups, that play fundamental roles in cell wall permeability and host-pathogen interactions. Mycolic acid modifications are incorporated into the meromycolate chain by a family of six highly similar S-adenosyl methionine (SAM)-dependent mycolic acid methyltransferases (MA-MTs: PcaA, CmaA2, MmaA1-4). Chemical inhibition studies using the multitargeting MAMT inhibitor dioctylamine have shown that simultaneous loss of mycolic acid modification results in the loss of cell viability and intrinsic resistance to established antituberculosis drugs. Given that cyclopropane mycolic acid synthases (CMAS) were found as the primarily targets of the compound and cyclopropane-deficient Mtb is severely growth attenuated in the mouse model of infection, attributed to the induction of an enhanced immune response, strongly indicates these enzymes as promising targets for antimycobacterial drug development.

Targeting CMAS with small druglike molecules has been hindered due to unsuitable in vitro assays for high throughput screening (HTS). We previously showed that

nitrobenzoxadiazole (NBD) competition displacement probes provide essential reagents for CMAS drug discovery, but their utility for HTS was not addressed. Here we show that NBD probe displacement is suitable for HTS and provides a highly effective approach to identify multitarget CMAS inhibitors. Our results herein show that the acyl binding sites of CMAS accommodate dioctylamine-like amphipathic small molecules of broad chemical diversity, wherein a selected collection of CMAS ligands were found to simultaneously inhibit multiple pathways of mycolic acid modification in vivo. The crystal structures of CmaA2-inhibitor complexes corroborate the hypothesis that amine-based ligands inhibit CMAS function through mimicking the carbocation reaction intermediate. Additionally, these data provide a foundation for structure-guided inhibitor design. Furthermore, Mtb kill-curve analysis suggests that compounds that simultaneously inhibit MA-MTs are bacteriostatic, and not bactericidal as previous thought.

## **Introduction**

Tuberculosis is a highly contagious airborne disease caused by the bacterium *Mycobacterium tuberculosis* (Mtb) that has plagued mankind for centuries and was once thought as a death sentence. Globally, tuberculosis (TB) is the leading cause of human mortality by a single infectious agent (World Health Organization, 2018). Drug-sensitive TB is often curable with the 6 to 9-month first-line standard combination drug regimen, but the emergence of multidrug-resistant Mtb strains has complicated therapeutic options (Dheda et al., 2017). The persistent threat of drug-resistant Mtb in addition to the lengthy duration of antibiotic therapy has placed an urgent need for the discovery of new antitubercular agents with novel modes of action and the capacity to shorten the duration of curative TB treatment.

Mycolic acids are the signature high-molecular-weight  $\alpha$ -alkyl- $\beta$ -hydroxy fatty acids found incorporated into the outer asymmetric bilayer of the mycobacterial cell wall. Within the inner leaflet, mycolic acids are esterified to the non-reducing termini of arabinan units of the underlying arabinogalactan, generating a cell wall lipid coat of unusually low fluidity and permeability, that in part contributes to intrinsic antibiotic resistance (Brennan and Nikaido, 1995; Liu et al., 1996). In the outer solvent-extractable leaflet, mycolic acids intercalate as lipid conjugates and have been found to play a critical role in host-pathogen interactions (Dao et al., 2008; Rao et al., 2005, 2006; Welsh et al., 2013). Mtb synthesizes three mycolic acid types:  $\alpha$ -mycolate, methoxymycolates, and ketomycolates that are characterized by distinct modifications incorporated at two positions along the meromycolate chain, proximal and distal (Figure 3). The proximal position is strictly cyclopropanated, whereas the distal position harbors either a *cis*-cyclopropane ring or oxygenated function group ( $\alpha$ -methyl methylether or  $\alpha$ -methyl ketone). The meromycolate chain in  $\alpha$ -mycolates contain two *cis*-cyclopropane rings. Oxygenated mycolates contain a proximal *cis*- or methyl-branched *trans*-cyclopropane ring but vary in their distal modification. Through extensive genetic studies, a family of MA-MTs have been found to be responsible for incorporating the various mycolic acid modifications (Barkan et al., 2010; Dubnau et al., 2000; Glickman, 2003; Glickman et al., 2000, 2001, Yuan et al., 1997, 1998a). This family of enzymes are highly similar with respect to primary and tertiary structure, but perform distinct site-specific chemical transformations (Figure 6A to C). PcaA and MmaA2 incorporate *cis*-cyclopropane rings into the proximal and distal positions of  $\alpha$ -mycolates, respectively (Glickman, 2003; Glickman et al., 2000). MmaA1 and CmaA2 function in *trans*-cyclopropane synthesis of oxygenated mycolates (Barkan et al., 2010; Glickman et al.,

2001; Yuan et al., 1997). CmaA2 and MmaA2 have a functionally redundant role for incorporating *cis*-cyclopropane rings into  $\alpha$ - and oxygenated mycolates (Barkan et al., 2010). Incorporation of a distal hydroxy group by MmaA4 produces a fundamental precursor that is subsequently methylated by MmaA3 or oxidized by an unknown oxidase, generating methoxy- and ketomycolates respectively (Behr et al., 2000; Dubnau et al., 2000; Quémard et al., 1997; Yuan et al., 1998a).

Extensive prior data has revealed that Mtb mycolic acid modifications play important roles in membrane permeability and virulence (Barkan et al., 2009; Dao et al., 2008; Dubnau et al., 2000; Glickman et al., 2000; Rao et al., 2005, 2006, Yuan et al., 1997, 1998a). Mtb harboring cell walls with differentially modified mycolic acids as a result of overexpressing either *mmaA1* or *mmaA3* or genetically inactivating *mmaA4* results in altered cellular uptake of many substances and drug susceptibility, in addition to significantly hindering growth in suboptimal growth temperatures (Dubnau et al., 2000; Yuan et al., 1997, 1998a). Notably, the  $\Delta mmaA4$  mutant was recently shown to be exceptionally sensitive to rifampicin treatment (Sambandan et al., 2013). Moreover, simultaneous inhibition of mycolic acid modification with the multitargeting MA-MT inhibitor dioctylamine (DOA) resulted in a synergistic effect with ciprofloxacin and isoniazid, wherein the observed synergy with ciprofloxacin was attributed to enhanced cell wall penetration (Barkan et al., 2009). This may equally explain the observed synergy with isoniazid and/or possibly their combined effect on mycolic acid synthesis. With respect to pathogenesis, Mtb  $\Delta pcaA$  and  $\Delta cmaA2$  mutants are differentially recognized by the murine immune system. The  $\Delta pcaA$  mutant is hypostimulatory upon macrophage infection, shows an early growth defect in the lung with a persistence defect upon activation of the adaptive immune response, and was unable to

establish a chronic lethal infection (Glickman et al., 2000; Rao et al., 2005). In contrast, the  $\Delta cmaA2$  mutant is hyperstimulatory upon macrophage infection, is hypervirulent in the mouse model of infection, induces extensive tissue damage, and causes premature death of the host (Rao et al., 2006). Recently, a cyclopropane-deficient Mtb strain was reported to be severely growth attenuated upon murine infection with an enhanced immune response, although it is currently unknown whether this heightened immune activity is beneficial or detrimental to the host (Barkan et al., 2012). In addition, the  $\Delta mmaA4$  mutant stimulates increased IL-12 production and is unable to establish a chronic lethal infection (Dao et al., 2008). Together, these results indicate MA-MTs as attractive drug targets, but small molecule inhibitors against this family of enzyme are lacking as in vitro assays suitable for high throughput screening are currently unavailable.

We previously showed that NBD probes are suitable CMAS ligands for competition displacement assay development, but their utility in HTS screening was not investigated (*see* Chapter 2). Herein we address the suitability of NBD probe displacement as an HTS assay platform and assess the multitargeting capacity of the identified inhibitors. Through HTS screening and confirmatory competition displacement assays, we show that the acyl binding sites of CMAS accommodate an array of small druglike molecules with amphipathic nature similar to dioctylamine. Moreover, we show that identified multitargeting CMAS ligands inhibit multiple pathways of mycolic acid modification *in vivo*. The molecular basis of inhibition was attributed to mimicking the common carbocation reaction intermediate, as established through crystallographic analysis of CmaA2-inhibitor complexes. Given the prior report indicating that simultaneous inhibition of mycolic acid modification is lethal to

Mtb, we tested our multitargeting MA-MT inhibitors in kill-curve assays, wherein the data suggests that this multitargeting approach is bacteriostatic.

## **Results**

### *Differential scanning fluorimetry small molecule screening identifies high affinity cyclopropane mycolic acid synthase ligands*

CMAS target-based inhibitor screening is currently prohibited due to poor in vitro enzymatic activity, therefore we initiated MA-MT drug discovery using differential scanning fluorimetry (DSF) as an assay surrogate. DSF is a rapid and inexpensive fluorescence-based screening technique that provides an indication of ligand binding through a change in protein thermal stability. As thermal denaturation of proteins demonstrate variable propensity to DSF detection, we first tested purified recombinant CMAS (CmaA2, MmaA2, and PcaA) in the presence and absence of SAM against a series of buffers, pH 5.5 - 8.5. CMAS enzymes were used because they were shown to be the primary targets of dioctylamine. CmaA2 was the only CMAS to demonstrate measurable temperature-dependent unfolding (Figure 14A to F).

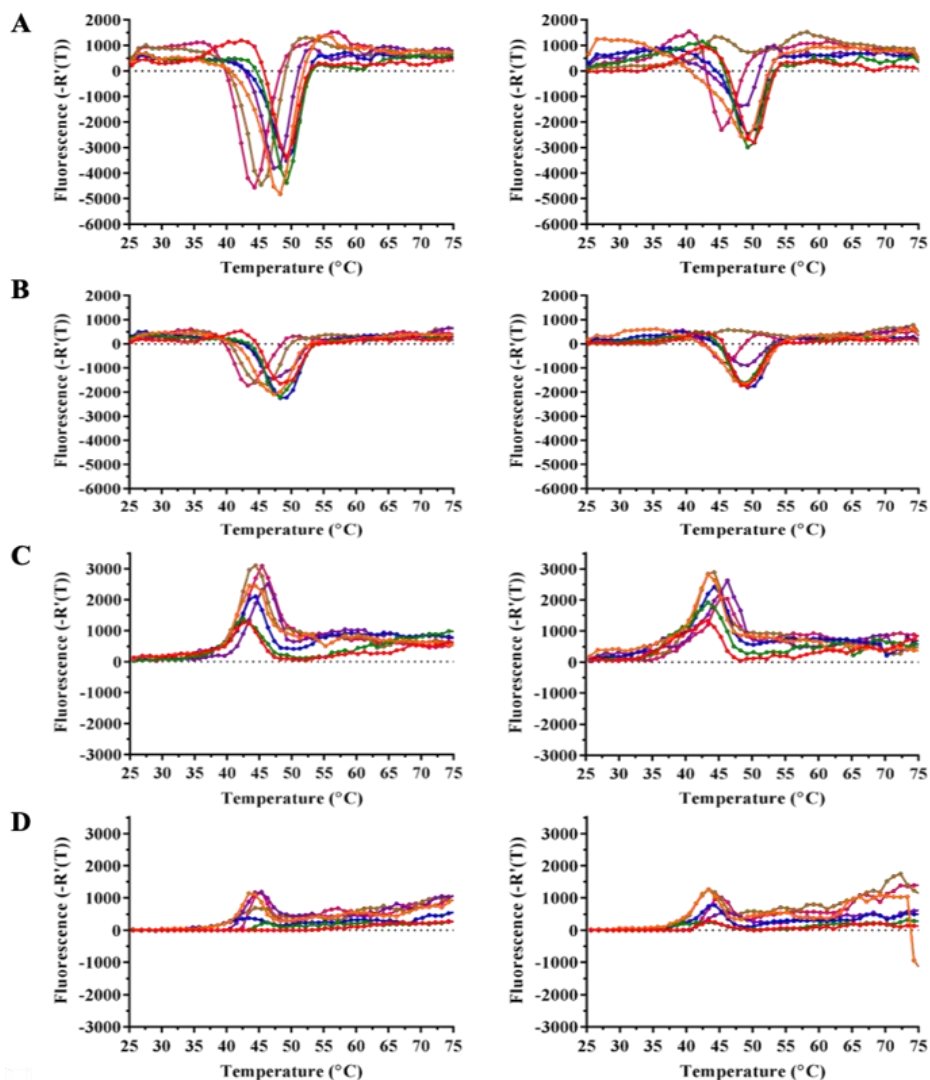


**Figure 14. Thermal denaturation profiles of cyclopropane mycolic acid synthases in various buffer conditions.**

Purified recombinant cyclopropane mycolic acid synthases were thermally denatured in various buffers in the presence or absence of 200  $\mu\text{M}$  *S*-adenosyl methionine (SAM). A) 2  $\mu\text{M}$  CmaA2, left, and 2  $\mu\text{M}$  CmaA2 + SAM, right; B) 5  $\mu\text{M}$  CmaA2, left, and 5  $\mu\text{M}$  CmaA2 + SAM, right; C) 2  $\mu\text{M}$  MmaA2, left, and 2  $\mu\text{M}$  MmaA2 + SAM, right; D) 5  $\mu\text{M}$  MmaA2, left, and 5  $\mu\text{M}$  MmaA2 + SAM, right; E) 2  $\mu\text{M}$  PcaA, left, and 2  $\mu\text{M}$  PcaA + SAM, right; F) 5  $\mu\text{M}$  PcaA, left, and 5  $\mu\text{M}$  PcaA + SAM, right. Buffers tested at 100 mM were: sodium citrate pH 5.5 (red), MES pH 6.0 (orange), PIPES pH 6.5 (green), MOPS pH 7.0 (blue), HEPES pH 7.5 (purple), imidazole pH 8.0 (brown), and BICINE pH 8.5 (pink). Experiments were performed in triplicate with similar results.

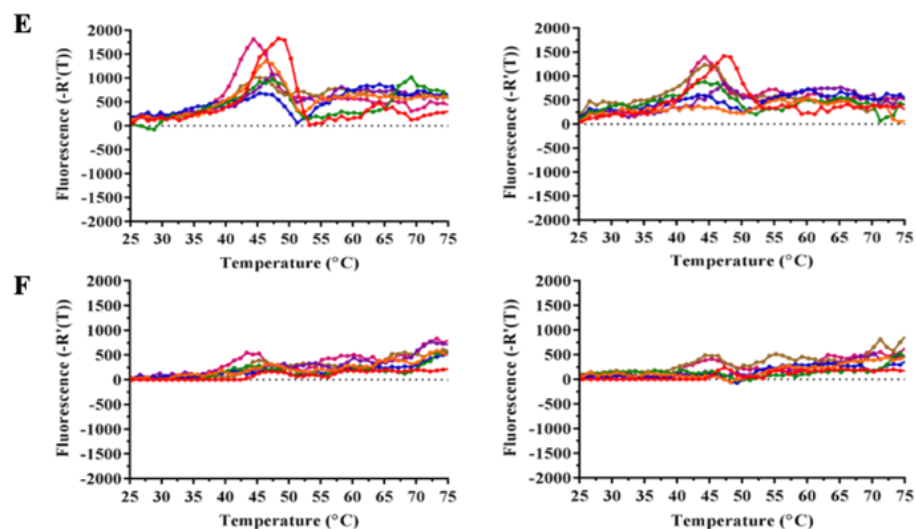
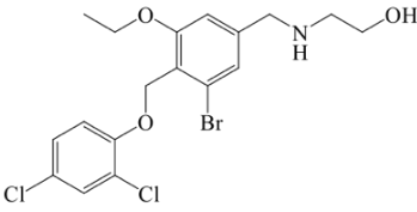
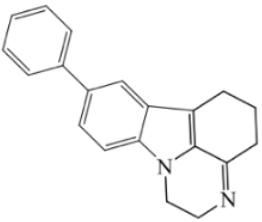
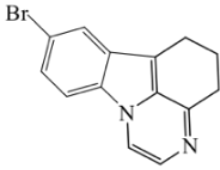
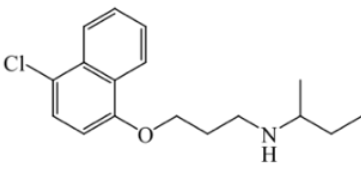
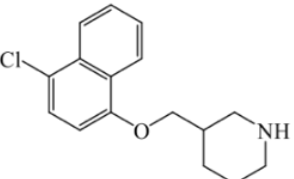


Figure 14, Continued.

We then screened a collection of 2,506 whole-cell active small molecule inhibitors against the CmaA2-SAM binary complex. The inhibitor collection was created from hits identified from an approximately 105,000 small molecule in-house diversity library assayed against Mtb mc<sup>2</sup>7000, in addition to a set of active molecules against Mtb H<sub>37</sub>Rv obtained from Southern Research Institute (Ananthan et al., 2009). We tested the collection using a concentration of about 25  $\mu$ M and found only five molecules that showed a shift in the melting temperature ( $\Delta T_m$ ) of CmaA2 by  $\geq 3$   $^{\circ}$ C (25  $\mu$ M DOA,  $\Delta T_m = 3$   $^{\circ}$ C) (Table 3). The five molecules cluster into three chemically distinct classes. Compound **1** ( $\Delta T_m$  of 3  $^{\circ}$ C) consists of a multi-substituted benzene core with hydrophobic substituents located distal to a terminal ethanolamine. Compounds **2** and **3** are 8-substituted pyrazinocarbazoles whereby



Compound	Chemical Structure	$\Delta T_m$
1		3°C
2		4.5°C
3		3.5°C
4		4°C
5		3°C

**Table 3. Chemical structures of five small molecules identified as CmaA2 thermal stabilizers via differential scanning fluorimetry screening.**

The change in melting temperatures ( $\Delta T_m$ ) were determined as the difference between the  $T_m$  of CmaA2 supplemented with S-adenosyl methionine in the presence and absence of small molecule ligands.

the aryl substituted Compound **2** provided a  $\Delta T_m$  of 4.5 °C, whereas the bromine- substituted analog provided a  $\Delta T_m$  of 3.5 °C. Compounds **4** and **5** are 4-chloronaphthoxyalkylamines whereby **4** provided greater CmaA2 thermal stability of  $\Delta T_m$  of 4 °C than the conformationally constrained **5**,  $\Delta T_m$  of 3 °C. Interestingly, All of the hit compounds are amine-containing amphiphiles that are in good structural agreement with DOA (Barkan et al., 2009).

We then tested all five DSF-identified molecules in our displacement assays as described in Chapter 2. All five molecules demonstrated dose-dependent displacement of the assay probes (Figure 15). Analysis of the dose-response plots showed that nearly all of the compounds were high affinity CMAS ligands (Table 4), with  $K_d$  values < 50 nM. Compounds **1** and **4** showed comparable binding differential between CMAS (CmaA2, **1**:  $K_d = 41 \pm 6$  nM, **4**:  $K_d = 36 \pm 5$  nM; MmaA2, **1**:  $K_d = 21 \pm 5$  nM, **4**:  $K_d = < 10$  nM; Binding differential (BD), **1**:  $BD_{CMAS} = 2.0$ ; **4**:  $BD_{CMAS} = 4.5$ ) as similarly observed with DOA (CmaA2, DOA:  $K_d = 134 \pm 20$  nM; MmaA2, DOA:  $K_d = 103 \pm 22$  nM;  $BD_{CMAS} = 1.3$ ). Compound **2** was a high affinity ligand of CmaA2 (**2**:  $K_d = 36 \pm 7$  nM), however the binding affinity could not be determined for MmaA2. Overall, Compound **5** was likely the most potent active site competitor of CMAS, as the binding affinity could not be established for either enzyme. The binding differential could not be calculated because the compound's affinity towards CMAS was higher than could be determined with the current assay conditions. Compound **3** exhibited a 45.8-fold binding differential, resulting from a substantially lower affinity towards MmaA2 (CmaA2, **3**:  $K_d = 31 \pm 5$  nM; MmaA2, **3**:  $K_d = 1,420 \pm 306$  nM;  $BD_{CMAS} = 45.8$ ). Whereas the majority of multitargeting CMAS ligands demonstrated  $IC_{50s} < 2 \mu M$  against Mtb mc<sup>2</sup>7000, the whole-cell activity of **3** was reduced

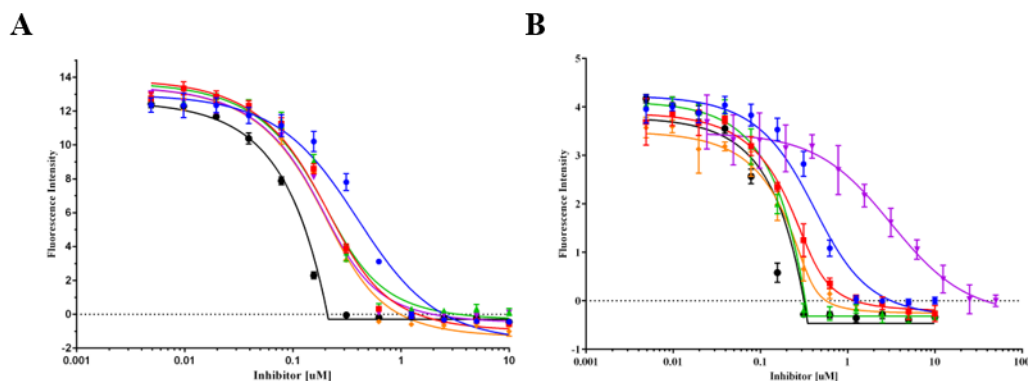


**Figure 15. Dioctylamine and differential scanning fluorimetry-identified small molecules are active site competitors of cyclopropane mycolic acid synthases.**

A) Selected compounds were titrated against CmaA2 complexed with S-adenosyl methionine and N<sup>1</sup>-methyl-N<sup>3</sup>-(7-nitrobenzo[c][1,2,5]oxadiazol-4-yl)propane-1,3-diamine (NBD-A). B) Selected compounds were titrated against MmaA2 complexed with S-adenosyl methionine and N<sup>1</sup>-(7-nitrobenz[c][1,2,5]oxadiazol-4-yl)propane-1,3-diamine (NBD-B). Compounds tested: Compound 1 (red), Compound 2 (green), Compound 3 (purple), Compound 4 (orange), and Compound 5 (black). Competition displacement fluorescence intensity data was fit to the Wang model (Wang, 1995). Titration experiments were performed in triplicate.

Compound No.	CmaA2 (K <sub>d</sub> , nM)	MmaA2 (K <sub>d</sub> , nM)	Binding Differential	Mtb (IC <sub>50</sub> , μM)	HDF (IC <sub>50</sub> , μM)	HepG2 (IC <sub>50</sub> , μM)
DOA	134 ± 20	103 ± 22	1.3	3.5	>100	-
1	41 ± 6	21 ± 5	2.0	0.8	3.7	>100
2	36 ± 7	<10	-	1.1	>100	-
3	31 ± 5	1,420 ± 306	45.8	7.2	-	-
4	36 ± 5	<10	4.5	1.5	22.7	7.0
5	<10	<10	-	0.6	11.4	-

**Table 4. K<sub>d</sub> and IC<sub>50</sub> values of differential scanning fluorimetry-identified small molecules.**

Equilibrium dissociation constants for the selected inhibitors were determined by fitting the competition displacement fluorescence intensity data to the Wang model (Wang, 1995). The data represents the mean ± standard error from triplicate experiments.

by 4.8 to 12-fold. Cytotoxicity testing using human dermal fibroblast (HDF) revealed that all of the compounds showed signs of cellular toxicity as the therapeutic indices [T.I. = (IC<sub>50</sub>

HDF)/(IC<sub>50</sub> Mtb)] were significantly less than 50, with the exception of Compound **2**. Additional cytotoxicity testing using human HepG2 cells were performed with compounds that were identified to inhibit multiple pathways of mycolic acid modification (see *Multitargeting CMAS ligands inhibit multiple pathways of mycolic acid modification*). Unlike the HDF cytotoxicity observed with **1**, this compound was not cytotoxic to HepG2 cells. In contrast, compound **4** was toxic to both cell types.

*CmaA2 high throughput screening identifies structurally diverse multitarget cyclopropane mycolic acid synthase ligands*

To establish the CmaA2-NBD-A displacement assay as an HTS platform, we screened our in-house Mtb-active small molecule collection against the CmaA2-NBD-A complex. Prior DSF-screening efforts solely identified five high affinity molecules that clustered into three structurally distinct classes. Given the fact that our collection contains many structural analogs to the DSF-identified compounds, this suggested that a multitude of potential multitargeting CMAS ligand may have gone unidentified. Based on this, we screened the collection at concentration of approximately 10  $\mu$ M in a 384-well format. The 96-plate HTS averaged a Z'-factor of 0.62 for the controls, indicating the HTS assay is of good quality (Figure 16). We identified 39 compounds exhibiting  $\geq 85\%$  inhibition (35 were  $\geq 2\sigma$  from the population mean), resulting in a hit rate of 1.6 %. Four of the 5 compounds identified using DSF (**1**, **2**, **4**, and **5**) were identified in the HTS screen.

Of the 39 HTS hits, sufficient material for dose-response was available for 35. Of these, 30 compounds exhibited dose-dependent inhibition; their chemical structures are provided in Figure 17. Several phenoxyalkylimidazole analogs were identified (**H3** to **H18**), a structural class previously reported to have good antimycobacterial activity (Ananthan et al., 2009).

With the addition of **H19**, these seventeen compounds are all chemically analogous to **4** and **5** (**H1** and **H2**). We also identified **H21** that structurally clusters with **2** (**H20**) and **3**.

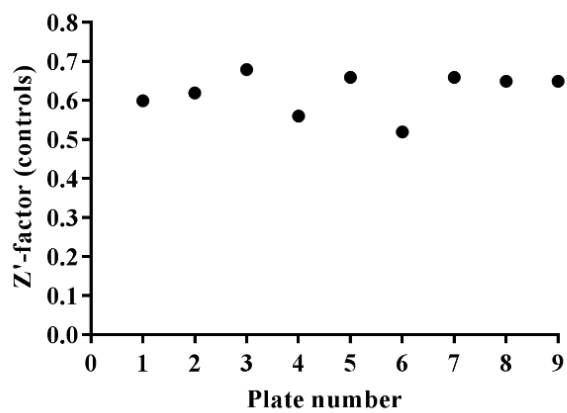


**Figure 16. CmaA2 high throughput screening plate Z'-factors**

The plate Z'-factor for the controls of each high throughput screening plate was calculated using Collaborative Drug Discovery software.

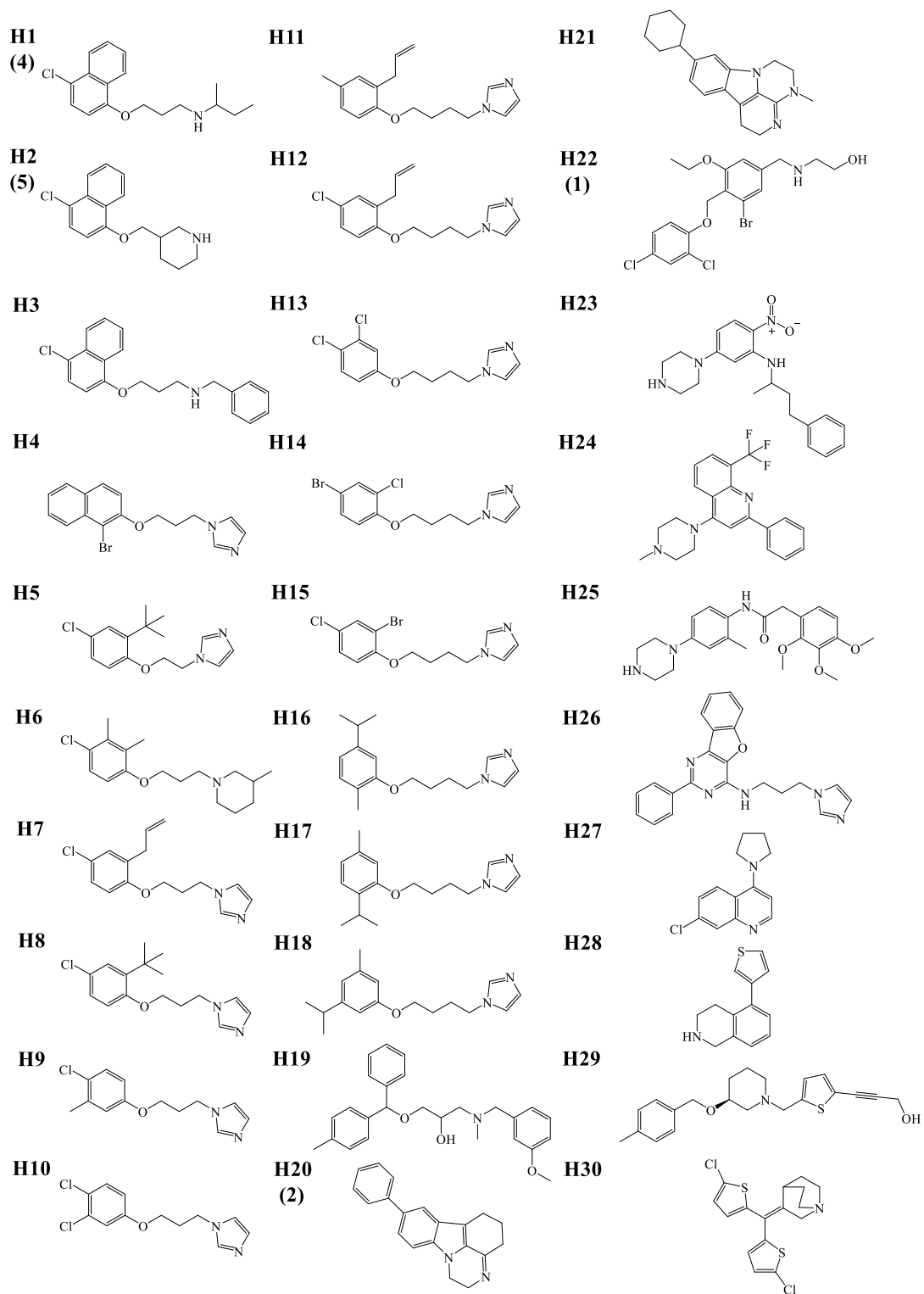


**Figure 17. Chemical structures of 30 compounds identified via CmaA2 high throughput screening**  
 Numbers in parenthesis denote compounds previously found with differential scanning fluorimetry screening (see Table 3).

Of the 30 confirmed hits, 16 were commercially available in the quantities needed so that we could establish their binding affinity and multitargeting capacity towards CMAS. The chemical structures and biochemical data for these 16 confirmed hits are provided in Figure 18 and Table 5, respectively. Most inhibitors exhibited high binding affinity towards CmaA2 ( $K_d < 100$  nM), however not all showed similar affinities for MmaA2. Using a criterion defined by binding affinity and whole-cell activity of DOA (an approximate  $K_d \leq 150$  nM for both CMAS, similar binding differential, and Mtb mc<sup>2</sup>7000  $IC_{50} < 3.5$   $\mu$ M), we

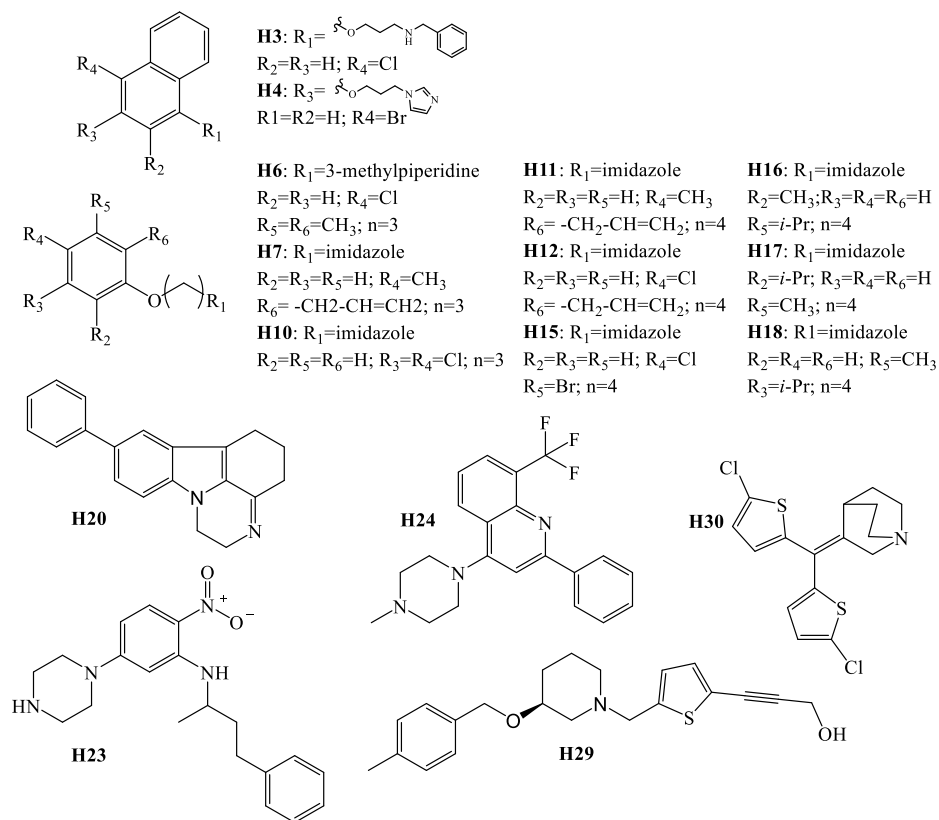


**Figure 18. Chemical structures of commercially available CmaA2 ligands identified via high throughput screening.**

Compound	CmaA2 (K <sub>d</sub> , nM)	MmaA2 (K <sub>d</sub> , nM)	Binding Differential	Mtb (IC <sub>50</sub> , μM)	HDF (IC <sub>50</sub> , μM)	HepG2 (IC <sub>50</sub> , μM)
<b>H3</b>	83 ± 8	58 ± 12	1.4	1.2	>100	-
<b>H4</b>	93 ± 11	359 ± 98	3.9	5.8	-	-
<b>H6</b>	43 ± 2	97 ± 13	2.3	5.6	-	-
<b>H7</b>	27 ± 3	1,300 ± 198	48.1	16.5	-	-
<b>H10</b>	234 ± 19	2,626 ± 434	11.2	7.3	-	-
<b>H11</b>	37 ± 3	158 ± 32	4.2	6.8	-	-
<b>H12</b>	44 ± 7	268 ± 44	6.1	3.9	-	-
<b>H15</b>	181 ± 15	1,181 ± 148	6.5	3.1	-	-
<b>H16</b>	83 ± 7	826 ± 116	10.0	7.4	-	-
<b>H17</b>	517 ± 41	583 ± 122	1.1	6.2	-	-
<b>H18</b>	441 ± 44	1717 ± 254	3.9	6.9	-	-
<b>H21</b>	908 ± 108	3606 ± 956	4.0	8.8	-	-
<b>H23</b>	88 ± 8	40 ± 13	2.2	1.5	11.6	3.7
<b>H24</b>	88 ± 5	124 ± 14	1.4	2.3	>100	-
<b>H29</b>	54 ± 9	19 ± 4	2.8	0.4	9.3	-
<b>H30</b>	37 ± 3	402 ± 33	10.9	2.2	-	-

**Table 5. K<sub>d</sub> and IC<sub>50</sub> values of selected compounds identified through CmaA2 high throughput screening.**

Equilibrium dissociation constants for the selected inhibitors were determined by fitting the competition displacement fluorescence intensity data to the Wang model (Wang, 1995). The data represents the mean ± standard error from triplicate experiments. N/A represents data not available. Human dermal fibroblast cell (HDF) and human liver carcinoma cell (HepG2) cytotoxicity assays were performed as a single titration experiment.

identified a chemically diverse set of four novel compounds (**H3**, **H23**, **H24**, and **H29**) with high affinity towards CMAS (CmaA2: K<sub>d</sub> = 54 - 88 nM; MmaA2: K<sub>d</sub> = 19 - 124 nM), < 3-fold binding differential, and good growth inhibitory activity of Mtb mc<sup>2</sup>7000 (IC<sub>50</sub>s < 2.5 μM). HDF cytotoxicity assays suggest that **H3** and **H24** were not cytotoxic, whereas **H23** and **H29** showed signs of cytotoxicity. Additional cytotoxicity testing using human HepG2 cells were performed with Compound **H23** as it was the only novel compound identified in CmaA2 HTS that is later shown to inhibit multiple pathways of mycolic acid modification



(see *Multitargeting CMAS ligands inhibit multiple pathways of mycolic acid modification*).

**H23** was additionally cytotoxic to HepG2 cells.

As nearly all reported CmaA2-ligand crystal structures are complexed with S-adenosyl homocysteine (SAH) and our displacement assays were performed with SAM, we reassessed the binding affinities of a diverse subset of inhibitors to determine whether preferential binding occurred between the CMAS-SAM and CMAS-SAH binary complexes (Barkan et al., 2009; Huang et al., 2002). Overall, the compounds showed similar binding affinity towards the CMAS-SAH and CMAS-SAM complexes, but generally trended slightly higher towards CMAS-SAH (Table 6). Whether inhibition of CMAS function results from inhibitor binding to the CMAS-SAM, CMAS-SAH, or both has not been established.

Compound	CmaA2 (K <sub>d</sub> , nM)	MmaA2 (K <sub>d</sub> , nM)	Binding Differential	CmaA2, K <sub>d</sub> (SAM/SAH)	MmaA2, K <sub>d</sub> (SAM/SAH)
1	< 10	< 10	-	-	-
2	< 10	< 10	-	-	-
4	< 10	< 10	-	-	-
H3	76 ± 18	60 ± 17	1.3	1.1	1.0*
H4	50 ± 11	186 ± 35	3.7	1.9	1.9
H7	<10	726 ± 125	-	-	1.8
H10	92 ± 14	1,233 ± 220	13.4	2.5	2.1
H11	14 ± 3	88 ± 25	6.3	2.6	1.8
H15	123 ± 24	514 ± 93	4.2	1.5	2.3
H17	45 ± 9	422 ± 78	9.4	11.5	1.4
H23	29 ± 5	< 10	-	3	-
H24	183 ± 29	123 ± 28	1.5	2.1*	1.0
H29	75 ± 11	16 ± 5	4.7	1.4*	1.2
H30	21 ± 4	154 ± 17	7.3	1.8	2.6

**Table 6. K<sub>d</sub> values of selected compounds identified through differential scanning fluorimetry and high throughput screening in the presence of S-adenosyl homocysteine.**

Equilibrium dissociation constants for the selected inhibitors were determined by fitting the competition displacement fluorescence intensity data to the Wang model (Wang, 1995). The data represents the mean ± standard error from triplicate experiments. Higher S-adenosyl methionine (SAM)/S-adenosyl homocysteine (SAH) ratio indicates the fold increase in binding affinity towards cyclopropane mycolic acid synthase (CMAS) in complex with SAH. The values marked with asterisks are an exception. In these cases, the SAM/SAH ratio (actually calculated as SAH/SAM) indicates the fold increase in binding affinity towards the CMAS-SAM complex, as the compounds showed higher affinities for the CmaA2-SAM complex.

*CmaA2 high throughput screening the Sanofi proprietary Mycobacterium tuberculosis whole cell active collection*

To further expand the set of potential multitargeting CMAS inhibitors, we screened a proprietary set of 2,035 Mtb whole-cell active growth inhibitors acquired from Sanofi against the CmaA2-NBD-A complex. Sanofi is a biopharmaceutical company dedicated to drug discovery and development for a variety of human diseases. The collection was screened against CmaA2 using a concentration of approximately 20 μM in a 384-well format. The average Z'-factor for the controls of the 9-plate HTS was 0.52, indicating the

assay performed well. We identified 10 compounds having a Z-score value  $\geq 2\sigma$  from the population mean, resulting in a hit rate of 0.5 %.

Of the 10 hits, sufficient material for 9 compounds were provided by Sanofi to establish the binding affinity and multitarget capacity towards CMAS. Seven compounds demonstrated dose-dependent inhibition of CMAS-NBD-A(B) complex formation (Table 7). The chemical structures of the 7 hit compounds have been disclosed, but cannot be provided herein due to the proprietary nature of the compounds. However, the compounds show extensive structural diversity and are all amine-based amphiphiles that perfectly agrees with the previously identified multitargeting CMAS ligands. The highest affinity CMAS ligands identified from the Sanofi collection were X-33515 (CmaA2/MmaA2  $K_d < 10$  nM) and X-3870D (CmaA2,  $K_d = 173$  nM; MmaA2,  $K_d = 14$  nM;  $BD_{CMAS} = 12.3$ ). The X-33515 structural analog, X-32454, was also a CmaA2 high affinity ligand (CmaA2,  $K_d < 10$  nM) but showed substantially lower binding affinity towards MmaA2 (MmaA2,  $K_d = 484$  nM). Finally, the opposite result occurred for X-3709B. The compound is structurally similarly to X-33515, but showing higher affinity towards MmaA2 than CmaA2 (CmaA2,  $K_d = 600$  nM; MmaA2,  $K_d = 43$  nM;  $BD_{CMAS} = 14$ ). The whole cell activity and cytotoxicity data for these four potential multitargeting CMAS inhibitors have not been disclosed.

Compound No.	CmaA2 (K <sub>d</sub> , nM)	MmaA2 (K <sub>d</sub> , nM)	Binding Differential
X-6905C	>20000	>20000	-
X-1306B	2,726	3021	1.1
X-3709B	600	43	14
X-9901F	790	9121	11.5
X-33515	< 10	< 10	-
X-3870D	173	14	12.3
X-8767F	1018	95	10.7
X-58831	>20000	>20000	-
X-32454	< 10	484	-

**Table 7. Cyclopropane mycolic acid synthase equilibrium dissociation constants for hit molecules identified via screening the Sanofi *Mycobacterium tuberculosis* whole cell active collection.**

Equilibrium dissociation constants for the selected inhibitors were determined by fitting the competition displacement fluorescence intensity data to the Wang model (Wang, 1995). Dose-response assays were performed as a single titration experiment.

*Small molecule mycolic acid methyltransferase screening via the automated ligand identification system*

The Automated Ligand Identification System, ALIS, is a high/ultra-throughput screening technology that integrates rapid size exclusion and reverse phase chromatographic separation systems with mass spectrometry to identify small molecule ligands of protein targets (Annis et al., 2007). Briefly, proteins targets are first incubated with mass-encoded compound pools to establish protein-ligand complexes. The complexes are then separated from non-binding small molecule components using a size-exclusion chromatographic step. Subsequently, the complexes are dissociated, liberating bound small molecules that are then separated via reverse phase chromatography and identified by high resolution mass spectrometry.

In collaboration with the pharmaceutical company Merck, a collection of 347 mycobacterial proteins, including five Mtb MA-MTs, were screened against a 57,917 small molecule library using ALIS technology. Approximately 97 % of the compounds subjected to testing were derived from a proprietary Merck collection. The remaining compounds were primarily contributed by TB Alliance, University of Dundee, Infection Disease Research Institute, and our laboratory. Purified recombinant Mtb PcaA, CmaA2, and MmaA2-4 were shipped to Merck for screening saturated with SAM. Following ALIS screening, Merck associates performed the primary analysis using a variety of selectivity metrics. Their results were provided to our laboratory for follow-up personal analysis.

Screening the library against all five MA-MTs afforded a combined total of 3,194 binding events. The total number of observed binding events for each MA-MT is provided in Table 8. The highest number of binding events were identified for CmaA2 and MmaA4,

<b>Enzyme</b>	<b>Total Binding Events</b>
<b>PcaA</b>	575
<b>CmaA2</b>	924
<b>MmaA2</b>	320
<b>MmaA3</b>	356
<b>MmaA4</b>	1019

**Table 8. Total number of binding events identified for each mycolic acid methyltransferase via automated ligand identification system screening.**

with approximately 1,000 each. To identify putative multitarget MA-MTs compounds, we pooled and filtered the primary analysis results for all 3,194 compounds by the selectivity metric “number of targets the compound binds to”. This selectivity metric describes the total number of binding events found for each compound.

Figure 19A to F shows the MA-MT selectivity profiles with respect to selectivity metric. Of the 1,019 binding events identified for MmaA4, 251 were found as target-specific compounds (Figure 19A). Similarly, 924 binding events were identified for the CmaA2 with 58 target-specific compounds. Significantly fewer target-specific compounds were identified for PcaA, MmaA2, and MmaA3 (11, 4, and 2, respectively). Compounds that were found to bind two and three targets bound the same three MA-MT pairs, with the 2-target compounds having the higher selectivity and abundance (Figure 19B and C). In Figure 19D to F, the 4-, 5-, and 6-targeting compounds show a much broader diversity of MA-MT interactions. The 4-targeting compounds with the highest specificity towards MA-MTs were those that bound three targets (36 out of 55 total compounds, 65 %), either PcaA:CmaA2:MmaA4 or CmaA2:MmaA2:MmaA4. Of the remaining 19 compounds, the majority bound solely to CMAS with an overall reduction in selectivity. The 5- and 6-targeting compounds showed the least multitarget capacity although this was anticipated as binding stringency towards all five MA-MTs is highest. Surprisingly, 16 of the 29 6-targeting compounds were found to bind four of five MA-MTs. Two compounds were identified to bind all five MA-MTs, but the number of targets the compounds binds to needed to be raised to 9. Surprisingly, Compound **4** was identified to bind CmaA2 and MmaA4 but not to MmaA2 as previously demonstrated using our displacement assays. To identify the compound cluster numbers with the most multitargeting MA-MT compounds, we filtered

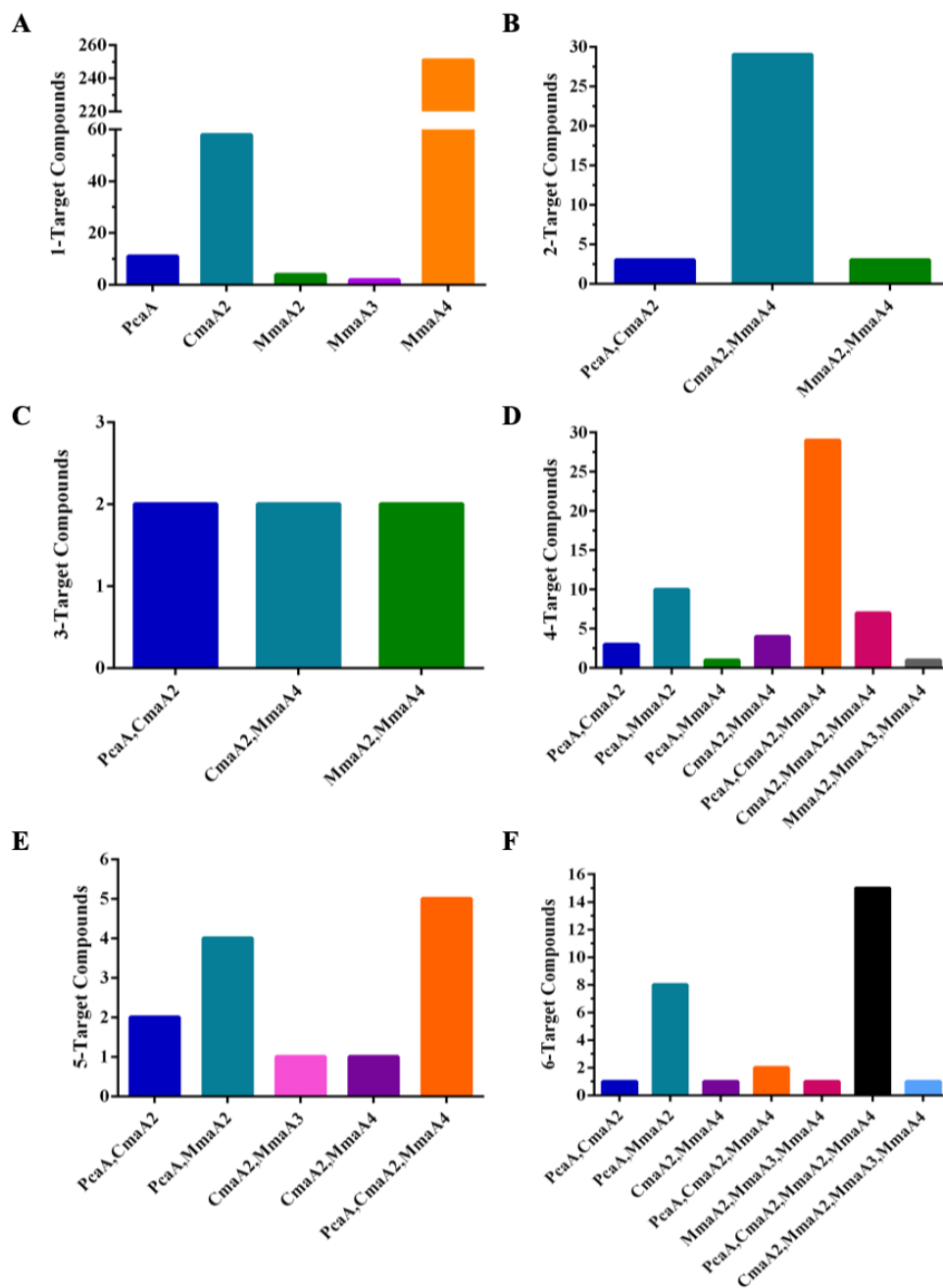


**Figure 19. Automated ligand identification system screening identified putative multitarget mycolic acid methyltransferase compounds.**

The 3,194 compounds identified as mycolic acid methyltransferase binders were filtered by number of binding events from 1 to 6. The number of compounds in each target specificity class is plotted against their identified mycolic acid methyltransferase target(s).

the collection of compounds that bound up to six targets by their cluster number. Seven compound clusters (33, 105, 155, 196, 318, 387, and 411) were identified to contain at least three multitargeting MA-MT compounds. With respect to all protein targets tested in the ALIS screen, the multitarget MA-MT compounds found within these clusters, predominantly bound MA-MTs. Given the breadth of compounds within each cluster, these clusters are not MA-MT specific.

*Multitargeting cyclopropane mycolic acid synthase ligands inhibit multiple pathways of mycolic acid modification in vivo*

DSF and HTS screening identified various compounds that shared the capacity to multitarget CMAS with similar whole cell activity as DOA, strongly suggesting that these compounds might also inhibit multiple pathways of mycolic acid modification. Compounds **1 (H22)**, **4 (H1)**, **H3**, **H23**, **H24**, and **H29** were selected because they were all structurally distinct high affinity CMAS ligands with similar binding differential and showed good growth inhibitory activity of Mtb mc<sup>2</sup>7000 (Table 4 and Table 5). To test whether these selected compounds inhibit mycolic acid modification, we incubated exponential growth phase cultures of *Mycobacterium bovis* BCG-Russia (BCG-R), a slow growing pathogenic mycobacterium that synthesizes all three mycolate types found in the cell wall of Mtb, with 10  $\mu$ M inhibitor in the presence of <sup>14</sup>C-actetic acid. After 8 hours of incubation, <sup>14</sup>C-labeled mycolic acids were isolated and prepared for analysis via radio two-dimensional thin layer chromatography (2D-TLC). Figure 20A shows the mycolate composition of BCG-R in the absence of inhibitor. BCG-R harbors an overall similar mycolate composition as Mtb mc<sup>2</sup>7000 but slightly lower  $\alpha$ -mycolate abundance (Coxon et al., 2013). BCG-R treated with dioctylamine resulted in the accumulation of predominately unsaturated  $\alpha$ - and



ketomycolates species with a near complete depletion of methoxymycolates (Figure 20B). Accumulation of hydroxymycolate, the oxygenated mycolate precursor that migrates slower than ketomycolate, in the absence of methoxymycolate is consistent with loss of MmaA3 function. The overall mycolate phenotype of BCG-R treated with dioctylamine is consistent with the prior report by Barkan et al. (Barkan et al., 2009).

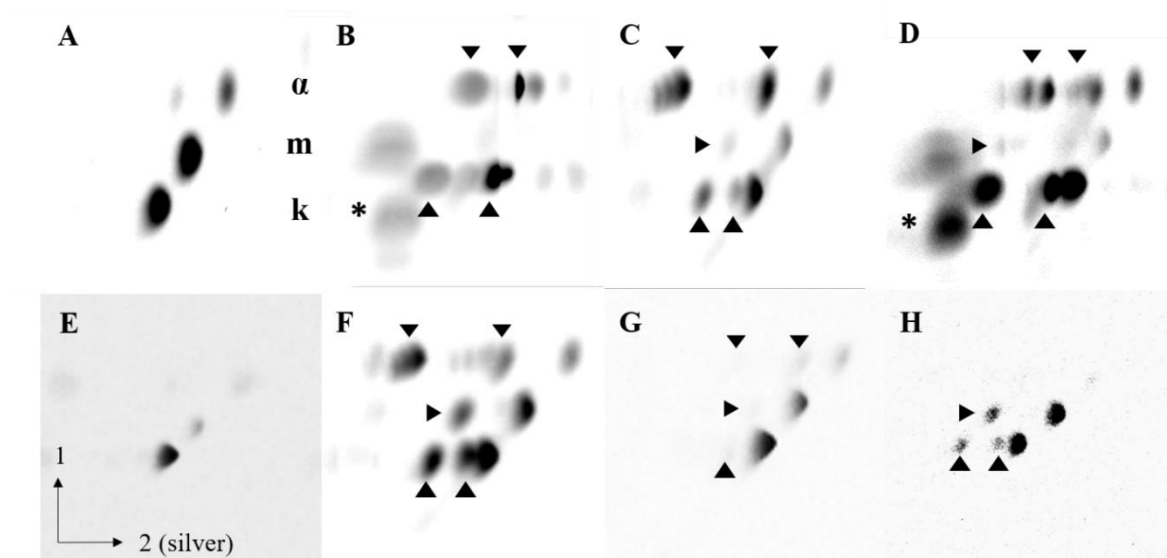


**Figure 20. Multitargeting cyclopropane mycolic acid synthase ligands inhibit mycolic acid cyclopropanation biosynthesis in vivo.**

Whole-cell active growth inhibitors of *Mycobacterium tuberculosis* that demonstrated high affinity towards CmaA2 and MmaA2 were incubated at 10  $\mu$ M with exponential growth phase cultures of *Mycobacterium bovis* BCG (Russia) for 8 hrs. Mycolic acids methyl esters were chromatographed by radio two-dimensional thin layer chromatography. Samples were separated by polarity (dimension 1), then by silver (dimension 2).  $\alpha$ -mycolate ( $\alpha$ ), methoxy mycolate (m), and keto mycolate (k) are indicated to the right in the vehicle (dimethyl sulfoxide) control (A). Compounds tested: B) dioctylamine; C) Compound 1; D) Compound 4; E) H3; F) H23; G) H24; H) H29. Unsaturated mycolic acid derivatives are indicated by arrowheads ( $\alpha$ -mycolates: mature, right, monounsaturated, middle, diunsaturated, left; methoxymycolates: mature (*cis* and *trans*), right, *cis*-unsaturated, left; ketomycolates: mature (*cis* and *trans*), right, *trans*-unsaturated, middle, *cis*-unsaturated, left; hydroxymycolate, \*).

Compounds **1**, **4** and **H23** demonstrated substantial but incomplete inhibition of cyclopropanation in all mycolate types (Figure 20C, D, and F). With respect to  $\alpha$ -mycolates, mono- and diunsaturated species predominate their mature dicyclopropanated parents. **H23** demonstrated a more profound inhibitory effect on  $\alpha$ -mycolate cyclopropanation, when compared to **1** and **4**, as the major mycolate derivative was diunsaturated. The lack of proximal and distal cyclopropanation of  $\alpha$ -mycolates is consistent with the simultaneous inhibition of PcaA and MmaA2 function (Glickman, 2003; Glickman et al., 2000). Methoxymycolate synthesis and their cyclopropane modifications were inhibited by all three compounds, but significantly more depleted when treated with **1** and **4** than **H23**. As similarly observed with DOA, treatment with **4** resulted in methoxymycolate depletion and hydroxymycolate accumulation. The simultaneous reduction of methoxymycolate synthesis with an accumulation of hydroxymycolate suggests that **4** inhibits MmaA3 function. Hydroxymycolate accumulation may result from inhibiting ketomycolate synthesis, but ketomycolate depletion was not observed (Barkan et al., 2009). In contrast to **4**, the inhibitory effect on methoxymycolate synthesis by **1** and **H23** did not result in hydroxymycolate accumulation. Moreover, all three compounds showed incomplete inhibition of cyclopropane synthesis of ketomycolates, but the inhibitory effect was more profound with **4** and **H23** than **1**. These data suggest that these compounds additionally inhibit CmaA2 function. Together, these data suggest that the compounds simultaneously inhibit PcaA, CmaA2, and MmaA2 function, whereas **4** may additionally inhibit the function of MmaA3. Of the three inhibitors tested above, **H23** demonstrated the highest selectivity towards CMAS. Compounds **H3** and **H24** both showed weak to no inhibition of MA-MT activity (Figure 20E and G). Compound **2** was within the selection criteria but never tested.

**H29** was the most potent whole-cell active compound identified by HTS (Mtb mc<sup>2</sup>7000: IC<sub>50</sub> = 0.4 μM), but demonstrated a minimal inhibitory effect on CMAS function but showed nearly complete inhibition of α-mycolate synthesis. This mycolate phenotype is nearly identical to that previously reported for Mtb mc<sup>2</sup>7000 treated with thiacetazone, a compound that has been identified to target the β-hydroxyacyl-ACP dehydratase complexes, HadAB/BC (Coxon et al., 2013). In agreement with our competition displacement assay results, molecules identified as potent acyl binding site competitors of multiple CMAS, generally, elicit substantial inhibition of cyclopropanation in vivo.

To further test whether **1** demonstrates dose-dependent inhibition of mycolic acid modification, exponential growth phase cultures of BCG-R were grown in <sup>14</sup>C-acetic acid with escalating concentrations of the inhibitor followed by mycolic acid analysis via 2D-TLC. Treatment with 2.5 μM **1** (Figure 21A and B) resulted in the accumulation of predominately monounsaturated α-mycolates with a slight accumulation of diunsaturated species. Unsaturated α-mycolates progressively accumulated in the presence of 5 and 10 μM inhibitor, with diunsaturated mycolates as the major species at 10 μM. The subtle decrease in methoxymycolates that accompanied increased α-mycolates at 2.5 μM was more pronounced as the concentration was increased to 5 and 10 μM (Figure 21B to D). Ketomycolate cyclopropanation was least effected, but dose-dependent inhibition is clearly observed though the accumulation of *cis*-unsaturated species. These data suggest that PcaA and MmaA2 are the primary targets of the compound, with a modest inhibitory effect of CmaA2 function. As hydroxymycolate accumulation did not coincide with methoxymycolate depletion, MmaA3 is likely an indirect target of the compound.

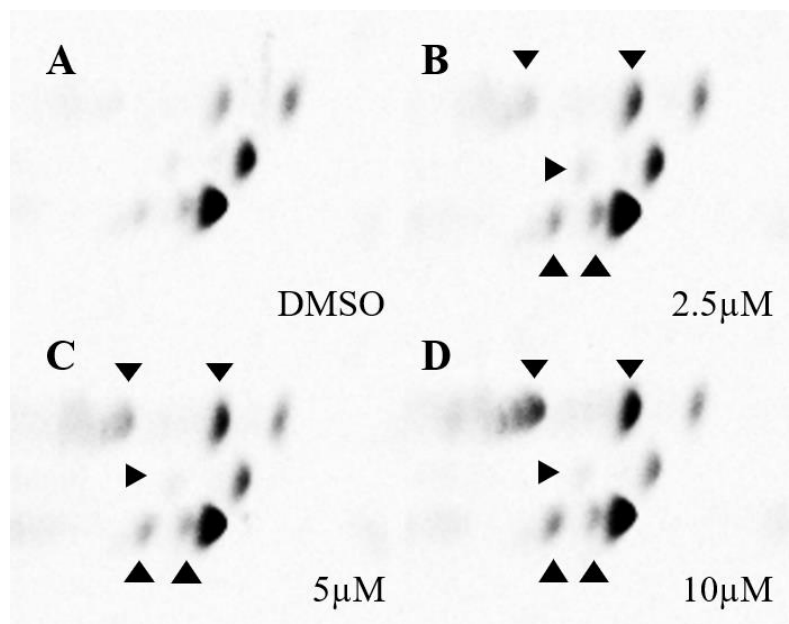


**Figure 21. Compound 1 is a dose-dependent inhibitor of multiple pathways of mycolic acid modification.** Exponential growth phase cultures of *Mycobacterium bovis* BCG-Russia were incubated in the presence of  $^{14}\text{C}$ -acetic acid and vehicle (A) or 2.5 to 10  $\mu\text{M}$  Compound 1 (B-D) for 8 hrs. Radiolabeled mycolates were isolated and analyzed by two-dimensional thin layer chromatography. Unsaturated mycolic acid derivatives are indicated by arrowheads ( $\alpha$ -mycolates: mature, right, monounsaturated, middle, diunsaturated, left; methoxymycolates: mature (*cis* and *trans*), right, *cis*-unsaturated, left ketomycolates: mature (*cis* and *trans*), right, *trans*-unsaturated, middle, *cis*-unsaturated, left).

To test whether **4** demonstrates dose-dependent inhibition of mycolic acid modification, the same approach was taken as previously described for **1**. BCG-R treated with **4** resulted in multiple phenotypic changes in mycolic acid modification: accumulation of di-unsaturated  $\alpha$ -mycolates, significant depletion in methoxymycolates, and a near complete loss of ketomycolate cyclopropanation (Figure 22B to D). At 2.5  $\mu\text{M}$ , mono- and diunsaturated  $\alpha$ -mycolates accumulate, methoxymycolates deplete, and oxygenated mycolate cyclopropanation is substantially inhibited. Unlike **1**, the decrease in methoxymycolates did not accompany  $\alpha$ -mycolate accumulation at 2.5  $\mu\text{M}$  of **4** but was

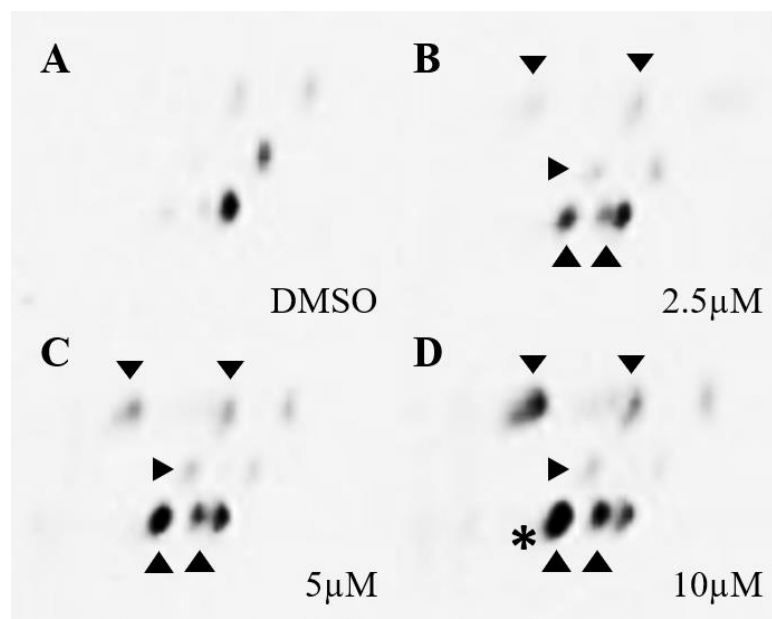


**Figure 22. Molecule 4 is a dose-dependent inhibitor of multiple pathways of mycolic acid modification.** Exponential growth phase cultures of *Mycobacterium bovis* BCG-Russia were incubated in the presence of  $^{14}\text{C}$ -actetic acid and vehicle (A) or 2.5 to 10  $\mu\text{M}$  Molecule 4 (B-D) for 8 hrs. Radiolabeled mycolates were isolated and analyzed by two-dimensional thin layer chromatography. Unsaturated mycolic acid derivatives are indicated by arrowheads ( $\alpha$ -mycolates: mature, right, monounsaturated, middle, diunsaturated, left; methoxymycolates: mature (*cis* and *trans*), right, *cis*-unsaturated, left ketomycolates: mature (*cis* and *trans*), right, *trans*-unsaturated, middle, *cis*-unsaturated, left, hydroxymycolate, \*).

more pronounced at higher concentrations of the compound, 5 and 10  $\mu\text{M}$ . At 5  $\mu\text{M}$ ,  $\alpha$ - and oxygenated mycolates predominately accumulate as their unsaturated derivatives. At 10  $\mu\text{M}$ , unsaturated mycolate abundance progressively increased to a level that the majority of  $\alpha$ -mycolates were mono- and diunsaturated with the most abundant species observed as their diunsaturated derivatives. In addition, methoxymycolates abundance was further depleted with a near complete loss of ketomycolate cyclopropanation. These data clearly show dose-dependent inhibition of multiple pathways of mycolic acid modification and suggests that the function of PcaA, CmaA2, MmaA2, and MmaA3 were all inhibited by the compound.

To test whether **H23** demonstrates dose-dependent inhibition of mycolic acid modification, the same approach was taken as previously described for **1** and **4**. Unlike the 4-fold concentration range tested for **1** and **4**, a broader 100-fold was used for **H23** (Figure 23B to D). BCG-R treated with **H23** showed no inhibition of mycolic acid modification at 0.1  $\mu\text{M}$ , but inhibition of  $\alpha$ -mycolate cyclopropanation was initially observed with a concentration as low as 1  $\mu\text{M}$ , marked by a slight accumulation of diunsaturated  $\alpha$ -mycolates. At 10  $\mu\text{M}$ , methoxymycolates showed substantial depletion with a concomitant accumulation of  $\alpha$ -mycolates, as similarly observed with **1**, **4**, and DOA. At this concentration,  $\alpha$ -mycolates were predominately unsaturated with the diunsaturated derivative as the principle mycolate. The data in Figure 23D shows major discrepancies with the **H23** data presented in Figure 20F. First, the vehicle controls show widely different mycolate profiles that complicate data interpretation for this compound. As the vehicle control in Figure 20 solely contains mature mycolates, whereas the vehicle control in Figure 23 shows unsaturated derivatives of all mycolic acid types. The data presented in Figure 20F shows that **H23** inhibits mycolic acid cyclopropanation of all mycolate types with a minor inhibitory effect on methoxymycolate synthesis. In contrast, the data in Figure 23D suggests that **H23** inhibits  $\alpha$ -mycolate cyclopropanation and methoxymycolate biosynthesis, with a negligible inhibitory effect on ketomycolate cyclopropanation. Despite the vehicle control discrepancies and broader concentration range used, this data shows that **H23** inhibits mycolic acid modification in a dose-dependent fashion; but unlike the data presented in Figure 20F that suggests that CMAS (PcaA, CmaA2, and MmaA2) are the primary targets of the compound, Figure 23D suggests that **H23** inhibits the function of PcaA, MmaA2, and MmaA3, with a negligible inhibitory effect of CmaA2 function.

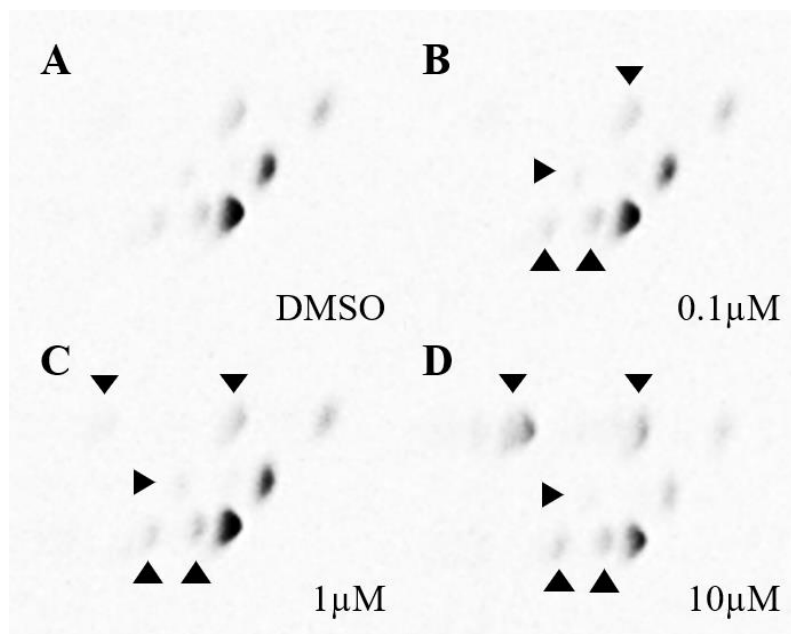


**Figure 23. Molecule H23 inhibits multiple pathways of mycolic acid modification.**

Exponential growth phase cultures of BCG-Russia were incubated in the presence of  $^{14}\text{C}$ -actetic acid and vehicle (A) or 0.1 to 10  $\mu\text{M}$  Molecule H23 (B-D) for 8 hrs. Radiolabeled mycolates were isolated and analyzed by 2D-TLC. Unsaturated mycolic acid derivates are indicated by arrowheads ( $\alpha$ -mycolates: mature, right, monounsaturated, middle, diunsaturated, left; methoxymycolates: mature (*cis* and *trans*), right, *cis*-unsaturated, left ketomycolates: mature (*cis* and *trans*), right, *trans*-unsaturated, middle, *cis*-unsaturated, left).

#### *Crystal structures of CmaA2 in complex with Compound 1 and Compound 4*

To further demonstrate that **1** and **4** bind specifically to the acyl binding site of CmaA2 and to establish the molecular basis of inhibition, we solved the structure of CmaA2 in complex with the inhibitors. These compounds both inhibited BCG-R mycolic acid modification to a similar extent as dioctylamine. Statistics for the crystallographic data collection and structure refinement are provided in Table 9. The crystal structure of CmaA2 bound to **1** and **4** were solved at 2.2 Å and 2.0 Å, respectively (Figure 24A and B). Both structures showed an overall similar fold as CmaA2 bound with DOA, with an average rmsd

of  $0.29 \pm 0.02$  Å. The terminal nitrogen atoms of the inhibitors similarly locate to the base of the active site tunnel where they reside within 1 Å to the nitrogen (N9) of DOA but differ in orientation. Relative to N9, the basic amine (N4) of **1** drifted  $\sim 0.6$  Å away from, with an  $\sim 45^\circ$  tilt towards, the bicarbonate ion. This positions the O3 oxygen atom of the ion within

		CmaA2-SAH-1	CmaA2-SAH-4
Data	Space group	I4122	I4122
	Unit cell dimensions		
	a, b, c (Å)	106.58, 106.58, 227.29	106.49, 106.49, 226.4
	$\alpha, \beta, \gamma$ ( $^\circ$ )	90, 90, 90	$\hat{9}0, \hat{9}0, \hat{9}0$
	Resolution <sup>a</sup>	48.25 - 2.20 (2.24 - 2.20)	48.18 - 2.04 (2.23 - 2.04)
	No. unique reflections	$\bar{3}359\bar{8}$	41496
	R <sub>merge</sub> (%) <sup>a</sup>	0.08 (0.69)	$\bar{0}.0\bar{9}$ ( $\bar{0}.8\bar{6}$ )
	I/ $\sigma$ <sup>a</sup>	31.7 (3.0)	39.6 (2.2)
	Redundancy <sup>a</sup>	10.1 (10.4)	14.5 (12.8)
	Completeness (%) <sup>a</sup>	99.9 (99.9)	99.8 (99.4)
Refinement	Resolution (Å)	48.25 - 2.20	48.18 - 2.04
	No. unique reflections	33598	41496
	R <sub>work</sub> /R <sub>free</sub> (%)	15.8, 18.1	16.1, 17.7
	R <sub>free</sub> test set (%)	5.95	4.82
	Wilson B-factor (Å <sup>2</sup> )	44.3	40.7
	Bulk solvent k <sub>sol</sub> (e/Å <sup>3</sup> ), B <sub>sol</sub>	0.36, 44.1	0.37, 53.3
	F <sub>o</sub> , F <sub>c</sub> correlation	0.97	0.97
	No. atoms	2552	2606
	No. protein atoms	2369	2399
	No. solvent atoms	127	156
	No. ligands	3	3
	RMSD bonds	0.01	0.006
	RMSD angles	0.98	0.75
	Average B, all atoms (Å <sup>2</sup> )	53	52
	Sidechain outliers (%)	1.99	1.97
	Ramachandran outliers (%)	0.35	0.35

**Table 9. Data collection and refinement statistics for CmaA2 in complex with Compound 1 and 4**  
<sup>a</sup>, values in parenthesis are for the highest resolution shell



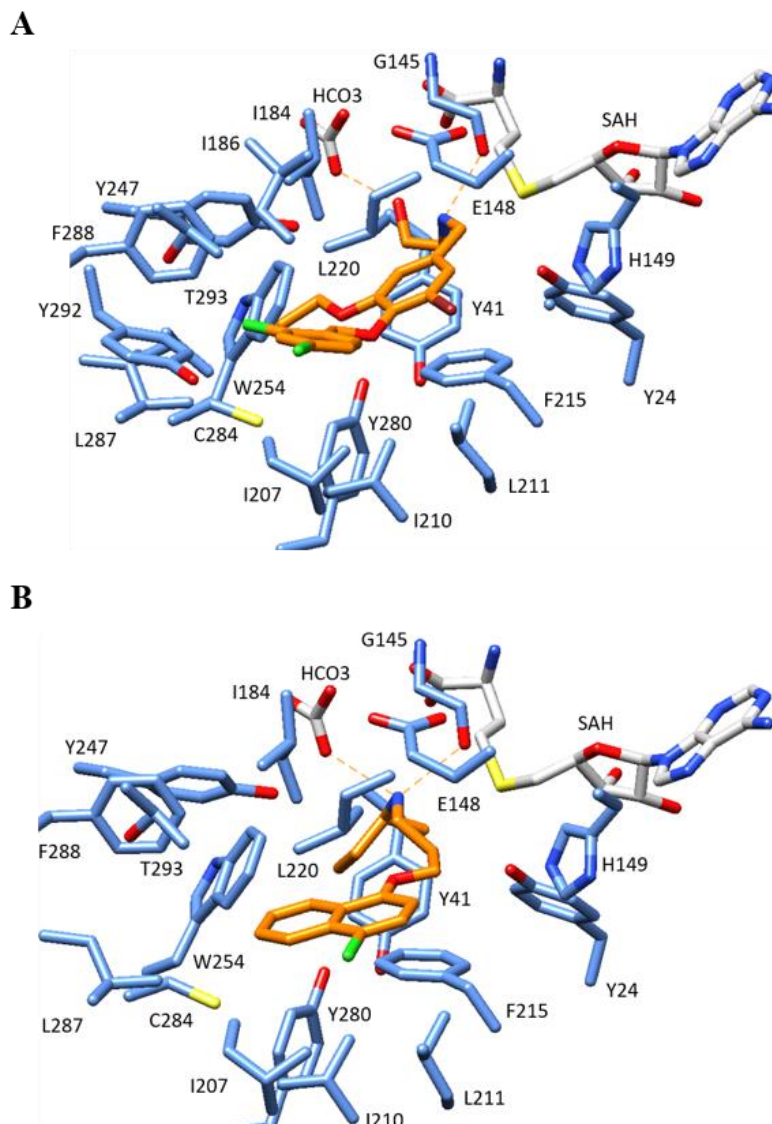


**Figure 24. Crystal structures of CmaA2 in complex with Compounds 1 and 4.**

A) Amplified view of Compound 1 and B) Compound 4 bound to the active site of CmaA2. Amino acid residues at a distance within 5 Å from the inhibitor are shown as light blue sticks (inhibitors: orange represents carbon, red represents oxygen, blue represents nitrogen, green represents chlorine, and maroon represents bromine); the bicarbonate ion and S-adenosyl homocysteine are represented in grey. Hydrogen bonds are shown as orange dashed lines.

a distance of 3.0 Å of both N4 and O1 atoms of the N-linked ethanol, where O3 was 4.2 Å away from N9 of DOA. In addition, this location of N4 maintains the hydrogen bond with

the backbone oxygen of G145, at distance of  $\sim 2.8$  Å, as observed for N9 of DOA. Whereas the nitrogen atoms of **1** and DOA similarly orient, they substantially differ from the nitrogen atom (N10) of **4**. With respect to N9 of DOA, N10 of **4** tilts  $\sim 45^\circ$  towards the sulfur atom of SAH. Unlike N9 of DOA, that forms a single hydrogen bond with the backbone oxygen of G145, N10 forms an additional hydrogen bond ( $\sim 2.9$  Å) with O3 of the bicarbonate ion. Like the aliphatic chains of DOA, the hydrophobic substituents of **1** and the 4-chloronaphthyl ring system of **4** position to the exclusively hydrophobic entrance. With regards to **1**, the multisubstituted benzene core is parallel-displaced to F215, with a  $20^\circ$  ring plane angle and a centroid distance of about 4.0 Å, indicating that the inhibitor is stabilized through  $\pi$ - $\pi$  stacking. The ethoxy group positioned meta, relative to the terminal amine substituent, resides in a small hydrophobic pocket within a distance of 4.5 Å of Y247, L251, Y280, C284, F288, whereas the meta-positioned bromine atom is solvent exposed and resides within an approximate distance of 5 Å from the protein-solvent interface and I207, L211, F215, G218, and L220. The para-positioned dichloro-substituted benzene ring extends further towards the protein-solvent interface, where it resides within a distance of 4 Å of I207, I210, C284, L287, and F288. With regards to **4**, the naphthyl ring system is positioned approximately 3.0 Å closer to the protein-solvent interface and away from F215 than the multisubstituted benzene core in **1**. At this location, the naphthyl ring resides within the van der Waals radii of an array of hydrophobic amino acid residues (I184, I207, I210, L211, F215, L220, C284, and L287) and positions with near perfect orientation as the NBD fluorophore in the CmaA2-SAH-NBD-A ternary structure, previously described in Chapter 2. Together, these data strongly suggest that high affinity amphipathic inhibitors of CMAS

likely will require a basic nitrogen positioned to the catalytic core, mimicking the carbocation reaction intermediate, with a hydrophobic extension localized to the entrance.

*Crystal structure of CmaA2 in complex with H23 and S-adenosyl homocysteine*

To investigate the molecular basis of CmaA2 recognition towards **H23**, a multitargeting CMAS ligand identified by HTS that structurally similar to **1** and inhibited multiple pathways of mycolic acid modification in vivo, we solved the structure of CmaA2 in complex with the compound. Unlike **1** that contains a multi-substituted benzene core with a tethered benzene ring at the para position, with respect to the terminal nitrogen atom, this aromatic ring is positioned meta in **H23**. Analysis of the structure of CmaA2 in complex with **1** suggested that bulky aromatic substituents at the meta position should be sterically hindered. As **H23** is a high affinity CmaA2 ligand, the binding mode may be unique. The crystal structure of the complex was solved at 2.1 Å resolution with a P4<sub>3</sub>2<sub>1</sub>2 spacegroup symmetry. This space group is unlike all of the previously solved CmaA2 complex structures (DOA, DDDMAB, NBD-A, **1**, and **4**) that were I4<sub>1</sub>22 (Barkan et al., 2009; Huang et al., 2002). Statistics for the crystallographic data collection and structure refinement are provided in Table 10. Subsequent to molecular replacement phasing, the initial difference map indicated that the α10 helix was incorrectly positioned. Upon correcting the atomic positions of the amino acids within the helix, superimposing the structure with the CmaA2-SAH-**4** complex revealed that the α10 underwent a drastic change in conformation (Figure 25A, left). This conformational change rotates α10 approximately 90° towards α11, resulting in an approximate 12 Å shift of M201 Cα (α10 N-terminus) and a 0.6 Å shift of I214 Cα (α10 C-terminus). This conformational change was attributed to the displacement of Y280 by the tethered benzene ring in the N-(1-methyl-3-phenylpropyl) group of **H23**, located at

the meta position (Figure 25A, right). The phenol side chain of Y280 rotated approximately 130° with a 10 Å shift of the hydroxyl group away from the active site towards the bulk

CmaA2-SAH-H23		
Data collection	Space group	P43212
	Unit cell dimensions	
	a, b, c (Å)	111.92, 111.92, 185.56
	$\alpha$ , $\beta$ , $\gamma$ (°)	90, 90, 90
	Resolution <sup>a</sup>	48.73 - 1.90 (2.35 - 1.90)
	No. unique reflections	93051
	R <sub>merge</sub> (%) <sup>a</sup>	0.06 (0.43)
	I/ $\sigma$ I <sup>a</sup>	46 (4.8)
	Redundancy <sup>a</sup>	13.4 (6.9)
	Completeness (%) <sup>a</sup>	99.9 (99.9)
Refinement	Resolution (Å)	48.73 - 1.90
	No. unique reflections	93051
	R <sub>work</sub> /R <sub>free</sub> (%)	14.4, 16.8
	R <sub>free</sub> test set (%)	2.15
	Wilson B-factor (Å <sup>2</sup> )	25
	Bulk solvent k <sub>sol</sub> (e/Å <sup>3</sup> ), B <sub>sol</sub> (Å <sup>2</sup> )	0.36, 46.7
	Fo, Fc correlation	0.97
	No. atoms	5483
	No. protein atoms	4749
	No. solvent atoms	620
	No. ligands	6
	RMSD bonds	0.02
	RMSD angles	1.45
	Average B, all atoms (Å <sup>2</sup> )	30
	Sidechain outliers (%)	2.19
	Ramachandran outliers (%)	0.35

**Table 10. Data collection and refinement statistics for CmaA2 in complex with H23 and S-adenosyl homocysteine**

<sup>a</sup>, values in parenthesis are for the highest resolution shell

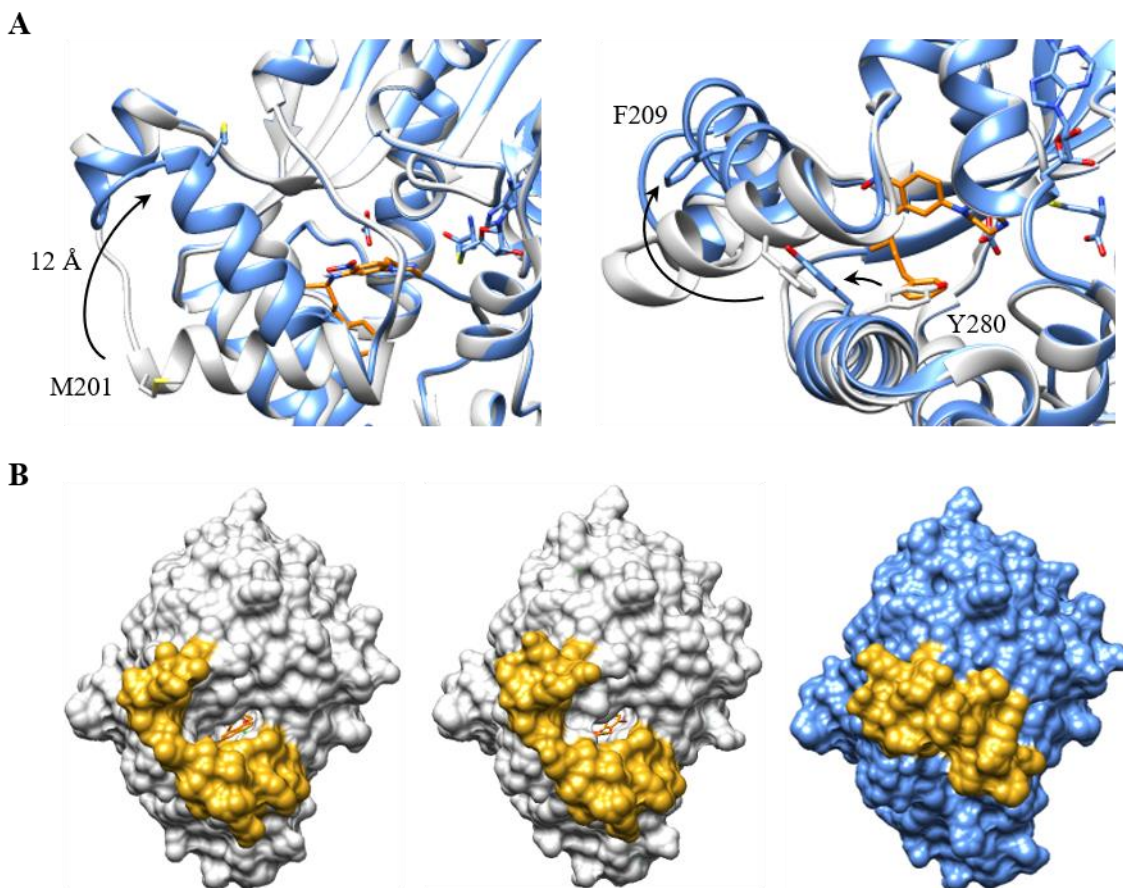


**Figure 25. H23 induces an active site occluding conformational change upon binding CmaA2.**

A) Superimposition of the  $\alpha$ -carbon trace of CmaA2 in complex with Compound 4 (grey) and H23 (blue). H23 is displayed as sticks, whereby orange represents carbon, red represents oxygen, and blue represents nitrogen. The bicarbonate ion and S-adenosyl homocysteine are represented as blue sticks, with the heteroatoms colored as previously mentioned, with the addition to sulfur represented in yellow. For clarity, only the polypeptide chain of CmaA2 bound to Molecule 4 is shown. B) Space filled models of CmaA2-SAH-4 (left), CmaA2-SAH-1 (middle), and CmaA2-SAH-H23 (right). Residues D188-T212 within the  $\alpha$ 9 and  $\alpha$ 10 helices are labelled in yellow.

solvent. This rotation likely provoked a steric clash with F209 causing  $\alpha$ 10 to rotate  $90^\circ$  towards  $\alpha$ 11. Surface modeling of the complex showed that the conformational shift resulted in the near complete occlusion of the acyl binding site (Figure 25B), whereas the active sites are all in an open conformation when bound to **1** and **4** (Figure 24A and B). As previously

described for the nitrogen atoms in DOA, **1**, and **4** in the CmaA2-bound structures, the terminal piperazine nitrogen atom (N13) in **H23** locates to the catalytic core. Whereas N9 of DOA forms a hydrogen bond with the backbone oxygen of G145 at a distance of 3.2 Å, N13 of **H23** forms stronger hydrogen bond interactions with the backbone oxygens of G145 and Y41, both within a 2.8 Å distance. The multisubstituted benzene core is parallel displaced with F215, with centroid distances of 3.9 Å apart, indicating that the inhibitor is stabilized through  $\pi$ - $\pi$  interactions. The meta-positioned N-(1-methyl-3-phenylpropyl) group resides in a novel, exclusively hydrophobic pocket composed of I207, L211, I214, F215, L220, L251, W254, L284, L287, and F288. The para-positioned nitro group interacts with an ordered water molecule, within a distance of 3.0 Å, in the active site but is not involved in any direct interactions with the polypeptide chain. Analysis of the crystal packing surface showed that the  $\alpha$ 10 loop in the closed conformation plays a critical role in crystal lattice formation, suggesting that loop closure may be an artifact of crystallization. As the crystal structure of CmaA2 in complex with **4** was crystallized in a nearly identical crystallization condition, but lacks active site closure, this indicates that the conformation change is unlikely a crystallographic artifact.

#### *Crystal structure of CmaA2 in complex with H29 and 5'-methylthioadenosine*

To determine the molecular interactions between CmaA2 and **H29** we solved the crystal structure of the complex. **H29** was the most potent HTS-identified whole cell active growth inhibitor of Mtb mc<sup>2</sup>7000 ( $IC_{50} = 0.4 \mu\text{M}$ ). The compound demonstrated high affinity towards both CmaA2-SAM ( $K_d = 54 \pm 9 \text{ nM}$ ) and MmaA2-SAM ( $K_d = 19 \pm 4 \text{ nM}$ ) but a poor inhibitor of mycolic acid cyclopropanation in vivo (Figure 20H). However, the compound was interesting because it is structurally similar to DOA as it contains an internal

basic amine flanked by hydrophobic constituents. The structural similarity suggested that the two molecules may bind to the CmaA2 active site in a similar fashion. To test this, we solved the crystal structure of CmaA2 in complex with **H29** at 2.7 Å resolution. Statistics for the crystallographic data collection and structure refinement are provided in Table 11.

		CmaA2-MTA-H29
Data collection	Space group	I4122
	Unit cell dimensions	
	a, b, c (Å)	106.62, 106.62, 225.33
	$\alpha, \beta, \gamma$ (°)	90, 90, 90
	Resolution <sup>a</sup>	45.13 - 2.70 (3.20 - 2.70)
	No. unique reflections	18305
	R <sub>merge</sub> (%) <sup>a</sup>	0.12 (3.7)
	I/ $\sigma$ <sup>a</sup>	80.1 (3.7)
	Redundancy <sup>a</sup>	16.6 (16.5)
	Completeness (%) <sup>a</sup>	99.9 (99.9)
Refinement	Resolution (Å)	45.13 - 2.70
	No. unique reflections	18305
	R <sub>work</sub> /R <sub>free</sub> (%)	16.7, 21.5
	R <sub>free</sub> test set (%)	10
	Wilson B-factor (Å <sup>2</sup> )	45.8
	Bulk solvent k <sub>sol</sub> (e/Å <sup>3</sup> ), B <sub>sol</sub> (Å <sup>2</sup> )	0.35, 31.9
	F <sub>o</sub> , F <sub>c</sub> correlation	0.95
	No. atoms	2435
	No. protein atoms	2369
	No. solvent atoms	16
	No. ligands	3
	RMSD bonds	0.008
	RMSD angles	0.92
	Average B, all atoms (Å <sup>2</sup> )	45
	Sidechain outliers (%)	1.59
	Ramachandran outliers (%)	0.35

**Table 11. Data collection and refinement statistics for CmaA2 in complex with H29 and S-adenosyl homocysteine**

<sup>a</sup>, values in parenthesis are for the highest resolution shell

Incomplete electron density was observed for the SAH cofactor and was therefore completely modelled as 5'-methylthioadenosine (MTA). Superimposition of the CmaA2 structures in complex with **H29** and DOA showed an overall similar fold with a rmsd for C $\alpha$  of 0.25 Å (Figure 26A). The two ligands showed near perfect superimposition as they both orient in a U-shaped conformation with their basic amines positioned at site of methyl transfer with their hydrophobic constituents extending towards the catalytic site entrance. At the catalytic core, the basic amines reside within a distance of 1.2 Å to one another. Although the amines similarly locate in the active site, they differ in their interactions with protein backbone. The secondary amine N09 of DOA resides within a distance of 3.2 Å of the peptide backbone oxygen of G145, whereas the tertiary amine of **H29** lacks this intermolecular contact. At the entrance, the hydrophobic constituents of **H29** and DOA locate within van der Waals radii of identical amino acid residues (I184, I207, I210, L211, F215, L220, L251, C284, L287, and F288) (Figure 26B). Specifically, the thiophene ring resides in a slightly off-plane sandwich geometry to F215, with a 25° ring plane angle and a centroid distance of about 4.4 Å, indicating the inhibitor is stabilized through  $\pi$ - $\pi$  stacking. The attached 2-propyn-1-ol substituent points directly towards the bulk solvent with the hydroxy group within a distance of 5.0 Å from the protein-solvent interface. The 3-[(4-methylphenoxy)methyl] substituent attached to the piperidine core resides within 4.4 Å of I184, Y247, L251, C284, L287, F288, Y280, I210, and L220 as the lipophilic group extends towards the active site entrance. Despite the poor CMAS inhibitory activity of **H29** in vivo, this structural analysis of the CmaA2-**H29** interaction provides a molecular framework to rationally drug design 1,3-disubstituted piperidine analogs for improving specificity and binding affinity towards these enzyme targets.



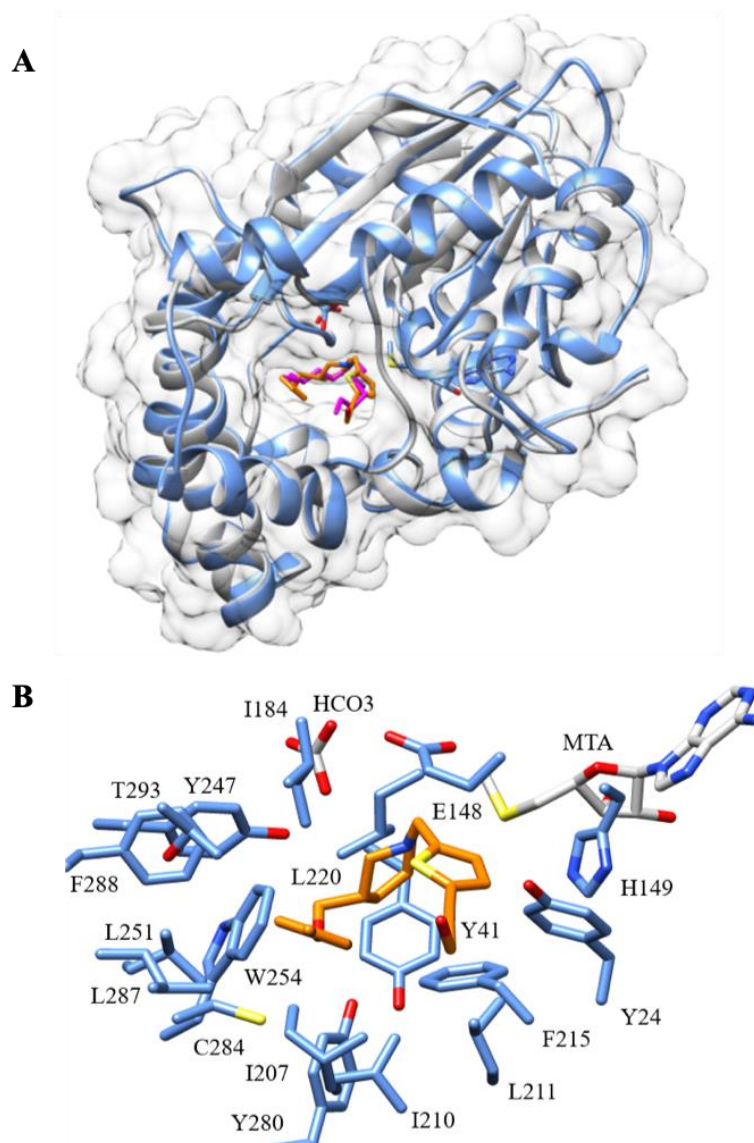


**Figure 26. H29 and dioctylamine similarly orient in the active site of CmaA2.**

A) Spaced filled model of the superimposition of H29 and dioctylamine (DOA) bound to the active site of CmaA2. Ribbon representations of the CmaA2-5'-methylthioadenosine-H29 complex shown in light blue and CmaA2-DOA shown in grey. B) Amplified view of H29 bound to the active site of CmaA2. Amino acid residues at a distance within 5 Å from the inhibitor are shown as light blue sticks (H29: orange represents carbon, red represents oxygen, blue represents nitrogen, yellow represents sulfur, magenta represents carbon). The bicarbonate ion and 5'-methylthioadenosine are represented in grey.

### *Crystal structure of CmaA2 in complex Compound 2 and S-adenosyl homocysteine*

To determine the molecular interactions between CmaA2 and Compound **2** (H20) we solved the crystal structure of the complex. Compound **2** was a high affinity ligand of CMAS (CmaA2:  $K_d = 36 \pm 7$  nM; MmaA2:  $K_d < 10$  nM) and showed good whole cell growth inhibition of Mtb mc<sup>2</sup>7000 ( $IC_{50} = 1.1$   $\mu$ M), but was a poor inhibitor of MA-MT function in vivo. The crystal structure of CmaA2 in complex with SAH and **2** was solved at 1.9 Å. Statistics for the crystallographic data collection and structure refinement are provided in Table 12. After modelling **2** into the active site, the subsequent difference map showed positive electron density adjacent to the terminal imine nitrogen atom (N16) that is located ~5 Å away from the sulfur atom of SAH. As with all of our previously described crystal structures, CmaA2 was co-crystallized with the inhibitor in the presence of SAM. However, SAH is typically modelled into the cofactor binding site as electron density for the methyl group is not observed. This positive density suggested that **2** was methylated during crystallization. Methylated-**2** (**m2**) was then modelled into the electron density. After structure refinement, **m2** perfectly modelled all available electron density in the active site, indicating that CmaA2 methylated **2** (Figure 27).

To confirm the presence of **m2** in crystalline CmaA2, crystal samples were prepared and subjected to ESI-MS. Mass spectral analysis of **2** released from CmaA2-SAH complex showed that the principle **2** species was **m2** ( $m/z$   $[M+H]^+$ : 301.1699 (calc.), 301.1713 (found)). There are two hypotheses for **m2** formation. First, compound **2** was directly methylated by SAM. Second, compound **2** was catalytically methylated by CmaA2. Neither hypothesis has currently been tested.

CmaA2-SAH-H20		
Data collection	Space group	I4122
	Unit cell dimensions	
	a, b, c (Å)	106.69, 106.69, 226.74
	$\alpha, \beta, \gamma$ (°)	90, 90, 90
	Resolution <sup>a</sup>	41.73 - 1.90 (2.04 - 1.90)
	No. unique reflections	52637
	R <sub>merge</sub> (%) <sup>a</sup>	0.81 (0.60)
	I/ $\sigma$ <sup>a</sup>	84.3 (1.5)
	Redundancy <sup>a</sup>	8.6 (8.8)
	Completeness (%) <sup>a</sup>	99.8 (100)
Refinement	Resolution (Å)	41.73 - 1.9
	No. unique reflections	51637
	R <sub>work</sub> /R <sub>free</sub> (%)	17.0, 19.3
	R <sub>free</sub> test set (%)	3.87
	Wilson B-factor (Å <sup>2</sup> )	38.9
	Bulk solvent k <sub>sol</sub> (e/Å <sup>3</sup> ), B <sub>sol</sub> (Å <sup>2</sup> )	0.37, 50.9
	F <sub>o</sub> , F <sub>c</sub> correlation	0.97
	No. atoms	2589
	No. protein atoms	2392
	No. solvent atoms	143
	No. ligands	3
	RMSD bonds	0.017
	RMSD angles	1.18
	Average B, all atoms (Å <sup>2</sup> )	51
	Sidechain outliers (%)	1.98
	Ramachandran outliers (%)	0.35

**Table 12. Data collection and refinement statistics for CmaA2 in complex with H20 and S-adenosyl homocysteine**

*a*, values in parenthesis are for the highest resolution shell

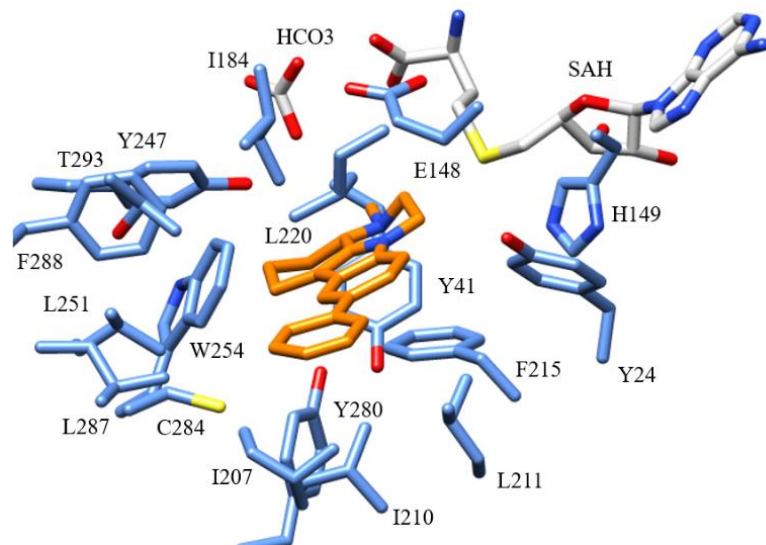


**Figure 27. Crystal structures of CmaA2 in complex with Compound 2 and S-adenosyl homocysteine.** Amplified view of Compound 2 bound to the active site of CmaA2. Amino acid residues at a distance within 5 Å from the inhibitor are shown as light blue sticks (inhibitors: orange represents carbon, red represents oxygen, blue represents nitrogen; the bicarbonate ion and S-adenosyl homocysteine are represented in grey).

*Mycobacterium tuberculosis* bactericidal assessment of mycolic acid modification inhibitors

DOA was previously reported as a bactericidal compound against Mtb, but direct evidence showing loss in colony forming units (CFUs) was not demonstrated (Barkan et al., 2009). To reevaluate the putative bactericidal properties of this compound, we grew Mtb mc<sup>2</sup>7000 in escalating concentrations of DOA (5X, 10X, and 20X the IC<sub>50</sub>, IC<sub>50</sub> = 3.5 μM). Culturing Mtb mc<sup>2</sup>7000 in the presence of 5X DOA (17 μM) resulted an approximate 100-fold reduction in CFUs on day 14, but was not reduced further on day 21 (Figure 28A). However, the cultures grown in 10X (35 μM) and 20X (70 μM) DOA were completely sterilized on day 7. These data clearly show that DOA treatment is lethal to Mtb.

To test the hypothesis that simultaneous inhibition of MA-MTs by **1**, **4**, and **H23** are bactericidal, we cultured mycobacterial cells with escalating concentrations of the inhibitors as described for DOA. We previously showed that BCG-R treated with 10  $\mu$ M **4** results in a mycolate composition that nearly phenocopies the inhibitory effect of DOA (Figure 20B and D). However, unlike the bactericidal activity found for DOA, **4** was bacteriostatic (Figure 28A and B). Together, these data suggest that cell death resulting from DOA treatment is likely due to off-target effects and simultaneous inhibition of mycolic acid modification is not lethal to Mtb. BCG-R cultures treated with 5X and 10X **1** and **H23** resulted in bacterial growth stasis but were completely sterilized with 20X on day 21 (Figure 28C and D). These data clearly show that **1** and **H23** are bactericidal compounds, but given their reduced potency in inhibiting mycolic acid modification, the compounds likely kill Mtb by inhibiting other protein targets.

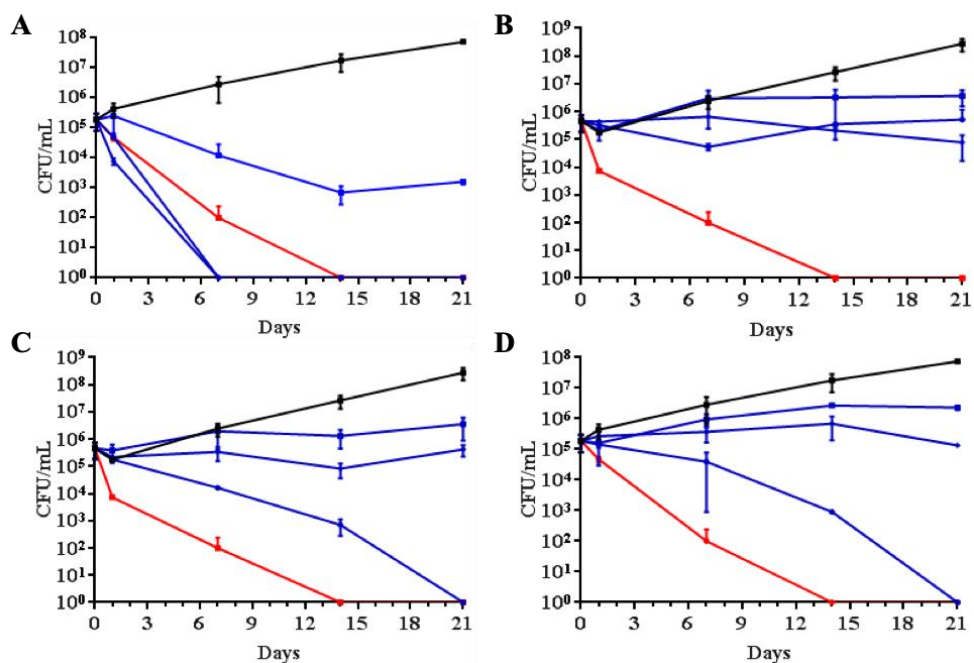


**Figure 28. *Mycobacterium tuberculosis* kill-curve analysis of multitargeting cyclopropane mycolic acid synthase inhibitors.**

*Mycobacterium tuberculosis* mc<sup>2</sup>7000 was cultured for 21 days in 7H9-dextrose media supplemented with various concentrations (5X, 10X, and 20X IC<sub>50</sub>) of multitargeting cyclopropane mycolic acid synthase inhibitors. On day 0, 1, 7, 14, and 21, bacterial culture CFUs were determined by dilution plating. A) dioctylamine (17.5  $\mu$ M, 35  $\mu$ M, 70  $\mu$ M), B) Compound 4 (7.5  $\mu$ M, 15  $\mu$ M, 30  $\mu$ M), C) Compound 1 (4  $\mu$ M, 8  $\mu$ M, 16  $\mu$ M), D) Compound H23 (7.5  $\mu$ M, 15  $\mu$ M, 30  $\mu$ M). The experiment was performed in duplicate.

## Materials and Methods

### *Cloning, expression, and protein purification of recombinant Mycobacterium tuberculosis mycolic acid methyltransferases*

*cmaA2* (Rv0503c), *mmaA2-4* (Rv0642c, Rv0643c, Rv0644c), and *pcaA* (Rv0470c) genes were amplified from H<sub>37</sub>Rv genomic DNA via polymerase chain reaction. *cmaA2* was cloned into pET28b-TEV whereas *mmaA2-4* and *pcaA* were cloned into pMCSG7. Positive clones, confirmed via DNA sequencing, were transformed into *E. coli* BL21 (DE3) for protein expression. Cell cultures were grown at 37 °C, in in Luria-Bertani broth, until an

OD<sub>600</sub> of ~ 0.8. The cultures were then chilled in an ice water bath for 20mins. Protein expression was induced with 500  $\mu$ M IPTG and protein production was allowed to proceed for 16 - 18 hr at 18 °C. Cell pellets were harvested and homogeneously suspended in an equal volume of 50 mM Tris-HCl, pH 8.0, 300 mM NaCl and lysed on French press. Recovered supernatants were loaded onto GE Healthcare Ni Sepharose 6 Fast Flow resin and washed with 30-column volumes of 50 mM Tris-HCl, pH 8.0, 300 mM NaCl, 30 mM imidazole. His-tagged recombinant protein was eluted using 50 mM Tris-HCl, pH 8.0, 300 mM NaCl, 500 mM imidazole, then setup for his-tag removal via TEV proteolysis in 20 mM Tris-HCl, pH 8.0, 150 mM NaCl, 1 mM DTT for 2 hrs at 25 °C. The final purified protein was obtained after collecting the flow through fraction of a second pass through the Ni resin. As 6Xhis-TEV-PcaA was observed to be a poor TEV protease substrate, the his-tag was not removed. Purified CMAS were buffer exchanged into 20 mM Tris-HCl, pH 8.0 and 50 mM NaCl using the concentrate and dilute method. All proteins were concentrated to 20 mg/mL and flash frozen in liquid nitrogen prior to storage at -80°.

*Differential scanning fluorimetry: buffer and inhibitor screening*

The differential scanning fluorimetry (DSF) buffer screen was performed in a 96-well format with a 20 $\mu$ L assay volume at a final buffer concentration of 100mM. Buffers used: sodium citrate pH 5.5, MES pH 6.0, PIPES pH 6.5, MOPS pH 7.0, HEPES 7.5, imidazole pH 8.0, and BICINE pH 8.5. CMAS were assayed at 2  $\mu$ M and 5  $\mu$ M in the presence of 200  $\mu$ M S-adenosyl methionine. DSF was conducted in a Stratagene MX3005P (Agilent Technologies) real-time PCR instrument, utilizing 4.9X sypro orange (Ex: 492 nm, Em: 610 nm), with a temperature gradient of 1 °C/min<sup>-1</sup> from 25 - 75 °C. CmaA2 melting

temperatures ( $T_m$ ) were determined as the temperature corresponding to the curve minima in the dissociation plot.

The CmaA2-SAM complex was screening against 2,506 Mtb whole cell active compounds collection in a similar fashion as previously described above for buffer screening. The small molecule collection was created from hits identified from an approximately 105,000 small molecule in-house diversity library screened against Mtb mc<sup>2</sup>7000, in addition to a set of active molecules against Mtb H<sub>37</sub>Rv obtained from Southern Research Institute. The compound collection was screened at 25  $\mu$ M against 2  $\mu$ M recombinant CmaA2 supplemented with 200  $\mu$ M S-adenosyl methionine in 40 mM MOPS pH 7.0 buffer. 25  $\mu$ M dioctylamine and DMSO (2.5%) were used as the positive and negative controls, respectively.

#### *CmaA2 high throughput small molecule inhibitor screening*

The CmaA2 high throughput screen was performed in Costar 384-well all black assay plates, 50 $\mu$ L assay volume, in three steps. All liquid handling was performed using a Cybio Vario instrument. First, 24  $\mu$ L of 100 mM NaH<sub>2</sub>PO<sub>4</sub>, pH 7.4, was transferred to each well in the assay plate, followed by the addition of 1 $\mu$ L of 100 % DMSO or 50X (500  $\mu$ M) inhibitor stock (1  $\mu$ M inhibitor stock was used for screening Sanofi library). After mixing thoroughly, 25  $\mu$ L of 2X enzyme master mix (600 nM CmaA2 supplemented with 600  $\mu$ M S-adenosyl methionine and 1.2  $\mu$ M fluorescent probe (NBD-A) was transferred to the assay plate. The plates were sealed and incubated overnight at 25 °C for 15 - 18 hrs then the fluorescence intensity of each well was measured (Ex: 475 nm, Em: 530 nm). 10  $\mu$ M Molecule 4 (Enamine, EN:Z57056244) was used as the positive control and 2 % DMSO was



used as the negative control. Analysis of the screening data was performed using Collaborative Drug Discovery software.

#### *Mycobacterium tuberculosis in vitro growth inhibition assay*

Mtb mc<sup>2</sup>7000 was cultured in 7H9 media supplemented with 10 % oleic acid-albumin-dextrose-catalase, 0.05% tyloxapol, and 25 µg/ml pantothenic acid. When the culture reached an OD<sub>600</sub> = 1.0, the culture was subsequently diluted to OD<sub>600</sub> = 0.1 in 7H9-dextrose media. 7H9-dextrose media: 0.5 % dextrose, 0.085 % NaCl, 0.25 µg/mL malachite green, 0.05 % tyloxapol, and 25 µg/ml pantothenic acid. Inhibitor stocks were made with 100% DMSO. Growth inhibition assays were performed in 96-well assay plates with a final assay volume of 200 µL of 7H9-dextrose media with 2 % DMSO. The assays were performed as follows: 4 µL of 100 % DMSO or desired compound stock were added to the assay plate, followed by 196 µL of Mtb culture (OD<sub>600</sub> = 0.1). The assay plates were sealed and incubated for 7 days at 37 °C. On day 7, 4 µL of 0.25 mg/mL resazurin solution (dissolved in sterile water) was added to each well throughout the plate and cultured for an additional 2 days. On day 9, resorufin fluorescence was measured (Ex: 544 nm, Em: 490 nm). Data analysis was performed using Collaborative Drug Discovery software.

#### *Automated ligand identification system screening*

The protocol used by Merck to perform the ALIS screen is confidential.

#### *Mycolic acid preparation and two-dimensional thin layer chromatography analysis*

*M. bovis* BCG Russia was cultured to OD<sub>600</sub> of 0.3 - 0.5 in a final volume of 50 -200 mL in 7H9 media. The media was supplemented with <sup>14</sup>C-labeled acetic acid to a concentration of 1 mCi/ml, where the bacteria were grown for an additional 6 hr. The bacteria were harvested, and mycolic acids were prepared for TLC analysis as previously

described (Glickman et al., 2001). Two-dimensional TLC plates were prepared by immersing 90 % of the plate area in 10 % silver nitrate and activated at 130 °C for 20 min. The mycolic acid samples were run along the line devoid of silver nitrate (first dimension). Subsequently, the TLC plate was rotated 90° then developed for five to six times into the silver nitrate impregnated area (second dimension). After separation completion, autoradiograms were developed using a Kodak BioMax Transcreen LE intensifying screen at -80C.

#### *Crystallization of CmaA2 ternary complexes and data collection*

CmaA2 in complex SAM and Compound 1 (Chembridge, CB:7732198), Compound 4 (Enamine, EN:Z57056244), H20 (VitasM labs, STL:055938), H23 (Chembridge, CB:6139451), and H29 (Chembridge, CB:79538770) were crystallized using the hanging-drop vapor diffusion method. For co-crystallization of CmaA2-inhibitor complexes, the following procedure was carried out. A 2 mL solution containing 30 µM (1 mg/mL) CmaA2, 200 µM S-adenosyl methionine, and 200 µM compounds were incubated at 25 °C for 1 hr. The protein solutions were then concentrated to 10 mg/mL and mixed with equal portions of mother liquor to a final volume of 4 µL. Mother liquors used: 0.1 M HEPES pH 7.4 and 1.1 M trisodium citrate (Compound 1), 0.1 M HEPES pH 7.6 and 1.1 M trisodium citrate (Compound 4), 0.1 M HEPES pH 7.6 and 1.2 M trisodium citrate (H20), 0.1 M Bis-Tris Propane pH 6.4 and 52 % tacsimate pH 7.0 (H23), and 0.1 M Bis-Tris Propane pH 7.0 and 56 % tacsimate pH 7.0 (H29). Crystals were ready for data collection in approximately one week. Crystals were cryo-protected in mother liquor supplemented with 20% glycerol prior to flash freezing in liquid nitrogen. Diffraction data was collected at beamlines 19- and 23-ID at the Advanced Photon Source, Argonne National Laboratory. Diffraction data for the

CmaA2-MTA-H29 was collected on a Rigaku R-Axis diffractometer. These data were processed and reduced using HKL2000 (Otwinowski and Minor, 1997).

*Structure determination and model refinement*

The structure of CmaA2-SAH-**1**, CmaA2-SAH-**2**, CmaA2-SAH-**4**, CmaA2-SAH-**H20**, and CmaA2-SAH-**H29** were all solved by molecular replacement using Phaser in Phenix (Afonin et al., 2010). CmaA2-DOA (PDB code: 3HEM) was used as the search model with all non-protein atoms excluded. The crystals were all in the space group  $I4_122$ , with one molecule in the asymmetric unit with dimensions closely approximating  $a = b = 106.5$  and  $c = 226.8$  Å and  $\alpha = \beta = \gamma = 90^\circ$ . Subsequent to molecular replacement phasing, rigid body refinements were performed in PHENIX refine. The initial structure refinements produced  $R_{\text{work}}$  and  $R_{\text{free}}$  of 24.3 % and 26.5 %, 25.1 % and 26.4 %, 26.0 % and 28.2 %, 21.0 % and 23.8 %, for CmaA2 in complex with **1**, **4**, **H20**, and **H29**, respectively (Afonin et al., 2010). SAH, bicarbonate ion, and small molecule inhibitors were then manually modelled. With further model building and PHENIX refinement cycles, water molecules were added to by examining the  $F_o - F_c$  maps. The final  $R_{\text{work}}$  and  $R_{\text{free}}$  values were as follows: (**1**: 15.8 % and 18.1%), (**4**: 16.1 %, 17.7 %), (**H20**: 17.0 %, 19.3 %) and (**H29**: 16.7 % and 21.5 %). The final models contained amino acid residues 12-302.

The structure of CmaA2-SAH-**H23** was all solved by molecular replacement using Phaser in Phenix (Afonin et al., 2010). CmaA2-DOA (PDB code: 3HEM) was used as the search model with all non-protein atoms excluded. The crystals were all in the space group  $P4_32_12$ , with two molecules in the asymmetric unit with dimensions closely approximating  $a = b = 111.92$  and  $c = 185.56$  Å and  $\alpha = \beta = \gamma = 90^\circ$ . Subsequent to molecular replacement phasing, rigid body refinement was performed in PHENIX refine. The initial structure

refinement produced a  $R_{\text{work}}$  and  $R_{\text{free}}$  of 31.1 % and 33.6 % (Afonin et al., 2010). Subsequently, SAH, bicarbonate ion, and H23 were manually modelled. With further model building and PHENIX refinement cycles, 620 water molecules were added by examining the  $F_o - F_c$  maps. The final  $R_{\text{work}}$  and  $R_{\text{free}}$  values were 14.4 % and 16.8 %. The final model contained amino acid residues 12-302.

#### *Mycobacterium tuberculosis* kill-curve assays

Mtb mc<sup>2</sup>7000 was cultured in 7H9 media supplemented with 10% oleic acid-albumin-dextrose-catalase, 0.05% tyloxapol, and 25  $\mu\text{g/ml}$  pantothenic acid. When the culture reached an  $\text{OD}_{600} = 1.0$ , the culture was subsequently diluted to  $\text{OD}_{600} = 0.1$  in 7H9-dextrose media. 7H9-dextrose media: 0.5 % dextrose, 0.085 % NaCl, 0.25  $\mu\text{g/mL}$  malachite green, 0.05 % tyloxapol, and 25  $\mu\text{g/ml}$  pantothenic acid. Kill-curve assay cultures were carried out in 5mL 7H9-dextrose media with 2% DMSO in 30mL Corning sterile bottles. To 4.85 mL of 7H9-dextrose media, either 100  $\mu\text{L}$  of 100% DMSO or desired inhibitor stock was added followed by the addition of 50  $\mu\text{L}$  of  $\text{OD}_{600} = 0.1$  Mtb culture (approximately  $1 \times 10^5$  CFU/mL final,  $\text{OD}_{600} = 0.001$ ). Inhibitor stocks were made up in 100% DMSO. Cultures were incubated for 21 days at 37 °C with continuous shaking. On days 0, 1, 7, 14, and 21, 50 $\mu\text{L}$  culture CFUs were determined by dilution plating onto 7H10-OADC agar plates.

#### **Discussion**

Our data clearly establishes NBD fluorescence probe displacement as a powerful approach for identifying multitarget CMAS ligands and reveals that the enzyme family binds dioctylamine-like amphiphiles of broad structural diversity. We previously showed that NBD fluorescence-enhancement probes are suitable reagents for CMAS competition

displacement assays and multitarget assessment, but their use for high throughput drug screening was not addressed. Our data showed that the NBD-based competition displacement assay is highly amenable to HTS, and have revealed that the CMAS active sites bind drug-like molecule of immense structural diversity. Approximately half of the identified CMAS ligands were analogs of **4** and **5** whereas the other half were structurally diverse, largely determined by differences in the hydrophobic constituents. The terminal nitrogen atoms were most commonly found as a secondary/tertiary amine, largely within nonaromatic heterocycles, or within an imidazole ring. These data strongly suggest that CMAS ligands will require a terminal basic amine to mimic the common carbocation reaction intermediate. This is corroborated by multiple CmaA2-inhibitor complex structures showing that the basic amines similarly locate at the catalytic core. We were unable to identify a multitarget compound devoid of cytotoxicity, however this may be alleviated through structure-guided design. Given that the hydrophobic entrance encompasses the largest portion of the active site, designing CMAS ligands that perfectly contour the active site that maximize their van der Waals intermolecular interactions may be most beneficial.

Post-primary analysis of the ALIS screening data indicates that the proprietary Merck collection likely contains a myriad of compounds and compound clusters that have capacity to multitarget the MA-MT family of enzymes. The majority of compounds identified showed multiple binding events towards CMAS but the majority included MmaA4. Despite very few inhibitors found to bind all three CMAS enzymes, many inhibitors bind at least two. Inferring from our competition displacement and in vivo studies, compounds that bind to at least two CMAS will likely bind to all three. To date, two compounds have been identified to target MmaA4, DOA and S-adenosyl-N-decyl-

aminoethyl (Barkan et al., 2009)(Vaubourgeix et al., 2009). The latter compound is a SAM analog that may inhibit host SAM-dependent methyltransferases resulting in cytotoxicity. ALIS screening identified a myriad of highly selective MmaA4 compounds. As in vitro assays have not been established for MmaA4, and the crystal structure has been solved in complex with multiple ligands, a structure-guided fluorescence polarization assay design approach described in Chapter 2 may provide an assay platform to initiate drug discovery of this currently intractable enzyme (Vaubourgeix et al., 2009). As ketomycolates have been strongly implicated in virulence, immune modulation, biofilm and host lipid droplet formation, assay development and inhibitor studies with compounds identified in the ALIS screen may provide a novel approach to shorten tuberculosis treatment through small-molecule inhibition of MmaA4 (Dao et al., 2008; Dkhar et al., 2014; Dubnau et al., 2000; Peyron et al., 2008; Sambandan et al., 2013).

The majority of compounds identified via HTS that demonstrated similar CMAS binding affinity, binding differential, and Mtb whole cell activity as DOA, were found to inhibit multiple pathways of mycolic acid modification in vivo. Given the dose-dependent inhibitory effect on mycolic acid modification BCG-R, we have attributed simultaneous inhibition of mycolic acid methyltransferases to Mtb growth inhibition, but further validation of on-target activity is required. Of primary importance, is determining whether the CMAS ligands identified in this study inhibit mycolic acid modification in Mtb. If the compounds are confirmed to inhibit multiple pathways of mycolic acid modification in Mtb, testing whether MA-MTs are direct targets of the compounds will require overexpressing MA-MTs individually to assess their ability to reverse the inhibitory effect of target-specific modifications. In addition, overexpressing multiple MA-MTs simultaneously should

provide resistance to the inhibitor. The caveat to the is experiment is that MA-MTs are nonessential enzymes. MA-MTs may simply act as target decoys, therefore causing a dilution effect of the cytoplasmic inhibitor concentration. The cytoplasmic concentration may be reduced to a level that is unable to inhibit the off-targets responsible for growth inhibition, rendering Mtb less susceptible to the compounds. To test whether off-target effects are the cause of Mtb growth inhibition, inhibitor susceptibility testing is required against cyclopropane-deficient Mtb (Barkan et al., 2012). Off-target inhibitors should demonstrate enhanced potency as the strain lacks four (PcaA, CmaA2, MmaA1, and MmaA2) of the six established MA-MTs. Lack of growth inhibition may result from on-target activity or poor cellular penetration. Although the latter is less probable as proximal *cis*- and *trans*-cyclopropanation have been shown to contribute to the relative impermeability of the cell wall (George et al., 1995; Liu et al., 1996; Yuan et al., 1997). The latter could be assessed through cell penetration assays using a radio-labelled inhibitor or liquid chromatography mass spectrometry methods (Barkan et al., 2009; Sarathy et al., 2013). Alternatively, carefully designed inducible CRISPR interference (CRISPRi) knockdown strains that phenocopy the cell wall of inhibitor-treated bacilli will be important cellular tools in future studies. Inducing a phenotype similar to those observed from DOA or other multitarget CMAS inhibitor treatment, while determining the number of colony forming units, would provide a genetic-based method for assessing whether simultaneous inhibition of MA-MTs are bactericidal or bacteriostatic to Mtb. In the case that the simultaneous loss of mycolic acid modification is confirmed to be bacteriostatic, as we believe based on Mtb kill-curve analysis, this inhibitory effect on the cell wall mycolate composition may provide a means to enhance drug penetration and reduce host toxicity by

lowering the dose of other antimycobacterials within a combination antitubercular drug regimen.

The novel conformation change of the CmaA2 active site entrance loop may indicate a potential molecular mechanism whereby Mtb inhibits CmaA2 function to alter its virulence. Prior studies have shown that fine structural changes to TDM induce altered host inflammatory responses, that profoundly affects the outcome of infection (Dao et al., 2008; Rao et al., 2005, 2006). Mtb synthesizes oxygenated mycolic acids harboring *trans*-cyclopropane rings to suppress Mtb-induced inflammation and virulence, mediated through TDM (Rao et al., 2006). As compared to WT, the Mtb  $\Delta$ *cmaA2* mutant displays a more aggressive infection with severe granulomatous inflammation, resulting in a hypervirulent strain with accelerated host mortality (Rao et al., 2006). In contrast, Mtb synthesizes  $\alpha$ -mycolates harboring proximal *cis*-cyclopropane rings to generate a mycolate composition sufficient for establishing a lethal chronic infection (Rao et al., 2005). Loss of PcaA function by inactivating the *pcaA* gene results in an overall inverted mycolate composition, with the TDM fraction harboring ketomycolate as the major mycolate species. Mice infected with the  $\Delta$ *pcaA* mutant displayed a less severe histopathology than WT, resulting in a population of mice that all survived whereas WT had perished. With respect to host macrophage TNF- $\alpha$  secretion, TDM derived from the  $\Delta$ *pcaA* mutant was hypoinflammatory, whereas TDM derived from the  $\Delta$ *cmaA2* mutant was hyperinflammatory. Together these data show that alteration in the fine chemical structure of TDM, by two enzymes required for proximal cyclopropanation, can significantly alter the course of infection. Recently, in vitro kinase screening showed that PcaA is a substrate for multiple eukaryotic-like serine/threonine protein kinases (STPKs), primarily PknF and PknH (Corrales et al., 2012). Phosphorylation



sites were identified as T183 and T168. T183 resides on the active site entrance loop whereas T168 locates within the protein core. The phosphomimetic T183D T186D mutant was enzymatically less active than WT PcaA, and unable to complement the lack of proximal cyclopropanation when overexpressed in the *M. bovis* BCG  $\Delta pcaA$  mutant. Although, T183 was the major phosphorylation site, phenotypic rescue was not examined for the T183D mutant alone. In the same study, it was shown that MmaA2 was not a substrate for any of the six STPKs tested. In addition, MmaA4 has been shown to be a protein substrate for PknJ (Jang et al., 2010). To date, phosphorylation of CmaA2 by STPKs has not been reported, despite extensive research directed towards elucidating these kinase substrates (Richard-Greenblatt and Av-gay, 2017). Analysis of the primary structure of CMAS) predicts that T198 of CmaA2 and T183 of PcaA reside at identical positions in the active site entrance loop (Figure 6A). By superimposing the crystal structures of PcaA and CmaA2 in the open conformation, we show that these amino acids reside at a similar location (Figure 29A). Interestingly, the active site loop (16 residues, T173-L188) of PcaA is highly flexible whereas the loop of CmaA2 is short (G196-P200) with increased order as it is flanked by two  $\alpha$ -helices,  $\alpha$ 9 and  $\alpha$ 10. In the open conformation, the oxygen atom (OG1) of T198 is within a distance of 4 Å of the carbon atom (CD) of P200 (Figure 29B). This predicts that subsequent to T198 phosphorylation, the phosphate group would likely result in a steric clash with P200. Removal of this steric impairment may require a conformation shift, resulting in active site closure. In the CmaA2-SAH-H23 structure, P200 shifts approximately ~10 Å towards the  $\alpha$ 11 helix with OG1 of T198 pointing directly to the bulk solvent with a near complete occlusion of the acyl binding site. This suggests a model that active site closure resulting from CmaA2 phosphorylation, prevents cyclopropanation of *trans*-unsaturated

mycolate substrates through inhibiting AcpM docking, that results in the accumulation of unsaturated oxygenated mycolates in TDM, thereby enhancing Mtb virulence. In sum, we hypothesize that Mtb alters its virulence by differential presentation of TDM variants, that is temporally regulated by fine adjustments in proximal CMAS function through protein phosphorylation.

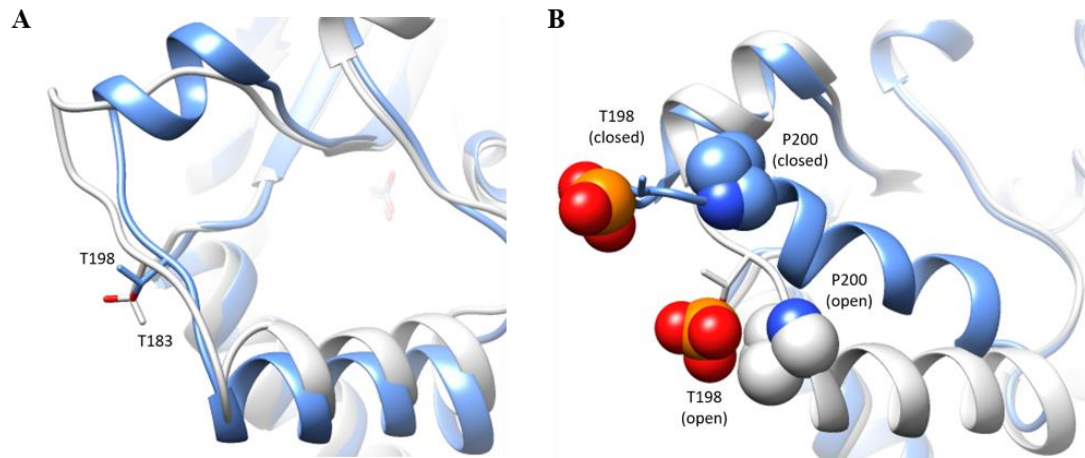


**Figure 29. Putative model for CmaA2 active site closure via T198 phosphorylation.**

A) Superimposition of PcaA (PDB entry: 1L1E, grey) and CmaA2 in complex with S-adenosyl homocysteine (SAH) and Compound 4 (CmaA2-SAH-4, blue). CmaA2 T198 resides at an identical position to PcaA T183, an established phosphorylation site by serine-threonine kinase PknF. B) Superimposition of CmaA2-SAH-4 (open conformation) and CmaA2-SAH in complex with Compound H23 (closed conformation). In the open conformation, T198 resides within 5 Å of P200. The crystal structure data suggests a putative model by which CmaA2 active site closure results due to CmaA2 T198 phosphorylation by a serine-threonine kinase. Upon phosphorylation, phospho-T198 may induce a steric clash with P200, whereby a conformation change would be required to relieve steric hinderance, resulting in active site loop closure.

## CHAPTER IV

### CONCLUSIONS

The identification of various multitarget CMAS ligands with equilibrium dissociation constants near or below the assay detection limits strongly suggests that future structure-activity relationship studies will require higher affinity NBD probes. Generating an assay probe with significantly higher affinity than those currently used will provide a stronger competitor for future inhibitor studies, thereby allowing the determination of inhibitor binding affinities much higher than currently can be achieved. Incorporating a higher affinity probe will improve the assay dynamic range as a lower probe concentration is required. This would be achieved by decreasing  $[NBD]_{free}$  contributing to the background fluorescence while maintaining CMAS-NBD complex fluorescence output. Given the essential nature of a basic amine of CMAS ligands, enhancing probe binding affinity will entail modifying the constituents attached to the terminal nitrogen atom while maintaining the position of NBD in the acyl binding sites. As **5** was the highest affinity CmaA2 ligand and likely the highest affinity MmaA2 ligand, generating NBD-**5** is of primary importance. Any forthcoming NBD probes generated should be assessed for binding other members of the MA-MT family, specifically PcaA and MmaA4, as *in vitro* assays have not been established.

A promising alternative *in vitro* assay design strategy to engage all three CMAS enzymes is through the use of fluorescence polarization (FP). Intrinsic background fluorescence and low fluorescence brightness of NBD are disadvantageous characteristics of our current *in vitro* assays that could be alleviated through an FP approach. Although FP

assays require fluorescent probes with high fluorescence brightness, negligible background fluorescence background is achieved through ratiometric detection. Generation of FP-based fluorescent probes require a covalently-attached fluorophore to an established small molecule ligand. As the location of the attached fluorophore is critical for assay success, the crystal structure of CmaA2 in complex with **4** showed that the chlorine atom resides within about a 5 Å distance from the protein-solvent interface and may serve as a substitution site for fluorophore tethering. However, tether length optimization will be required. In addition, Compound **4** was a high affinity ligand of both CmaA2 and MmaA2, and based-on our in vivo data the compound may also bind PcaA. As CMAS enzymes are highly similar with respect to primary and tertiary structure, these data suggest that the compound likely binds to all three active sites in a similar fashion. Therefore, an FP probe generated by fluorescently-labeling Compound **4** is a promising strategy to establish in vitro assays for all three CMAS enzymes. Importantly, FP assays are well-suited for high throughput screening. An alternative and potentially higher affinity multitargeting probe could be generated by fluorescently labeling **5**.

By screening the CmaA2-SAM-NBD-A complex against a diverse collection of whole cell active small molecules, we identified a set of compounds that inhibit multiple pathways of mycolic acid modification in vivo, but further validation of on-target activity is required. Coupling CmaA2 HTS and multitarget assessment, we have established that the active sites of CMAS accommodates small drug-like molecules of broad structural diversity, specifically amine-based amphiphiles. According to our hit collection, the hydrophobic constituents show significant structural diversity, whereas the terminal amines were strongly favored within aliphatic heterocycles or imidazole. Three molecules, **1**, **4**, and **H23** were

found to inhibit multiple pathways of mycolic acid modification in vivo but further on-target validation is required, and can be testing using the following approaches. First, as BCG-R is routinely used to test on-target activity, strains overexpressing single MA-MT targets should reverse the inhibitory effect of the target-specific modification. Second, overexpressing multiple MA-MT targets should reverse the inhibitory effect of all target-specific modifications and demonstrate increased resistance to the compound. As MA-MTs are non-essential, increased resistance to the compound may result from a target decoy effect, wherein inhibitor binding to MA-MTs reduce the overall cytosolic concentration, prohibiting inhibition of the target responsible for Mtb growth inhibition. Third, to test MA-MTs as target decoys, it is imperative to test the inhibitory effect of the compound on a strain lacking the putative targets. As **1**, **4**, and **H23** inhibit multiple pathways of mycolic acid cyclopropanation in vivo, the compounds need to be tested for growth inhibition against a cyclopropane-deficient strain of Mtb, that is available (Barkan et al., 2012). Compounds demonstrating enhanced potency against this strain would strongly suggests that growth inhibition results from off-target effects. Conversely, the lack of growth inhibition would indicate that the MA-MTs are direct targets of the compounds or they poorly penetrate the cell wall. Provided that the compounds show similar cell wall penetration, these data would provide strong support to on-target MA-MT activity. Finally, to accurately relate simultaneous inhibition of mycolic acid modification with Mtb growth inhibition, experiments need to be conducted within the same strain, particularly in Mtb.

An alternative genetic approach to assess inhibition of mycolic acid modification as a therapeutic approach is to use the inducible CRISPR interference (CRISPRi) system to transcriptionally repress multiple MA-MTs simultaneously. In particular, the CRISPRi

system would be used to generate strains lacking mycolic acid modifications to the extent observed by the inhibitors identified via CmaA2 HTS. A caveat of this approach is that the four genes within the *mma* (*mmaA1-4*) locus reside in an operon, wherein CRISPRi knockdown of a gene within the locus may cause a polar effect on downstream genes. Of particular concern is knocking down *mmaA3* to reduce methoxymycolate synthesis, as repression of the downstream *mmaA4* will deplete both methoxy- and ketomycolates. An additional concern with repressing *mmaA3* is the accumulation of hydroxymycolate, a mycolate species rarely observed with the treatment of our compounds. If CRISPRi knockdown strains could be generated that phenocopy the mycolic acid phenotype of our inhibitors and result in Mtb growth inhibition or loss of cell viability, this would provide strong support for MA-MTs as viable targets for drug discovery. Although a bactericidal effect is the ideal result, as all first-line antimycobacterial drugs are bactericidal compounds, the ability to demonstrate growth stasis would be highly informative as altered cell wall mycolate composition has been shown to enhance drug penetration, result in synergistic killing with known antimycobacterial drugs, and an enhanced immune response upon murine infection.

The multitargeting CMAS inhibitors identified in this study, established through *in vitro* and *in vivo* studies, all showed an indication of cytotoxicity. To combat this unfavorable compound toxicity, structure-guided drug design and extensive testing of ALIS-identified compounds provide two potential avenues for future investigations. Crystallographic studies of CmaA2-inhibitor complexes clearly established the molecular basis of inhibitor binding the active site. The nitrogen atoms reside at the catalytic core, mimicking the carbocation reaction intermediate, whereas the hydrophobic constituents

locate to the extensively hydrophobic entrance. Given the highly polar nature of the catalytic core, we envisage that increasing hydrogen bond intermolecular interactions would provide enhanced binding affinity and selectivity towards this family of enzymes over host enzymes. As all of the multitarget MA-MT inhibitors identified in this study solely contain terminal alkylamines, with the exception to **1** that additionally harbors an N-linked ethanol, potential hydrogen bond networks through heteroatoms attached to the alky groups were not revealed. With respect to the hydrophobic entrance, we envisage that inhibitor optimization would entail altering the chemical structure to perfectly contour the hydrophobic architecture of the acyl binding site. Alternatively, ALIS screening identified a myriad of MA-MT binding compounds, with over 3,000 binding events found. As our primary goal in the study was to identify multitargeting inhibitors against the three CMAS enzymes, the compounds of primary importance are those of that bound to 1- to 3-targets. As our CmaA2 HTS assay identified three compounds that inhibited multiple mycolic acid cyclopropane synthases *in vivo*, compounds that were found to bind one or two CMAS via ALIS screening likely bind to all three family members. The compound structures within the Merck collection are currently proprietary and have not been disclosed. Requesting their disclosure is of utmost importance as they may provide inhibitors with reduced cytotoxicity. Identifying a multitarget CMAS inhibitor with a favorable toxicity profile would provide a means to further test this therapeutic approach in a mouse model of infection.

The biological relevance of the conformation change revealed from crystal structure analysis of CmaA2 in complex with **H23**, that completely occludes the active site, is currently unknown. Superimposition of the crystal structures of CmaA2 and PcaA showed that CmaA2 T198 resides at the same position as PcaA T183, an established phosphorylation

site. Importantly, of the three established CMAS enzymes that show proximal cyclopropane synthase activity, this threonine residue is conserved in PcaA and CmaA2 but not in MmaA2. PcaA was shown to be a substrate for multiple serine-threonine kinases, but not MmaA2. However, it is currently unknown whether CmaA2 is kinase substrate. Phosphorylated PcaA showed a significant reduction in enzymatic activity and a PcaA phosphomimetic transformed into the *M. bovis* BCG Pasteur  $\Delta pcaA$  mutant demonstrated an inability to complement the mutant mycolic acid phenotype. The virulence of the Mtb  $\Delta pcaA$  and  $\Delta cmaA2$  mutants have been shown to be drastically different, that has been attributed to the differences in the host immune response by changes in the fine chemical structure of TDM. With respect to host mortality, the Mtb  $\Delta pcaA$  was unable to establish a lethal infection whereas an infection with the  $\Delta cmaA2$  mutant resulted in premature death. Therefore, we hypothesize that Mtb alters its virulence by differential presentation of TDM variants, that may be temporally regulated by fine adjustments in proximal CMAS function through protein phosphorylation. Setting precedence to this hypothesis would require direct evidence for CmaA2 as serine-threonine kinase substrate, that could be assessed using a similar approach as was previously reported for PcaA (Corrales et al., 2012). Interestingly, a most recent report indicated a role of TDM and the PcaA-dependent cyclopropane modification in initiating angiogenesis towards the site of granuloma formation (Walton et al., 2018). With regards to CmaA2, a prior report showed that granulomas with the liver granulomas of 2-week old  $\Delta cmaA2$ -infected mice appear necrotic with an exaggerated induction of host angiogenesis (Rao et al., 2006). This enhanced vasculature surrounding the necrotic granuloma was not addressed in the report but is commonly found human tuberculosis lesions. Taken together, we hypothesize that CmaA2-dependent cyclopropane



modifications to TDM, controlled by the CmaA2 phosphorylation, may play a fundamental role in the induction of angiogenesis to the site of granuloma formation. Moreover, CmaA2 phosphorylation is likely to be temporally controlled as indefinite inhibition of CmaA2 function may have a deleterious effect on the host by inducing an exaggerated immune response resulting in premature death, thereby disrupting the pathogens ultimate goal, dissemination.

The presence of **m2** in the crystal structure of CmaA2 in complex with **2** suggests that the compound was a substrate. There are two hypotheses for **m2** formation. Either **2** was directly methylated by SAM or catalytically methylated by CmaA2. Neither hypothesis has been currently tested. To test the first, requires incubating SAM and **2** together then analyzing the mass spectrum of the reaction mixture over time. Detection of **m2** in the reaction mixture would indicate that SAM can directly methylate **2**. If no reaction occurs, this would suggest that CmaA2 catalytically methylated **2**. To test whether **2** is a CmaA2 substrate, a similar MS approach could be used as previously described or a continuous coupled enzyme assay using SAH hydrolase and Ellman's reagent (Barkan et al., 2009)(Corrales et al., 2012). Current CMAS in vitro assays require nonauthentic medium chain fatty acid substrates, that result in poor enzyme activity. Identifying **2** as a CmaA2 substrate may provide a rational approach for designing new substrates to kinetically monitor CMAS activity in vitro. As the carbocation reaction intermediate is likely to be transiently formed, using an amine-based substrate similar to **2** will unlikely be a viable substrate for a kinetic based assay as the compound will most definitely be an inhibitor, as the compound mimics a long-lived cation intermediate. Although a substrate analog of **2** may be generated

by replacing N16 with a carbon atom (C16) and incorporating a double bond between the adjacent C16 atom.

## REFERENCES

- Afonin, P. V., Hung, L.W., Terwilliger, T.C., Oeffner, R., Davis, I., McCoy, A., Richardson, J., Bunkoczi, G., Moriarty, N., Headd, J., et al. (2010). PHENIX: a comprehensive Python-based system for macromolecular structure solution. *Acta Crystallogr. D66*, 213 - 221.
- Aggarwal, A., Parai, M.K., Shetty, N., Wallis, D., Woolhiser, L., Hastings, C., Dutta, N.K., Galaviz, S., Dhakal, R.C., Shrestha, R., et al. (2017). Development of a novel lead that targets *M. tuberculosis* polyketide synthase 13. *Cell* 170, 249 - 259.
- Aguilar, P.S., and Cronan, J.E. (1998). A *Bacillus subtilis* gene induced by cold shock encodes a membrane phospholipid desaturase. *J. Bacteriol.* 180, 2194 - 2200.
- Alahari, A., Trivelli, X., Guérardel, Y., Dover, L.G., Besra, G.S., Sacchettini, J.C., Reynolds, R.C., Coxon, G.D., and Kremer, L. (2007). Thiacetazone, an antitubercular drug that inhibits cyclopropanation of cell wall mycolic acids in mycobacteria. *PLoS One* 2, 1 - 12.
- Alahari, A., Alibaud, L., Trivelli, X., Gupta, R., Lamichhane, G., Reynolds, R.C., Bishai, W.R., Guerardel, Y., and Kremer, L. (2009). Mycolic acid methyltransferase, MmaA4, is necessary for thiacetazone susceptibility in *Mycobacterium tuberculosis*. *Mol. Microbiol.* 71, 1263 - 1277.
- Altabe, S.G., Aguilar, P., Caballero, G.M., and Mendoza, D. De (2003). The *Bacillus subtilis* acyl lipid desaturase is a  $\Delta 5$  desaturase. *J. Bacteriol.* 185, 3228 - 3231.
- Ananthan, S., Faaleolea, E.R., Goldman, R.C., Hobrath, J. V., Kwong, C.D., Laughon, B.E., Maddry, J.A., Mehta, A., Rasmussen, L., Reynolds, R.C., et al. (2009). High-throughput screening for inhibitors of *Mycobacterium tuberculosis* H37Rv. *Tuberculosis* 89, 334 - 353.
- Annis, D.A., Nickbarg, E., Yang, X., Ziebell, M.R., and Whitehurst, C.E. (2007). Affinity selection-mass spectrometry screening techniques for small molecule drug discovery. *Curr. Opin. Chem. Biol.* 11, 518 - 526.
- Asselineau, J., and Lederer, E. (1950). Structure of the mycolic acids of mycobacteria. *Nature* 166, 782 - 783.
- Asselineau, C.P., Lacave, C.S., and Montrozier, H.L. (1970). Relations structurales entre les acides mycoliques insatures et les acides inferieurs insatures synthetises par *Mycobacterium phlei*. *Eur. J. Biochem.* 14, 406 - 410.
- Barkan, D., Liu, Z., Sacchettini, J.C., and Glickman, M.S. (2009). Mycolic acid cyclopropanation is essential for viability, drug resistance, and cell wall integrity of *Mycobacterium tuberculosis*. *Chem. Biol.* 16, 499 - 509.
- Barkan, D., Rao, V., Sukenick, G.D., and Glickman, M.S. (2010). Redundant function of cmaA2 and mmaA2 in *Mycobacterium tuberculosis* cis cyclopropanation of oxygenated mycolates. *J. Bacteriol.* 192, 3661 - 3668.
- Barkan, D., Hedhli, D., Yan, H.-G., Huygen, K., and Glickman, M.S. (2012).

- Mycobacterium tuberculosis* lacking all mycolic acid cyclopropanation is viable but highly attenuated and hyperinflammatory in mice. *Infect. Immun.* *80*, 1958 - 1968.
- Barry III, C.E., Lee, R.E., Mdluli, K., Sampson, A.E., Schroeder, B.G., and Slayden, R.A. (1998). Mycolic acids : Structure, biosynthesis and physiological functions. *Prog. Lipid Res.* *37*, 143 - 179.
- Basaraba, R.J., and Ojha, A.K. (2017). Mycobacterial biofilms: revisiting tuberculosis bacilli in extracellular necrotizing lesions. *Microbiol. Spectr.* *5*, 1 - 7.
- Beatty, W.L., Rhoades, E.R., Ullrich, H.-J., Chatterjee, D., Heuser, J.E., and Russell, D.G. (2000). Trafficking and release of mycobacterial lipids from infected macrophages. *Traffic* *1*, 235 - 247.
- Behr, M.A., Schroeder, B.G., Brinkman, J.N., Slayden, R.A., and Barry III, C.E. (2000). A point mutation in the *mma3* gene is responsible for impaired methoxymycolic acid production in *Mycobacterium bovis* BCG strains obtained after 1927. *J. Bacteriol.* *182*, 3394 - 3399.
- Vander Beken, S., Al Dulayymi, J.R., Naessens, T., Koza, G., Maza-Iglesias, M., Rowles, R., Theunissen, C., De Medts, J., Lanckacker, E., Baird, M.S., et al. (2011). Molecular structure of the *Mycobacterium tuberculosis* virulence factor, mycolic acid, determines the elicited inflammatory pattern. *Eur. J. Immunol.* *41*, 450 - 460.
- Belardinelli, J.M., and Morbidoni, H.R. (2012). Mutations in the essential FAS II  $\beta$ -hydroxyacyl ACP dehydratase complex confer resistance to thiacetazone in *Mycobacterium tuberculosis* and *Mycobacterium kansasii*. *Mol. Microbiol.* *86*, 568 - 579.
- Bell, E. (1981). Fluorescence: Solution Studies. In *Spectroscopy in Biochemistry*, (CRC Press), pp. 155 - 194.
- Berger, W.T., Ralph, B.P., Kaczocha, M., Sun, J., Balius, T.E., Rizzo, R.C., Haj-Dahmane, S., Ojima, I., and Deutsch, D.G. (2012). Targeting Fatty Acid Binding Protein (FABP) anandamide transporters - A novel strategy for development of anti-inflammatory and anti-nociceptive drugs. *PLoS One* *7*, 1 - 12.
- Bhamidi, S., Scherman, M.S., Rithner, C.D., Prenni, J.E., Chatterjee, D., Khoo, K., and Mcneil, M.R. (2008). The identification and location of succinyl residues and the characterization of the interior arabinan region allow for a model of the complete primary structure of *Mycobacterium tuberculosis* mycolyl arabinogalactan. *J. Biol. Chem.* *283*, 12992 - 13000.
- Bhatt, A., Fujiwara, N., Bhatt, K., Gurucha, S.S., Kremer, L., Chen, B., Chan, J., Porcelli, S.A., Kobayashi, K., Besra, G.S., et al. (2007). Deletion of *kasB* in *Mycobacterium tuberculosis* causes loss of acid-fastness and subclinical latent tuberculosis in immunocompetent mice. *Proc. Natl. Acad. Sci. U. S. A.* *104*, 5157 - 5162.
- Boehringer, D., Ban, N., and Leibundgut, M. (2013). 7.5-Å Cryo-EM structure of the mycobacterial fatty acid synthase. *J. Mol. Biol.* *425*, 841 - 849.
- Boissier, F., Bardou, F., Guillet, V., Uttenweiler-Joseph, S., Daffé, M., Quémard, A., and

- Mourey, L. (2006). Further insight into S-adenosylmethionine-dependent methyltransferases: Structural characterization of Hma, an enzyme essential for the biosynthesis of oxygenated mycolic acids in *Mycobacterium tuberculosis*. *J. Biol. Chem.* *281*, 4434 - 4445.
- Brennan, P.J., and Nikaido, H. (1995). The envelope of mycobacteria. *Annu. Rev. Biochem.* *64*, 29 - 63.
- Brown, A.K., Sridharan, S., Kremer, L., Lindenberg, S., Dover, L.G., Sacchettini, J.C., and Besra, G.S. (2005). Probing the mechanism of the *Mycobacterium tuberculosis*  $\beta$ -ketoacyl-acyl carrier protein Synthase III *mtFabH*: Factors influencing catalysis and substrate specificity. *J. Biol. Chem.* *280*, 32539 - 32547.
- Buist, P.H., and Maclean, D.B. (1981). The biosynthesis of cyclopropane fatty acids. I. Feeding experiments with oleic acid-9,10-*d*<sub>2</sub>, oleic acid-8,8,11,11-*d*<sub>4</sub>, and L-methionine-methyl-*d*<sub>3</sub>. *Can. J. Chem.* *59*, 828 - 838.
- Burstein, Y., and Shakked, Z. (2015). AcpM, the meromycolate extension acyl carrier protein of *Mycobacterium tuberculosis*, is activated by the 4'-phosphopantetheinyl transferase PptT, a potential target of the multistep mycolic acid biosynthesis. *Biochemistry* *54*, 2360 - 2371.
- Cambau, E., and Drancourt, M. (2014). Steps towards the discovery of *Mycobacterium tuberculosis* by Robert Koch, 1882. *Clin. Microbiol. Infect.* *20*, 196 - 201.
- Chan, J., Xing, Y., Magliozzo, R.S., and Bloom, B.R. (1992). Killing of virulent *Mycobacterium tuberculosis* by reactive nitrogen intermediates produced by activated murine macrophages. *J. Exp. Med.* *175*, 1111 - 1122.
- Chang, Y., and Fox, B.G. (2006). Identification of Rv3230c as the NADPH oxidoreductase of a two-protein DesA3 acyl-CoA desaturase in *Mycobacterium tuberculosis* H37Rv. *Biochemistry* *45*, 13476 - 13486.
- Cheng, X., and Roberts, R.J. (2001). AdoMet-dependent methylation, DNA methyltransferases and base flipping. *Nucleic Acids Res.* *29*, 3784–3796.
- Cole, S.T., Brosch, R., Parkhill, J., Garnier, T., Churcher, C., Harris, D., Gordon, S. V, Eiglmeier, K., Gas, S., Barry III, C.E., et al. (1998). Deciphering the biology of *Mycobacterium tuberculosis* from the complete genome sequence. *Nature* *393*, 537 - 544.
- Collins, M.D., Goodfellow, M., and Minnikin, D.E. (1982). A Survey of the structures of mycolic acids in *Corynebacterium* and related taxa. *J. Gen. Microbiol.* *128*, 129 - 149.
- Corrales, R.M., Molle, V., Leiba, J., Mourey, L., De Chastellier, C., and Kremer, L. (2012). Phosphorylation of mycobacterial PcaA inhibits mycolic acid cyclopropanation: Consequences for intracellular survival and for phagosome maturation block. *J. Biol. Chem.* *287*, 26187 - 26199.
- Costerton, J.W., Stewart, P.S., and Greenberg, E.P. (1999). Bacterial biofilms: A common cause of persistent infections. *Science.* *284*, 1318 - 1323.

- Courtois, F., and Ploux, O. (2005). *Escherichia coli* cyclopropane fatty acid synthase: Is a bound bicarbonate ion the active-site base? *Biochemistry* 44, 13583 - 13590.
- Courtois, F., Guérard, C., Thomas, X., and Ploux, O. (2004). *Escherichia coli* cyclopropane fatty acid synthase: Mechanistic and site-directed mutagenetic studies. *Eur. J. Biochem.* 271, 4769 - 4778.
- Coxon, G.D., Craig, D., Corrales, R.M., Vialla, E., Gannoun-Zaki, L., and Kremer, L. (2013). Synthesis, antitubercular activity and mechanism of resistance of highly effective thiacetazone analogues. *PLoS One* 8, 1 - 13.
- Cronan, J. E. J., Nunn, W.D., and Batchelor, J.G. (1974). Studies on the biosynthesis of cyclopropane fatty acids in *Escherichia coli*. *J. Bacteriol.* 348, 63 - 75.
- Daffé, M., and Etienne, G. (1999). The capsule of *Mycobacterium tuberculosis* and its implications for pathogenicity. *Tuber. Lung Dis.* 79, 153 - 169.
- Daffé, M., Brennan, P.J., and McNeil, M. (1990). Predominant structural features of the cell wall arabinogalactan of *Mycobacterium tuberculosis* as revealed through characterization of oligoglycosyl alditol fragments by gas chromatography/mass spectrometry and by <sup>1</sup>H and <sup>13</sup>C NMR analyses. *J. Biol. Chem.* 265, 6734 - 6743.
- Daniel, T.M. (2006). The history of tuberculosis. *Respir. Med.* 100, 1862 - 1870.
- Dao, D.N., Sweeney, K., Hsu, T., Gurcha, S.S., Nascimento, I.P., Roshevsky, D., Besra, G.S., Chan, J., Porcelli, S.A., and Jacobs, W.R. (2008). Mycolic acid modification by the *mmaA4* gene of *M. tuberculosis* modulates IL-12 production. *PLoS Pathog.* 4, 1 - 14.
- Davidson, L.A., and Takayama, K. (1979). Isoniazid inhibition of the synthesis of monounsaturated long-chain fatty acids in *Mycobacterium tuberculosis* H37Ra. *Antimicrob. Agents Chemother.* 16, 104 - 105.
- DeJesus, M., Gerrick, E., Xu, W., Park, S., Long, J., Boutte, C., Rubin, E., Schnappinger, D., Ehrt, S., Fortune, S., et al. (2017). Comprehensive essentiality analysis of the *Mycobacterium tuberculosis* genome. *MBio* 8, 1 - 17.
- Dheda, K., Gumbo, T., Maartens, G., Dooley, K.E., McNerney, R., Murray, M., Furin, J., Nardell, E.A., London, L., Lessem, E., et al. (2017). The epidemiology, pathogenesis, transmission, diagnosis, and management of multidrug-resistant, extensively drug-resistant, and incurable tuberculosis. *Lancet Respir. Med.* 5, 291 - 360.
- Dinadayala, P., Laval, F., Raynaud, C., Lemassu, A., Lanéelle, M.A., Lanéelle, G., and Daffé, M. (2003). Tracking the putative biosynthetic precursors of oxygenated mycolates of *Mycobacterium tuberculosis*: Structural analysis of fatty acids of a mutant strain devoid of methoxy- and ketomycolates. *J. Biol. Chem.* 278, 7310 - 7319.
- Dkhar, H.K., Nanduri, R., Mahajan, S., Dave, S., Saini, A., Somavarapu, A.K., Arora, A., Parkesh, R., Thakur, K.G., Mayilraj, S., et al. (2014). *Mycobacterium tuberculosis* keto-mycolic acid and macrophage nuclear receptor TR4 modulate foamy biogenesis

- in granulomas: a case of a heterologous and noncanonical ligand-receptor pair. *J. Immunol.* *193*, 295 - 305.
- Draper, P. (1998). The outer parts of the mycobacterial envelope as permeability barriers. *Front. Biosci.* *3*, 1253 - 1261.
- Dubnau, E., Laneelle, M.A., Soares, S., Benichou, A., Vaz, T., Prome, D., Prome, J.C., Daffe, M., Quemard, A., Lan elle, M.-A., et al. (1997). *Mycobacterium bovis* BCG genes involved in the biosynthesis of cyclopropyl keto- and hydroxymycolic acids. *Mol. Microbiol.* *23*, 313 - 322.
- Dubnau, E., Chan, J., Raynaud, C., Mohan, V.P., Lan elle, M.-A., Yu, K., Qu emard, A., Smith, I., and Daff e, M. (2000). Oxygenated mycolic acids are necessary for virulence of *Mycobacterium tuberculosis* in mice. *Mol. Microbiol.* *36*, 630 - 637.
- Ducasse-Cabanot, S., Cohen-gonsaud, M., Marrakchi, H., Nguyen, M., Zerbib, D., Bernadou, J., Daffe, M., Labesse, G., and Quemard, A. (2004). In vitro inhibition of the *Mycobacterium tuberculosis*  $\beta$ -ketoacyl-acyl carrier protein reductase MabA by isoniazid. *Antimicrob. Agents Chemother.* *48*, 242 - 249.
- Dyer, D.H., Lyle, K.S., Rayment, I., and Fox, B.G. (2009). X-ray structure of putative acyl-ACP desaturase DesA2 from *Mycobacterium tuberculosis* H37Rv. *Protein Sci.* *14*, 1508 - 1517.
- Etemadi, A.H. (1967). Use of pyrolysis gas chromatography and mass spectroscopy in the study of the structure of mycolic acids. *J. Gas Chromatogr.* *5*, 447 - 456.
- Fery-Forgues, S., Fayet, J.P., and Lopez, A. (1993). Drastic changes in the fluorescence properties of NBD probes with the polarity of the medium: involvement of a TICT state? *J. Photochem. Photobiol.* *70*, 229 - 243.
- Fox, B.G., Shanklin, J., Ai, J., Loehr, T.M., and Sanders-Loehr, J. (1994). Resonance raman evidence for an Fe-O-Fe center in stearyl-ACP desaturase. Primary sequence identity with other diiron-oxo proteins. *Biochemistry* *33*, 12776 - 12786.
- Fox, B.G., Lyle, K.S., and Rogge, C.E. (2004). Reactions of the diiron enzyme stearyl-acyl carrier protein desaturase. *Accounts Chemical Res.* *37*, 421 - 429.
- Gavalda, S., Bardou, F., Laval, F., Bon, C., Malaga, W., Chalut, C., Guilhot, C., Mourey, L., Daffe, M., and Quemard, A. (2014). The polyketide synthase Pks13 catalyzes a novel mechanism of lipid transfer in mycobacteria. *Chem. Biol.* *21*, 1660 - 1669.
- George, K.M., Yuan, Y., Sherman, D.R., and Barry III, C.E. (1995). The biosynthesis of cyclopropanated mycolic acids in *Mycobacterium tuberculosis*: Identification and functional analysis of CMAS-2. *J. Biol. Chem.* *270*, 27292 - 27298.
- Glickman, M.S. (2003). The mmaA2 gene of *Mycobacterium tuberculosis* encodes the distal cyclopropane synthase of the  $\alpha$ -mycolic acid. *J. Biol. Chem.* *278*, 7844 - 7849.
- Glickman, M.S., Cox, J.S., and Jacobs Jr., W.R. (2000). A novel mycolic acid cyclopropane synthetase is required for cording, persistence, and virulence of *Mycobacterium tuberculosis*. *Mol. Cell* *5*, 717 - 727.

- Glickman, M.S., Cahill, S.M., and Jacobs Jr., W.R. (2001). The *Mycobacterium tuberculosis* *cmaA2* gene encodes a mycolic acid *trans*-cyclopropane synthetase. *J. Biol. Chem.* 276, 2228 - 2233.
- Griffin, J.E., Gawronski, J.D., Dejesus, M.A., Ioerger, T.R., Akerley, B.J., and Sasseti, C.M. (2011). High-resolution phenotypic profiling defines genes essential for mycobacterial growth and cholesterol catabolism. *PLoS Pathog.* 7, 1 - 9.
- Grzegorzewicz, A.E., Korduláková, J., Jones, V., Born, S.E.M., Belardinelli, J.M., Vaquié, A., Gundi, V.A.K.B., Madacki, J., Slama, N., Laval, F., et al. (2012). A common mechanism of inhibition of the *Mycobacterium tuberculosis* mycolic acid biosynthetic pathway by isoxyl and thiacetazone. *J. Biol. Chem.* 287, 38434 - 38441.
- Grzegorzewicz, A.E., de Sousa-d'Auria, C., McNeil, M.R., Huc-Claustre, E., Jones, V., Petit, C., Angala, S. kumar, Zemanová, J., Wang, Q., Belardinelli, J.M., et al. (2016). Assembling of the *Mycobacterium tuberculosis* cell wall. *J. Biol. Chem.* 291, 18867 - 18879.
- Guangqi, E., Drujon, T., Correia, I., Ploux, O., and Guianvarc'h, D. (2013). An active site mutant of *Escherichia coli* cyclopropane fatty acid synthase forms new non-natural fatty acids providing insights on the mechanism of the enzymatic reaction. *Biochimie* 95, 2336 - 2344.
- Guianvarc'h, D., Drujon, T., Leang, T.E., Courtois, F., and Ploux, O. (2006). Identification of new inhibitors of *E. coli* cyclopropane fatty acid synthase using a colorimetric assay. *Biochim. Biophys. Acta* 1764, 1381 - 1388.
- Guianvarc'h, D., E, G., Drujon, T., Rey, C., Wang, Q., and Ploux, O. (2008). Identification of inhibitors of the *E. coli* cyclopropane fatty acid synthase from the screening of a chemical library: In vitro and in vivo studies. *Biochim. Biophys. Acta* 1784, 1652 - 1658.
- Hall-Stoodley, L., Costerton, J.W., and Stoodley, P. (2004). Bacterial biofilms: From the natural environment to infectious diseases. *Nat. Rev. Microbiol.* 2, 95 - 108.
- Hoffmann, C., Leis, A., Niederweis, M., Plitzko, J.M., and Engelhardt, H. (2008). Disclosure of the mycobacterial outer membrane: Cryo-electron tomography and vitreous sections reveal the lipid bilayer structure. *Proc. Natl. Acad. Sci.* 105, 3963 - 3967.
- Holla, S., Prakhar, P., Singh, V., Karnam, A., Mukherjee, T., Mahadik, K., Parikh, P., Singh, A., Rajmani, R.S., Ramachandra, S.G., et al. (2016). MUSASHI-mediated expression of JMJD3, a H3K27me3 demethylase, is involved in foamy macrophage generation during mycobacterial infection. *PLoS Pathog.* 12, 1 - 25.
- Hong, S., Cheng, T., Layre, E., Sweet, L., Young, D.C., Posey, J.E., Butler, W.R., Branch, D.B., Cheng, T., Layre, E., et al. (2018). Ultralong C100 mycolic acids support the assignment of *Segniliparus* as a new bacterial genus. *PLoS One* 7, 1 - 11.
- Huang, C., Smith, C. V., Glickman, M.S., Jacobs Jr., W.R., and Sacchettini, J.C. (2002). Crystal structures of mycolic acid cyclopropane synthases from *Mycobacterium tuberculosis*. *J. Biol. Chem.* 277, 11559 - 11569.



- Hunter, R.L. (2012). Pathology of post primary tuberculosis of the lung: An illustrated critical review. *Tuberculosis* *91*, 497 - 509.
- Inghosso, D., Fowler, A. V., Bleibaum, J., and Clarke, S. (1989). Sequence of the D-aspartyl/L-isoaspartyl protein methyltransferase from human erythrocytes. *J. Biol. Chem.* *264*, 20131 - 20139.
- Iwig, D.F., Grippe, A.T., McIntyre, T.A., and Booker, S.J. (2004). Isotope and elemental effects indicate a rate-limiting methyl transfer as the initial step in the reaction catalyzed by *Escherichia coli* cyclopropane fatty acid synthase. *Biochemistry* *43*, 13510 - 13524.
- Iwig, D.F., Uchida, A., Stromberg, J.A., and Booker, S.J. (2005). The activity of *Escherichia coli* cyclopropane fatty acid synthase depends on the presence of bicarbonate. *J. Am. Chem. Soc.* *127*, 11612 - 11613.
- Jackson, M. (2014). The mycobacterial cell envelope-Lipids. *Cold Spring Harb. Perspect. Med.* *4*, 1 - 22.
- Jang, J., Stella, A., Boudou, F., Levillain, F., Darthuy, E., Vaubourgeix, J., Wang, C., Bardou, F., Puzo, G., Gilleron, M., et al. (2010). Functional characterization of the *Mycobacterium tuberculosis* serine/threonine kinase PknJ. *Microbiology* *156*, 1619 - 1631.
- Jankute, M., Cox, J.A.G., Harrison, J., and Besra, G.S. (2015). Assembly of the mycobacterial cell wall. *Annu. Rev. Microbiol.* *69*, 405 - 423.
- Julián, E., Roldán, M., Sánchez-Chardi, A., Astola, O., Agustí, G., and Luquin, M. (2010). Microscopic cords, a virulence-related characteristic of *Mycobacterium tuberculosis*, are also present in nonpathogenic mycobacteria. *J. Bacteriol.* *192*, 1751 - 1760.
- Koch, R. (1882). Aetiologie der Tuberkulose. *Berliner Klin. Wochenschrift* *15*, 221–230.
- Kolattukudy, P.E., Fernandes, N.D., Azad, A.K., Fitzmaurice, A.M., and Sirakova, T.D. (1997). Biochemistry and molecular genetics of cell-wall lipid biosynthesis in mycobacteria. *Mol. Microbiol.* *24*, 263 - 270.
- Korf, J., Stoltz, A., Verschoor, J., De Baetselier, P., and Grooten, J. (2005). The *Mycobacterium tuberculosis* cell wall component mycolic acid elicits pathogen-associated host innate immune responses. *Eur. J. Immunol.* *35*, 890 - 900.
- Kremer, L., Nampoothiri, K.M., Lesjean, S., Dover, L.G., Graham, S., Betts, J., Brennan, P.J., Minnikin, D.E., Locht, C., and Besra, G.S. (2001). Biochemical characterization of acyl carrier protein (AcpM) and malonyl-CoA:AcpM transacylase (*mtFabD*), two major components of *Mycobacterium tuberculosis* fatty acid synthase II. *J. Biol. Chem.* *276*, 27967 - 27974.
- Kulka, K., Hatfull, G., and Ojha, A.K. (2012). Growth of *Mycobacterium tuberculosis* biofilms. *J. Vis. Exp.* *60*, 1 - 6.
- Lancet, D., and Pecht, I. (1977). Spectroscopic and immunochemical studies with nitrobenzoxadiazolealanine, a fluorescent dinitrophenyl analogue. *Biochemistry* *16*,

5150 - 5157.

- Laval, F., Laneelle, M., Deon, C., Monsarrat, B., and Daffe, M. (2001). Accurate molecular mass determination of mycolic acids by MALDI-TOF mass spectrometry. *Anal. Chem.* *73*, 4537 - 4544.
- Laval, F., Haites, R., Movahedzadeh, F., Lemassu, A., Chinn, Y.W., Stoker, N., Billman-Jacobe, H., and Daffé, M. (2008). Investigating the function of the putative mycolic acid methyltransferase UmaA: Divergence between the *Mycobacterium smegmatis* and *Mycobacterium tuberculosis* proteins. *J. Biol. Chem.* *283*, 1419 - 1427.
- Lea-smith, D.J., Pyke, J.S., Tull, D., McConville, M.J., Coppel, R.L., and Crellin, P.K. (2007). The reductase that catalyzes mycolic motif synthesis is required for efficient attachment of mycolic acids to arabinogalactan. *J. Biol. Chem.* *282*, 11000 - 11008.
- Lea, W.A., and Simeonov, A. (2012). Fluorescence polarization assays in small molecule screening. *Expert Opin. Drug Discov.* *6*, 17 - 32.
- Lederer, E. (1969). Some problems concerning biological C-alkylation reactions and phytosterol biosynthesis. *Q. Rev. Chem. Soc.* *23*, 453 - 481.
- Lehner, R., and Quiroga, A.D. (2016). Fatty acid handling in mammalian cells. In *Biochemistry of Lipids, Lipoproteins and Membranes*, (Elsevier), pp. 149 - 184.
- Lemassu, A., and Daffe, M. (1994). Structural features of the exocellular polysaccharides of *Mycobacterium tuberculosis*. *Biochem. J.* *297*, 351 - 357.
- Lenaerts, A.J., Hoff, D., Aly, S., Ehlers, S., Andries, K., Cantarero, L., Orme, I.M., and Basaraba, R.J. (2007). Location of persisting mycobacteria in a guinea pig model of tuberculosis revealed by R207910. *Antimicrob. Agents Chemother.* *51*, 3338 - 3345.
- Lindqvist, Y., Huang, W., Schneider, G., and Shanklin, J. (1996). Crystal structure of  $\Delta 9$  stearoyl-acyl carrier protein desaturase from castor seed and its relationship to other di-iron proteins. *EMBO J.* *15*, 4081 - 4092.
- Liu, J., Barry III, C.E., Besra, G.S., and Nikaido, H. (1996). Mycolic acid structure determines the fluidity of the mycobacterial cell wall. *J. Biol. Chem.* *271*, 29545 - 29551.
- Luckner, S.R., Machutta, C.A., Tonge, P.J., and Kisker, C. (2009). Crystal structures of *Mycobacterium tuberculosis* KasA show mode of action within cell wall biosynthesis and its inhibition by thiolactomycin. *Structure* *17*, 1004 - 1013.
- Lyonnet, B.B., Diacovich, L., Gago, G., Spina, L., Bardou, F., Lemassu, A., Quemard, A., and Gramajo, H. (2017). Functional reconstitution of the *Mycobacterium tuberculosis* long-chain acyl-CoA carboxylase from multiple acyl-CoA subunits. *FEBS J.* *284*, 1110 - 1125.
- Mahajan, S., Dkhar, H.K., Chandra, V., Dave, S., Nanduri, R., Janmeja, A.K., Agrewala, J.N., and Gupta, P. (2012). *Mycobacterium tuberculosis* modulates macrophage lipid-sensing nuclear receptors PPAR $\gamma$  and TR4 for survival. *J. Immunol.* *188*, 5593 - 5603.

- Marrakchi, H., Choi, K., and Rock, C.O. (2002a). A new mechanism for anaerobic unsaturated fatty acid formation in *Streptococcus pneumoniae*. *J. Biol. Chem.* *277*, 44809 - 44816.
- Marrakchi, H., Ducasse, S., Labesse, G., Montrozier, H., Margeat, E., Emorine, L., Charpentier, X., Daffe, M., and Quemard, A. (2002b). MabA (FabG1), a *Mycobacterium tuberculosis* protein involved in the long-chain fatty acid elongation system FAS-II. *Microbiology* *148*, 951 - 960.
- Marrakchi, H., Lan  elle, M.A., and Daff  , M. (2014). Mycolic acids: Structures, biosynthesis, and beyond. *Chem. Biol.* *21*, 67 - 85.
- Matsushashi, M. (1966). Biosynthesis in the bacterial cell wall. *Tanpakushitsu Kakusan Koso* *11*, 875 - 886.
- McNeil, M., Daffe, M., and Brennan, P.J. (1991). Location of the mycolyl ester substituents in the cell walls of mycobacteria. *J. Biol. Chem.* *266*, 13217 - 13223.
- Middlebrook, G., Dubos, R.J., and Pierce, C. (1947). Virulence and morphological characteristics of mammalian tubercle bacilli. *J. Exp. Med.* *86*, 175 - 184.
- Mikuřov  , K., Mikuř, M., Besra, G.S., Hancock, I., and Brennan, P.J. (1996). Biosynthesis of the linkage region of the mycobacterial cell wall. *J. Biol. Chem.* *271*, 7820 - 7828.
- Minnikin, D. (1982). In *The Biology of the Mycobacteria* (London: Academic).
- Minnikin, D.E., Minnikin, S.M., Parlett, J.H., Goodfellow, M., and Magnusson, M. (1984). Mycolic acid patterns of some species of *Mycobacterium*. *Arch. Microbiol.* *139*, 225 - 231.
- Ojha, A.K., Baughn, A.D., Sambandan, D., Hsu, T., Trivelli, X., Guerardel, Y., Alahari, A., Kremer, L., Jacobs, W.R., and Hatfull, G.F. (2008). Growth of *Mycobacterium tuberculosis* biofilms containing free mycolic acids and harbouring drug-tolerant bacteria. *Mol. Microbiol.* *69*, 164 - 174.
- Ojha, A.K., Trivelli, X., Guerardel, Y., Kremer, L., and Hatfull, G.F. (2010). Enzymatic hydrolysis of trehalose dimycolate releases free mycolic acids during mycobacterial growth in biofilms. *J. Biol. Chem.* *285*, 17380 - 17389.
- Olsen, I. (2015). Biofilm-specific antibiotic tolerance and resistance. *Eur. J. Clin. Microbiol. Infect. Dis.* *34*, 877 - 886.
- Olsen, J.G., Kadziola, A., von Wettstein-Knowles, P., Siggaard-Anderson, M., and Larsen, S. (2001). Structures of  $\beta$ -ketoacyl-acyl carrier protein synthase I complexed with fatty acids elucidate its catalytic machinery. *Structure* *9*, 233 - 243.
- Orme, I.M. (2011). Development of new vaccines and drugs for TB: limitations and potential strategic errors. *Future Microbiol.* *6*, 161 - 177.
- Orme, I.M. (2014). A new unifying theory of the pathogenesis of tuberculosis. *Tuberculosis* *94*, 8-14.
- Ortalo-Magne, A., Dupont, M., Lemassu, A., Anderson, A.B., Gounon, P., and Daffe, M. (1995). Molecular composition of the outermost capsular material of the tubercle

- bacillus. *Microbiology* 141, 1609 - 1620.
- Ortalo-Magne, A., Lemassu, A., Laneelle, M.-A., Bardou, F., Silve, G., Gounon, P., Marchal, G., and Daffe, M. (1996). Identification of the surface-exposed lipids on the cell envelopes of *Mycobacterium tuberculosis* and other mycobacterial species. *J. Bacteriol.* 178, 456 - 461.
- Otwinowski, Z., and Minor, W. (1997). Processing of X-ray diffraction data collected in oscillation mode. *Methods Enzymol.* 276, 307 - 326.
- Pawelczyk, J., and Kremer, L. (2014). The molecular genetics of mycolic acid biosynthesis. *Microbiol. Spectr.* 2, 1 - 20.
- Peyron, P., Vaubourgeix, J., Poquet, Y., Levillain, F., Botanch, C., Bardou, F., Daffe, M., Emile, J.F., Marchou, B., Cardona, P.J., et al. (2008). Foamy macrophages from tuberculous patients' granulomas constitute a nutrient-rich reservoir for *M. tuberculosis* persistence. *PLoS Pathog.* 4, 1 - 14.
- Phetsuksiri, B., Jackson, M., Scherman, H., McNeil, M., Besra, G.S., Baulard, A.R., Slayden, R.A., DeBarber, A.E., Barry, C.E., Baird, M.S., et al. (2003). Unique mechanism of action of the thiourea drug isoxyl on *Mycobacterium tuberculosis*. *J. Biol. Chem.* 278, 53123 - 53130.
- Pohl, S., Law, J.H., and Ryhage, R. (1963). The path of hydrogen in the formation of cyclopropane fatty acids. *Biochem. Biophys. Acta* 70, 583 - 585.
- Polacheck, J.W., Tropp, B.E., Law, J.H., and McCloskey, J.A. (1966). Biosynthesis of cyclopropane compounds: VIII. The conversion of leate to dihydrosterculate. *J. Biol. Chem.* 241, 3362 - 3364.
- Portevin, D., de Sousa-D'Auria, C., Montrozier, H., Houssin, C., Stella, A., Laneelle, M.-A., Bardou, F., Guilhot, C., and Daffe, M. (2005). The acyl-AMP ligase FadD32 and AccD4-containing acyl-CoA carboxylase are required for the synthesis of mycolic acids and essential for mycobacterial growth: Identification of the carboxylation product and determination of the acyl-CoA carboxylase component. *J. Biol. Chem.* 280, 8862 - 8874.
- Quemard, A. (2016). New insights into the mycolate-containing compound biosynthesis and transport in mycobacteria. *Trends Microbiol.* 24, 725 - 738.
- Quemard, A., Sacchetti, J.C., Dessen, A., Vilcheze, C., Bittman, R., and Jacobs Jr., W.R. (1995). Enzymatic characterization of the target for isoniazid in *Mycobacterium tuberculosis*. *Biochemistry* 34, 8235 - 8241.
- Quémard, A., Lanéelle, M., Marrakchi, H., Promé, D., Dubnau, E., and Daffé, M. (1997). Structure of a hydroxymycolic acid potentially involved in the synthesis of oxygenated mycolic acids of the *Mycobacterium tuberculosis* complex. *Eur. J. Biochem.* 250, 758 - 763.
- Qureshi, N., Sathyamoorthy, N., and Takayama, K. (1984). Biosynthesis of C30 to C56 fatty acids by an extract of *Mycobacterium tuberculosis* H37Ra. *J. Bacteriol.* 157, 46 - 52.

- Rachman, H., Strong, M., Ulrichs, T., Grode, L., Schuchhardt, J., Mollenkopf, H., Kosmiadi, G.A., Eisenberg, D., and Kaufmann, S.H.E. (2006). Unique transcriptome signature of *Mycobacterium tuberculosis* in pulmonary tuberculosis. *Infect. Immun.* *74*, 1233 - 1242.
- Rao, V., Fujiwara, N., Porcelli, S.A., and Glickman, M.S. (2005). *Mycobacterium tuberculosis* controls host innate immune activation through cyclopropane modification of a glycolipid effector molecule. *J. Exp. Med.* *201*, 535 - 543.
- Rao, V., Gao, F., Chen, B., Jacobs Jr., W.R., and Glickman, M.S. (2006). *Trans*-cyclopropanation of mycolic acids on trehalose dimycolate suppresses *Mycobacterium tuberculosis*-induced inflammation and virulence. *J. Clin. Invest.* *116*, 1660 - 1667.
- Rich, A. (1951). *The pathogenesis of tuberculosis* (Springfield, IL: Charles C Thomas).
- Richard-Greenblatt, M., and Av-gay, Y. (2017). Epigenetic phosphorylation control of *Mycobacterium tuberculosis* infection and persistence. *Microbiol. Spectr.* *5*, 1 - 23.
- Rock, C.O., and Cronan, J.E. (1996). *Escherichia coli* as a model for the regulation of dissociable (type II) fatty acid biosynthesis. *Biochem. Biophys. Acta* *1302*, 1 - 16.
- Rohacova, J., Marin, M.L., and Miranda, M.A. (2010). Complexes between fluorescent cholic acid derivatives and human serum albumin: A photophysical approach to investigate the binding behavior. *J. Phys. Chem. B* *114*, 4710 - 4716.
- La Rosa, V., Poce, G., Ortiz Canseco, J., Buroni, S., Rosalia Pasca, M., Biava, M., Raju, R.M., Cesare Porretta, G., Alfonso, S., Battilocchio, C., et al. (2012). MmpL3 Is the cellular target of the antitubercular pyrrole derivative BM212. *Antimicrob. Agents Chemother.* *56*, 324 - 331.
- Russell, D.G., Cardona, P., Kim, M., Allain, S., and Altare, F. (2009). Foamy macrophage and the progression of the human TB granuloma. *Nat. Immunol.* *10*, 943 - 948.
- Sacco, E., Suarez Covarrubias, A., O'Hare, H.M., Carroll, P., Eynard, N., Jones, T.A., Ba, K., Parish, T., Daffe, M., Backbro, K., et al. (2007). The missing piece of the type II fatty acid synthase system from *Mycobacterium tuberculosis*. *Proc. Natl. Acad. Sci.* *104*, 14628 - 14633.
- Sachdeva, S., Musayev, F.N., Alhamadsheh, M.M., Scarsdale, J.N., Wright, H.T., and Reynolds, K.A. (2008). Separate entrance and exit portals for ligand traffic in *Mycobacterium tuberculosis* FabH. *Chem. Biol.* *15*, 402 - 412.
- Sambandan, D., Dao, D.N., Weinrick, B.C., Vicheze, C., Gurchach, S.S., Ojha, A., Kremer, L., Besra, G.S., Hatfull, G.F., and Jacobs Jr., W.R. (2013). Keto-mycolic acid-dependent pellicle formation confers tolerance to drug-sensitive *Mycobacterium tuberculosis*. *MBio* *4*, 1 - 10.
- Sani, M., Houben, E.N.G., Geurtsen, J., Pierson, J., de Punder, K., van Zon, M., Wever, B., Piersma, S.R., Jiménez, C.R., Daffé, M., et al. (2010). Direct visualization by Cryo-EM of the mycobacterial capsular layer: A labile structure containing ESX-1-secreted proteins. *PLoS Pathog.* *6*, 1 - 10.

- Sarathy, J., Dartois, V., Dick, T., and Gengenbacher, M. (2013). Reduced drug uptake in phenotypically resistant nutrient-starved nonreplicating *Mycobacterium tuberculosis*. *Antimicrob. Agents Chemother.* *57*, 1648 - 1653.
- Schaeffer, M.L., Agnihotri, G., Kallender, H., Brennan, P.J., and Lonsdale, J.T. (2001). Expression, purification, and characterization of the *Mycobacterium tuberculosis* acyl carrier protein, AcpM. *Biochem. Biophys. Acta* *1532*, 67 - 78.
- Schluckebier, G., O’Gara, M., Saenger, W., and Cheng, X. (1995). Universal catalytic domain structure of AdoMet-dependent methyltransferases. *J. Mol. Biol.* *247*, 16 - 20.
- Schmid, K.M. (2016). Lipid metabolism in plants. In *Biochemistry of Lipids, Lipoproteins and Membranes*, pp. 113 - 147.
- Shi, Z., Karki, R.G., Oishi, S., Worthy, K.M., Bindu, L.K., Dharmawardana, P.G., Nicklaus, M.C., Bottaro, D.P., Fisher, R.J., and Burke Jr., T.R. (2005). Utilization of a nitrobenzoxadiazole (NBD) fluorophore in the design of a Grb2 SH2 domain-binding peptide mimetic. *Bioorg. Med. Chem. Lett.* *15*, 1385 - 1388.
- Singh, A., Varela, C., Bhatt, K., Veerapen, N., Lee, O.Y.C., Wu, H.H.T., Besra, G.S., Minnikin, D.E., Fujiwara, N., Teramoto, K., et al. (2016). Identification of a desaturase involved in mycolic acid biosynthesis in *Mycobacterium smegmatis*. *PLoS One* *11*, 1 - 20.
- Smith, S. (1994). The animal fatty acid synthase: one gene, one polypeptide, seven enzymes. *FASEB J.* *8*, 1248 - 1259.
- Srivastava, S., Chaudhary, S., Thukral, L., Shi, C., Gupta, R.D., Gupta, R., Priyadarshan, K., Vats, A., Haque, A.S., Sankaranarayanan, R., et al. (2015). Unsaturated lipid assimilation by mycobacteria requires auxiliary *cis-trans* enoyl CoA isomerase. *Chem. Biol.* *22*, 1577 - 1587.
- Stanley, S.A., Kawate, T., Iwase, N., Shimizu, M., Clatworthy, A.E., Kazyanskaya, E., Sacchettini, J.C., Ioerger, T.R., Siddiqi, N.A., Minami, S., et al. (2013). Diarylcoumarins inhibit mycolic acid biosynthesis and kill *Mycobacterium tuberculosis* by targeting FadD32. *Proc. Natl. Acad. Sci.* *110*, 11565 - 11570.
- Swanson, S., Gokulan, K., and Sacchettini, J.C. (2009). KasA, another brick in the mycobacterial cell wall. *Struct. Previews* *17*, 914 - 915.
- Takayama, K., and Qureshi, N. (1978). Isolation and characterization of the monounsaturated long chain fatty acids of *Mycobacterium tuberculosis*. *Lipids* *13*, 575 - 579.
- Takayama, K., Schnoes, H.K., Armstrong, E.L., and Boyle, R.W. (1975). Site of inhibitory action of isoniazid in the synthesis of mycolic acids in *Mycobacterium tuberculosis*. *J. Lipid Res.* *16*, 308 - 317.
- Takayama, K., Wang, C., and Besra, G.S. (2005). Pathway to synthesis and processing of mycolic acids in *Mycobacterium tuberculosis*. *Clin. Microbiol. Rev.* *18*, 81 - 101.

- Tehlivets, O., Scheuringer, K., and Kohlwein, S.D. (2007). Fatty acid synthesis and elongation in yeast. *Biochim. Biophys. Acta* 1771, 255 - 270.
- Teramoto, K., Suga, M., Sato, T., Wada, T., Yamamoto, A., and Fujiwara, N. (2015). Characterization of mycolic acids in total fatty acid methyl ester fractions from *Mycobacterium* species by high resolution MALDI-TOFMS. *Mass Spectrom.* 4, 1 - 7.
- Tomiyasu, I., and Yano, I. (1984). Separation and analysis of novel polyunsaturated mycolic acids from a psychrophilic, acid-fast bacterium, *Gordona aurantiaca*. *Eur. J. Biochem.* 139, 173 - 180.
- Trivedi, O.A., Arora, P., Sridharan, V., Tickoo, R., Mohanty, D., and Gokhale, R.S. (2004). Enzymic activation and transfer of fatty acids as acyl-adenylates in mycobacteria. *Nature* 428, 441 - 445.
- Vaubourgeix, J., Bardou, F., Boissier, F., Julien, S., Constant, P., Ploux, O., Daffé, M., Quémar, A., and Mourey, L. (2009). S-adenosyl-N-decyl-aminoethyl, a potent bisubstrate inhibitor of *Mycobacterium tuberculosis* mycolic acid methyltransferases. *J. Biol. Chem.* 284, 19321 - 19330.
- Vollmer, W., and Höltje, J.-V. (2004). The architecture of the murein (peptidoglycan) in gram-negative bacteria: vertical scaffold or horizontal layer(s)? *J. Bacteriol.* 186, 5978 - 5987.
- Walton, E.M., Cronan, M.R., Cambier, C.J., Rossi, A., Marass, M., Foglia, M.D., Brewer, J.W., Poss, K.D., Stainier, D.Y.R., Bertozzi, C.R., et al. (2018). Cyclopropane modification of trehalose dimycolate drives granuloma angiogenesis and mycobacterial growth through Vegf signaling. *Cell Host Microbe* 24, 514 - 525.
- Wang, Z.X. (1995). An exact mathematical expression for describing competitive binding of two different ligands to a protein molecule. *FEBS Lett.* 360, 111 - 114.
- Wang, A.Y., Grogan, D.W., and Cronan, J.E. (1992). Cyclopropane fatty acid synthase of *Escherichia coli*: Deduced amino acid sequence, purification, and studies of the enzyme active site. *Biochemistry* 31, 11020 - 11028.
- Watanabe, M., Aoyagi, Y., Mitome, H., Fujita, T., Naoki, H., Ridell, M., and Minnikin, D.E. (2002). Location of functional groups in mycobacterial meromycolate chains; the recognition of new structural principles in mycolic acids. *Microbiology* 148, 1881 - 1902.
- Wayne, L.G. (1994). Cultivation of *Mycobacterium tuberculosis* for research purposes. In *Tuberculosis: Pathogenesis, Protection, and Control*, (Washington, DC: ASM Press), pp. 73 - 83.
- Welsh, K.J., Hunter, R.L., and Actor, J.K. (2013). Trehalose 6,6'-dimycolate - A coat to regulate tuberculosis immunopathogenesis. *Tuberculosis* 93, S3 - S9.
- Wenskowsky, L., Schreuder, H., Derdau, V., Matter, H., Volkmar, J., Nazaré, M., Opatz, T., and Petry, S. (2018). Identification and characterization of a single high-affinity fatty acid binding site in human serum albumin. *Angew. Chemie - Int. Ed.* 57, 1044 - 1048.

- Wong, K., and Jacobs, W.R. (2016). Postprimary tuberculosis and macrophage necrosis: Is there a big conNEction? *MBio* 7, 1 - 6.
- Wong, H.C., Liu, G., Zhang, Y.M., Rock, C.O., and Zheng, J. (2002). The solution structure of acyl carrier protein from *Mycobacterium tuberculosis*. *J. Biol. Chem.* 277, 15874 - 15880.
- World Health Organization (2018). Global tuberculosis report.
- Xie, S., Lee, Y., Kim, E., Chen, L., Ni, J., Fang, L., Liu, S., Lin, S., Abe, J., Berk, B., et al. (2009). TR4 nuclear receptor functions as a fatty acid sensor to modulate CD36 expression and foam cell formation. *Proc. Natl. Acad. Sci.* 106, 13353 - 13358.
- Yang, Y., Kulka, K., Montelaro, R.C., Reinhart, T.A., Sissons, J., Aderem, A., and Ojha, A.K. (2014). A hydrolase of trehalose dimycolate induces nutrient influx and stress sensitivity to balance intracellular growth of *Mycobacterium tuberculosis*. *Cell Host Microbe* 15, 153 - 163.
- Yuan, Y., and Barry III, C.E. (1996). A common mechanism for the biosynthesis of methoxy and cyclopropyl mycolic acids in *Mycobacterium tuberculosis*. *Proc. Natl. Acad. Sci. U. S. A.* 93, 12828 - 12833.
- Yuan, Y., Lee, R.E., Besra, G.S., Belisle, J.T., and Barry III, C.E. (1995). Identification of a gene involved in the biosynthesis of cyclopropanated mycolic acids in *Mycobacterium tuberculosis*. *Proc. Natl. Acad. Sci. U. S. A.* 92, 6630 - 6634.
- Yuan, Y., Crane, D.C., Musser, J.M., Sreevatsan, S., and Barry III, C.E. (1997). MMAS-1, the branch point between *cis*- and *trans*-cyclopropane-containing oxygenated mycolates *Mycobacterium tuberculosis*. *J. Biol. Chem.* 272, 10041 - 10049.
- Yuan, Y., Zhu, Y., Crane, D.D., and Barry III, C.E. (1998a). The effect of oxygenated mycolic acid composition on cell wall function and macrophage growth in *Mycobacterium tuberculosis*. *Mol. Microbiol.* 29, 1449 - 1458.
- Yuan, Y., Mead, D., Schroeder, B.G., Zhu, Y., and Barry III, C.E. (1998b). The biosynthesis of mycolic acids in *Mycobacterium tuberculosis*: Enzymatic methyl(ene) transfer to acyl carrier protein bound meromycolic acid in vitro. *J. Biol. Chem.* 273, 21282 - 21290.
- Zalkin, H., Law, J.H., and Goldfine, H. (1963). Enzymatic synthesis of cyclopropane fatty catalyzed by bacterial extracts. *J. Biol. Chem.* 238, 1242-1249.
- Zhang, Y.M., and Rock, C.O. (2016). Fatty acid and phospholipid biosynthesis in prokaryotes. In *Biochemistry of Lipids, Lipoproteins and Membranes*, (Elsevier), pp. 73 - 112.
- Zhuang, Y. D., Chiang, P. Y., Wang, C.-W., and Tan, K. T. (2013). Environment-sensitive fluorescent turn-on probes targeting hydrophobic ligand-binding domains for selective protein detection. *Angew. Chemie - Int. Ed.* 52, 8124 - 8128.
- Zimhony, O., Vilche, C., and Jacobs Jr., W.R. (2004). Characterization of *Mycobacterium smegmatis* expressing the *Mycobacterium tuberculosis* fatty acid synthase I (fasI)



Gene. *J. Bacteriol.* *186*, 4051 - 4055.

Zuber, B., Chami, M., Houssin, C., Dubochet, J., Griffiths, G., and Daffé, M. (2008). Direct visualization of the outer membrane of mycobacteria and corynebacteria in their native state. *J. Bacteriol.* *190*, 5672 - 5680.